UNIVERSITY OF CALIFORNIA SAN DIEGO

SAN DIEGO STATE UNIVERSITY

Glassy Carbon Neural Probes for Cortical and Spinal Electrochemical and Electrophysiological Sensing and Stimulation

A Dissertation in partial satiation of the requirements
for the degree of Doctor of Philosophy
in

Bioengineering

by

Mieko Hirabayashi

Committee in charge

San Diego State University

Professor Sam Kassegne, Chair
Professor Joaquin Camacho

University of California San Diego

Professor Gert Cauwenberghs, Co-Chair
Professor Thomas Liu
Professor Jaime Pineda

2018

The Dissertation of Mieko Hirabayashi is approved and it is acceptable in quality and form for the publication on microfilm and electronically:

_____

_____

_____

_____

Chair

_____

Co-Chair

University of California San Diego

San Diego State University

2018

DEDICATION

I dedicate this to my husband Tom McDowell who has been there for me throughout this journey…I wouldn't have finished this without you or the wonderful children you have given me.

TABLE OF CONTENTS

LIST OF TABLES

LIST OF FIGURES

ACKNOWLEDGEMENTS

This research was funded by the National Science Foundation (NSF) Grant No. EEC-1028725 under the ERC program.

Thank you to the San Diego State University Department of Chemistry and Dr. David Pullman for allowing use and collection of Infrared and Raman spectroscopy data.

Thank you to the San Diego State Electron Spectroscopy lab for allowing use of the Scanning electron microscope and its facilities.

I would also like to thank my mentees, Nha Uyen Huynh, Shane Witsell, Alberto Perez, Laura Sandoval, Kyle Logan, Christopher Deutschman, and Will Ritchie who assisted with data collection, fabrication, and SEM during their time working with me.

Chapter 3 is a reprint of the journal article “In-Vitro Real-Time Coupled Electrophysiological and Electrochemical Signals Detection with Glassy Carbon Microelectrodes" published in the *Journal of The Electrochemical Society* (164, no. 5 (2017): B3113-B3121). Methods from this paper are in Chapter 2 sections 2.2.3 and 2.3.

Chapter 4 is a reprint of the journal article “Investigation of Interface Bonding Mechanisms between Glassy Carbon Microelectrodes and Polyimide Substrate through Fourier Transform Infrared Spectroscopy” accepted for publication to the *Journal of the Electrochemical Society*.

VITA

2009	Bachelor of Science, Bioengineering, University of California San Diego
2010	Research Associate at Advanced Brain Monitoring, Inc.
2011	Teaching Assistant, San Diego State University
2012	Master of Science, Bioengineering, San Diego State University
2013	Research Associate and Project Manager at San Diego State University MEMS lab
2014	Teaching and Research Assistant, San Diego State University
2018	Doctor of Philosophy, Bioengineering, University of California San Diego and San Diego State University Joint Doctoral Program,

PUBLICATIONS

1. **Hirabayashi, Mieko,** Kyle Logan, Christopher Deutschman, Thomas McDowell, Martha Torres, David Pullman, and Sam Kassenge. “Investigation of Interface Bonding Mechanisms between Glassy Carbon Microelectrodes and Polyimide Substrate through Fourier Transform Infrared Spectroscopy.” *Journal of the Electrochemical Society* 165, no. 8 (2018): B3060-B3070.

2. **Hirabayashi, Mieko**, Nha Uyen Huynh, Shane Witsell, Alberto Perez, Laura Sandoval, Naoya Yamada, and Sam Kassegne. "In-Vitro Real-Time Coupled Electrophysiological and Electrochemical Signals Detection with Glassy Carbon Microelectrodes." *Journal of The Electrochemical Society* 164, no. 5 (2017): B3113-B3121.

3. Vomero, Maria, Pieter van Niekerk, Vivian Nguyen, Nick Gong, **Mieko Hirabayashi**, Alessio Cinopri, Kyle Logan, Ali Moghadasi, Priya Varma, and Sam Kassegne. "A Novel Pattern Transfer Technique for Mounting Glassy Carbon Microelectrodes on Polymeric Flexible Substrates." *Journal of Micromechanics and Microengineering* 26, no. 2 (2016): 025018.

4. Kassegne, Sam, Maria Vomero, Pieter van Niekerk, **Mieko Hirabayashi**. “Glassy Carbon Microelectrodes for Neural Sensing and Stimulation,” 2016, Invited Review Article, Micro

Electronic Mechanical Devices Collection: Carbon: The Next Silicon? Book 2—Applications. Marc J. Madou, Victor H. Perez- Gonzalez, Bidhan Pramanick, Momentum Press Engineering.

5. Kassegne, Sam, Maria Vomero, Roberto Guagliò, **Mieko Hirabayashi**, Emre Özyilmaz, Sebastien Nguyen, Jesus Rodriguez, Eda Özyilmaz, Pieter van Niekerk, and Ajit Khosla. "Electrical impedance, electrochemistry, mechanical stiffness, and hardness tunability in glassy carbon MEMS μECoG electrodes." *Microelectronic Engineering* 133 (2015): 36-44.

6. **Hirabayashi, Mieko**, Beejal Mehta, Nasim W. Vahidi, Ajit Khosla, and Sam Kassegne. "Functionalization and characterization of pyrolyzed polymer based carbon microstructures for bionanoelectronics platforms." *Journal of Micromechanics and Microengineering* 23, no. 11 (2013): 115001.

7. Vahidi, Nasim W., **Mieko Hirabayashi**, Beejal Mehta, Mohammad Rayatparvar, Denni Wibowo, Varsha Ramesh, James Chi et al. "Bionanoelectronics platform with DNA molecular wires attached to high aspect-ratio 3D metal microelectrodes." *ECS Journal of Solid State Science and Technology* 3, no. 3 (2014): Q29-Q36.

8. **Hirabayashi, Mieko**, Beejal Mehta, Bao Nguyen, and Sam Kassegne. "DNA immobilization on high aspect ratio glassy carbon (GC-MEMS) microelectrodes for bionanoelectronics applications." *Microsystem Technologies* (2014): 1-7.

9. **Hirabayashi, Mieko**, Beejal Mehta, A. Khosla, and Sam Kassegne. "Functionalization of Pyrolyzed Carbon Structures for Bio-Nanoelectronics Platforms." *ECS Transactions* 50, no. 12 (2013): 325-331.

Fields of Study

Major field: Bioengineering

Studies in microfabrication, biosensors, and electrochemistry

Professor Sam Kassegne

ABSTRACT OF THE DISSERTATION

Glassy Carbon Neural Probes for Electrochemical and Electrophysiological Sensing and Stimulation

by

Mieko Hirabayashi

Doctor of Philosophy in Bioengineering

University of California San Diego, 2018

San Diego State University, 2018

This study demonstrates glassy carbon's ability to perform as multi-modal flexible penetrating neural probe array. The fabrication process of glassy carbon arrays allows for development of a single device with multiple electrode sites, flexible body, and penetrating probes capable of penetrating neural tissue making the device suitable for various types of brain or spinal cord implant. Furthermore, the investigation into the carbon surface properties makes the device suitable for detecting electrical or electrochemical signals and electrical stimulation of neurons. Here, glassy carbon's ability to detect electrophysiology and electrochemical signals simultaneously recorded is shown in an *in vitro* set-up. Glassy carbon's ability to perform *in vivo* as an electrochemical and electrophysiological detector and stimulator is also demonstrated.

CHAPTER 1

Introduction

Damage or dysfunction of any portion of the central nervous system can have devastating effects on peoples' lives. Spinal cord injury can result in partial or complete loss of motor function in upper and lower limbs (De La Torre, 1981). Parkinson's disease, caused by dysfunction of dopaminergic neurons leads to loss of fine motor control (Hudspeth, 2013). Epilepsy, characterized by reoccurring seizures is thought to be caused by improper neural connections and/or dysregulation of neurotransmitter levels (Goldberg, 2103). These are just a few of the many neurological disorders that have devastating consequences for those suffering with the condition. While treatments do exist, many people with spinal cord injury never retain full function of the motor impairment, people suffering with Parkinson's disease experience schizophrenic-like auditory hallucinations from treatments, and those with epilepsy are often medicated with anti-convulsant that impair cognitive function. The reason for many of these unsuccessful treatments is due to a lack in fundamental understanding of the central nervous system (CNS). To better understand the CNS, an advancement in the development and use of implantable neural interfaces is necessary.

Within the realm of neural interfaces, sometimes referred to as neural probes, includes neural stimulators and electrochemical and electrophysiological sensors. These probes can be placed epidermally but are often implanted trans or sub-cutaneously or even directly on neural tissue to record or stimulate nearby neurons. With well-developed protocols, these probes can be used to sense electrical or electrochemical signals in response to behavioral or electrical stimulus giving insight into neural mechanisms and pathways and leading to a better understanding of the

brain. However, currently, most methods for investigating the brain and its function includes either electrical or electrochemical sensing (discussed in detail in sections 1.1 through 1.3); part of the reason is that most neural probes developed are not suitable for both electrical and electrochemical sensing. Thus, a need exists for the development of a single device implantable in either the brain or spinal cord and capable of simultaneously stimulating and detecting the resulting neurotransmitter release and change in electrophysiological potential. To do this, microfabrication methods were developed to generate glassy carbon microelectrodes on a biocompatible and flexible substrate made of polyimide stiff enough to penetrate neural tissue, as described chapter 2 section 1 and 2. Then, electrochemical methods described in section 2.3 were used to test and characterize the devices. To fully understand the durability and characteristics of the materials being used in the device, the interface of glassy carbon and polyimide were investigated using Fourier Transform Infrared Spectroscopy (FTIR). An *in vitro* study was then done to prove that these electrodes could simultaneously detect serotonin and electrophysiology *in vitro* as described in chapter 4. In order to prepare for *in vivo* testing, fundamental studies on the interaction between glassy carbon and neurotransmitters were completed and described in chapter 5. Finally, chapter 6 covers how design and surface modifications were implemented to allow for *in vivo* electrophysiological signal detection, electrical stimulation, and electrochemical detection.

1.1 Neural Probe Electrode Arrays

From an architectural point of view, neural probes come in many forms. Some are arrays of microfabricated electrodes while others are as simple as a single wire. The variations in the geometry and architectures of neural probes depends on the application. First, the design depends

on the location of the implant. Since the spinal cord is simply organized with the neural bodies in the center of the cord and the axons on the outside of the cord (Hudspeth, 2013), most signal detection and stimulation are done with penetrating electrodes that can reach the neural bodies. However, to minimize tissue damage, researchers have attempted to move from penetrating electrodes to epidural electrodes for stimulation (van den Brand, 2012). The brain, on the other hand, has a more complex structure. While some significant signaling happening on the surface, like the at the sensory motor cortex, other signaling, like the insular cortex associated with reward, learning, and empathy occurs only in the center (Hudspeth, 2013). Thus, sensing and stimulating electrodes designs for the brain are dictated by the location of the area of interest. While some applications only require surface electrodes, other cases may dictate a need for both surface and penetrating electrodes, or only penetrating electrodes. Figure 1 describes the various applications for neural probe architecture.

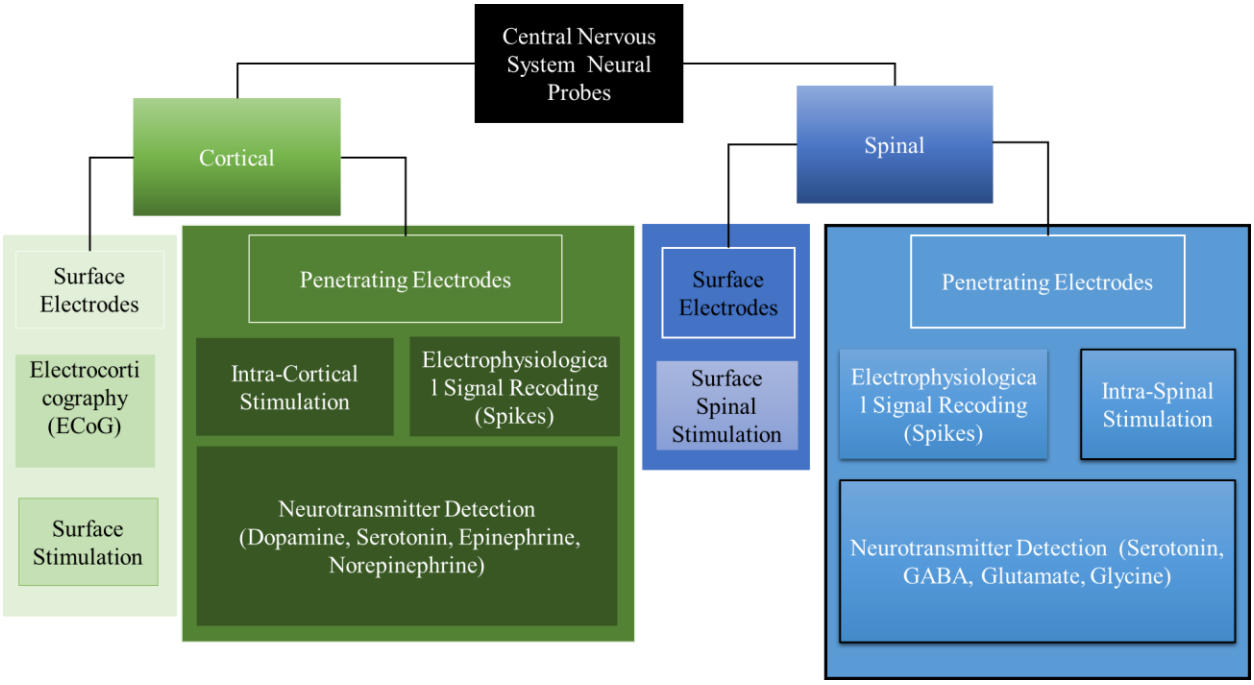

Figure 1: Various Applications of Neural Probes

1.1.1 Surface Microelectrodes

Surface arrays, most commonly used for Electrocorticography (ECoG), electrophysiological signal recording from the surface of the cortex, allow for detection of mu, beta, and gamma sensorimotor rhythms (Rothschild, 2010). To gather this information, an array of conductive sites that can be placed directly on neural tissues and carry the signal to an amplifier and recording equipment is required. Because of their simplicity, various types of surface microelectrode arrays have been developed, but recently, the most important aspect of the surface arrays have been its ability to last long term and conform to the neural tissue. The most recent innovation in these recording arrays often comes from the flexibility and conformity of the substrate it sits on. The most common substrates in recent years have been those that are

considered flexible and biocompatible, mainly Polydimethylsiloxane (PDMS), Parylene-C, and polyimides, but the more recent developments in ECoG technologies has been the implementation of hydrogels and scaffolds that allow the neural tissue to integrate better with the substrate (Scaini, 2018).

Similar surface arrays designs have been used for stimulation. Epidural stimulation, for example, whether in the spinal cord or cortex, has similar design requirements as ECoG surface arrays; these designs need to be flexible with a durable conductive site (Gad, 2013; Rembado, 2017; van den Brand, 2012). The biggest difference between stimulating and recording microelectrodes is the electrode site material. While the surface recording electrodes can be made of any biocompatible, conductive materials, stimulating electrodes, on the other hand require a high charge injection capacity and wide electrochemical window. Thus, most stimulating surface electrode are made from biocompatible metals with high charge injection capacity like platinum or iridium (Cogan, 2008).

1.1.2 Penetrating Neural Probes

While surface arrays have the benefit of being less invasive than penetrating probes, often penetrating probes are still needed. For recording arrays, penetrating probes are more suitable for acquiring signals from single or multi-unit neurons because spatial resolution through the depth of the brain that cannot be attained from surface signals (Rothschild, 2010). Many of the arrays currently used were inspired by the original Utah array, a 3D silicon-based probe with gold electrodes (Maynard, 1997), and the Michigan array (Rousche, 2001) a similar silicon and gold-based array that has longer probes because of its 2D design. These original designs are still used today but have also been modified by Black Rock Microsystems ® and Neuronexus ®.

Neuronexus, for instance, has made higher density electrode sites (Hetke, 2011) and moved to penetrating arrays made from polyimide, making them more flexible than the original (Kong, 2009). While Blackrock has kept the design of the probe mostly the same, it is still used and published in some of the most recent neuroscience publications (Nghiem, 2018).

Stimulating penetrating electrodes are more commonly used in research than the stimulating surface electrodes. Cortical stimulators include those meant for Deep Brain Stimulation (Kuncel, 2004), or a modification of the penetrating recording electrodes to increase charge injection capacity (Cogan, 2008). In the spinal cord, while researchers use versions of the Utah array (Branner, 2001), this design can be bulky and difficult to implant long term. Thus, researchers will often prefer the simplicity of small diameter iridium, stainless-steel, or even silver wires in place of arrays (Linderoth, 1995; Mushahwar, 2000; Seki, 2003).

1.2 Neurotransmitter Detection

Neurotransmitters are signaling molecules between individual neural cells. These molecules are released by vesicles in the synaptic cleft as a result of an action potential (a relative electrochemical voltage) reaching the end of an axon. In the synaptic cleft, the molecules diffuse to the dendrite of another neuron and bind to proteins specific to the neurotransmitter. This chemical basis of signaling happens at each neural connection and can be responsible for upregulation, downregulation, or simply termination of a process (Hudspeth, 2013). To some degree, some signaling of neurotransmitters is understood. For example, dopamine (DA) and serotonin (5-Hydtoytryptamine or 5-HT) are associated with mood and acetylcholine and nitric oxide are often associated with autonomic function regulation. Even some disease states are correlated with changes in neurotransmitters: increase of dopamine in the temporal lobe is

associated with schizophrenia, while deficit in dopamine in the substantia nigra is associated with Parkinson's disease (Hudspeth, 2013). However, specifically, how each one of these signaling molecules modulates a single function is not well understood. Thus, as we move toward a better understanding of cognition through electrophysiological signal analysis, we must also look at how neurons are talking to one another through chemical signaling. Researchers have begun to investigate these chemical communications through microdialysis and electrochemistry.

1.2.1 Microdialysis

Currently, microdialysis still remains the most widely used way to determine the types of neurotransmitters present in tissue. To do this, a dialysis probe is inserted into the tissue; this probe is permeable to small molecules and allows the entry of localized molecules into to the probe. The probe is then perfused with artificial cerebral spinal fluid and the dialysate is separated and analyzed using high pressure liquid chromatography (Robinson, 2003).

While this method is very straightforward and reliable, it has its drawbacks. The main drawback is its inability to resolve data in real time; without real time measurements, the exact cause of an increase in neurotransmitter cannot be known. Thus, in more recent years, researchers have begun to implement electrochemical methods of detecting neurotransmitters *in vivo* to gain better temporal resolution (Roberts, 2017).

1.2.2 Fast Scan Cyclic Voltammetry

Cyclic voltammetry (CV) is an electrochemical analytical method that uses a triangular input at scan rate in the range of mV/s. This input sends a current from the counter electrode that generates a voltage at the working electrode relative to the reference electrode. As the voltage

sweeps upward, the positive charge at the working electrode uptakes electrons from species in the analyte causing oxidation; as the voltage sweeps downward the working electrode gives up electrons causing reduction of species in the analyte. The output of the CV is a current vs. voltage plot, commonly known as a voltammogram, that can give insight into the species in the analyte or the electrode itself. Thus, this method of analysis has been used to characterize and detect neurotransmitters *in vitro* and *in vivo* (Roberts, 2017). However, while the information has more temporal resolution than microdialysis, the linear sweeping causes charging of the electrode which takes time to discharge before an accurate subsequent signal to be obtained (Millar, 1985). Various types of waveforms have been developed to address this issue, such as differential pulse voltammetry (DPV), but currently, fast scan cyclic voltammetry has become the standard for neurochemical detection.

Fast scan cyclic voltammetry (FSCV) is a variant of the traditional CV where the scan rate is increased to the order of volts or kilovolts per second rather than the standard millivolts per second. This is done partially to increase temporal resolution to the millisecond scale, the time scale of neural action potentials, making this method ideal for *in vivo* application, but also to decrease the amount of charging occurring on the electrode (Millar, 1985). Once collected, the voltammogram shows a background current that can obscure small oxidation currents, but this is easily remedied by digitally subtracting out a voltammogram collected before the release of the neurotransmitter.

In 1985, FCSV methods for neurotransmitter detection *in vivo* were developed to investigate dopamine concentrations in rat caudate nucleus (Roberts, 2017). These experiments laid the foundation for subsequent developments in the field to detect other catecholamines,

norepinephrine (Robinson, 2003) and epinephrine, and other neuro-signaling molecules like, 5-HT (Jackson, 1995), histamine (Van Gompel, 2010) and adenosine (Swamy, 2007), by altering the input waveform and/or the surface of the electrode (Lama, 2012). Other researchers made progress in obtaining spatial resolution by using microelectrode arrays in place of the single carbon fiber (Koehne, 2011; Yakushenko, 2014).

In the last decade, several significant developments have happened in the FSCV field. One large advancement has been the studies that have moved to primates. In 2012, Chang et. Al. at the Mayo Clinic developed the WINCS (Wireless Instantaneous Neurotransmitter Concentration System) and was able to perform measurements of dopamine concentrations in humans (Chang, 2012). Even more recently, Schwerdt et. Al. was able to establish the ability reliably detect dopamine in non-human primates for over 100 days using FSCV and carbon fiber electrodes (Schwerdt, 2017).

The technology is now becoming useful in elucidating mechanisms in at the cellular level. Abdalla used methods developed by Jackson *et al.* to determine basal extracellular 5-HT level; understanding the basal levels of 5-HT allows for further studies into what mechanisms exist to control the extracellular levels of 5-HT (Abdalla, 2017). Taleat *et al.* was able to use FSCV methods to detect levels of epinephrine in the presence of Adenosine Tri-Phosphate (ATP). Experiments showed the epinephrine oxidation peak could be reduced by putting it the presence in epinephrine, which suggests that the ATP phosphate was interacting with the ammonium group of the epinephrine. These findings give insight into the mechanisms that allow neurotransmitters to accumulate in secretory vesicles inside neuronal cells (Taleat, 2017).

1.2.3 Serotonin FSCV

In 1995, a decade after the first dopamine experiments, Jackson *et al.* demonstrated that serotonin (5-HT) could be detected using the same methods that were used with dopamine but complications like irreversible adsorption of the 5-HT and fouling of the electrode occurred (Jackson, 1995). Thus, changes in the input waveform (Jackson, 1995), surface coating of the electrode (Jackson, 1995; Pihel, 1996; Swamy 2007), and even post processing of the data were implemented (Fang, 2013). With these changes, as shown in Table 1, *in situ* studies were able to detect values as low as 200 nM with the standard *in vivo* set-up and 10 nM with a special *in vitro* set-up. While 200 nM is physiologically relevant, in order to obtain better temporal resolution, lower detection limits would be beneficial.

Table 1: Serotonin FSCV studies

Electrode	***Voltage Input***	***Scan Rate (V/s)***	***Lowest Detection Reported***	***Reference***
Carbon fiber	0.2-1- (-0.1)-0.2	1000	250 nM	(Griessenauer, 2010)
Overoxidized Polypyrrole-Coated carbon fiber	-0.4-1.4	300	1000 nM	(Pihel, 1996)
Deep Brain Stimulation Electrode (Human)	-0.6-1.4	400	100 nM	(Moran, 2018)
Carbon Fiber	0.2-1- (-0.6)-0.2	300	200 nM	(John, 2007)
Carbon-Fiber Disk (3 probe in vitro *set-up)*	-0.4-1.4	400	10 nM	(Fang, 2013)
Carbon Fiber coated with CNT and 5-HTP	-0.4-1.4	400	130 nM	(Swamy, 2007)

1.2.4 Electrochemical Carbon Microelectrodes

Unlike the passive recording done by neural probes for electrophysiological signal sensing, electrochemical recording requires the electrode to withstand an applied voltage; since many of the electrophysiological signal sensing arrays are made by thin film deposition, their tolerance to stimulation degrades over time as the metal slowly delaminates (Cogan, 2008; Zachek, 2010). However, carbon-based electrodes tend to have a wider electrochemical window than metal-based electrodes making them more suitable for electrochemical methods (Kassegne,

2015). Currently, the FSCV standard *in vivo* electrode has been carbon fiber. However, as the demand for better and smaller biosensors has increase, the applications of fullerene structures have become ubiquitous. Some of the most recent uses of fullerenes include the generation of Carbon Nano Fiber (CNF) (Zhang, 2017), Carbon Nanopipette Electrodes (CNPE) (Rees, 2015), and Carbon Nanotube Yarn (CNTY) (Schmidt, 2013).

Rees *et al.* developed CPNEs by first generating nanopipettes from quartz capillaries and then subsequently depositing carbon onto the capillaries with a tip that varied in size from 40 nm to 500 nm. With this device, they were able to perform fast scan cyclic voltammetry in drosophila and able to detect concentrations as low as 25 nM. Carbon nanofibers with a diameter of 10um generated by Zhang et. Al. from spinnable multiwalled carbon nanotubes (Zhang, 2017) were found to have sensitivity and selectivity to electroactive neurochemicals that could be enhanced by inducing defects through subsequent heating. CNT yarn, composed from several layers of parallel CNT structures have also become popular. These structures can be made disk shaped and because of the inherent surface roughness, can makes these electrodes more sensitive to electrochemical oxidization (Schmidt, 2013). In 2014, Du and colleagues were able to increase the sensitivity of the more traditionally carbon fiber by ‘blooming; graphene sheets on the surface. This was done by applying a solution containing graphene nanosheets to the carbon fiber and allowing the graphene to dry; copper nanoparticles were the electrochemically deposited onto the carbon fiber acting as a mold for the subsequent layer of graphene sheets applied. After the final application of the graphene solution the copper nanoparticles were dissolved out leaving flower-like blossoms on the surface of the CNF (Du, 2014).

While this CNT and graphene-based structures continue to be of interest, the dominant material properties in the direction of growths of the sp^2 hybridized plane poses a limitation for applications requiring electrical or mechanical isotropy. Furthermore, while these highly organized structures can be beneficial in purely electrical experiments, the sp^2 hybridization has the side effect of making the surface so stable that they are often too inert for *in vivo* applications that rely on electrochemical oxidation and/or reduction at the surface of the carbon; the oxygen containing functional groups in defects in the lattice of the carbon allow carbon require the ability to give up or uptake electrons (Hirst, 1998) . Thus, despite the elegance of sensors generated from CNTs and graphene, glassy carbon, a semi-amorphous, semi-crystalline carbon, has remained the 'gold standard' for electrochemistry.

Glassy carbon consists of interlaced ribbons of sp^2 hybridized carbon atoms connected through sp^3 bonds (Ferrari, 2000; Hirabayashi, 2013; Jenkins, 1971; Wang, 1990); at the end of each ribbon or in any discontinuity is the termination of the carbon lattice which most often ends in an oxygen containing functional group. These functional groups are randomly dispersed in glassy carbon even before electrochemical or chemical activation, making glassy carbon innately more suitable than the more ordered fullerene structures. Glassy carbon, typically synthesized through pyrolysis of a polymer precursor, when heated to high temperatures in an inert environment, form sp^2 graphitic planes in random orientations (Franklin, 1951). Earlier work in measurements to define the degree of sp^2 bonding showed that the number of sp^2 graphitic planes and their alignment with one another increases with increasing carbonization temperature (Franklin, 1951).

However, more recently, as microfabrication techniques have become more accessible, the introduction of microfabrication-based patterning using photosensitive polymer pre-cursors has given rise to the fabrication of glassy carbon structures through pyrolysis of photo-sensitive polymers. Through TEM (Transmission Electron Microscopy) and Raman spectroscopy, the ensuing patterned glassy carbon structure was shown to have both amorphous and crystalline properties that changed with increasing temperature in the same fashion as the polymer derived graphite (Ferrari, 2000; Hirabayashi, 2013; Sharma, 2012; Wang, 1990). The electrical properties of this pyrolytic carbon, commonly referred to as glassy carbon (GC) due to its isotropic low impedance, has led to its increasing use as electrode material (Sharma ,2012). Further, due its inertness and long-term corrosion resistance (Zachek, 2010), large electrochemical window, and its high charge injection capacity (Kassegne, 2015; Vomero, 2016) glassy carbon has demonstrated superior electrochemical sensing capabilities.

Table 2: Electrochemical Carbon Microelectrodes for Neurotransmitter Detection

Carbon Electrode	***Sensing Modality***	***In vivo/ In vitro***	***Reference***
Carbon Nano Fiber (CNF),	Ascorbic Acid/ DPV	*In vivo* (rat)	(Zhang, 2017)
Carbon Nanopipette Electrodes (CNPE)	Dopamine/ FSCV	*In vivo* (Fruit Fly)	(Rees, 2015)
Carbon Nanotube Yarn (CNTY)	Dopamine/ FSCV	In situ	(Schmidt 2013)
Glassy Carbon from pyrolyzed photoresist	Neurotransmitter (Various)/CV and FSCV	*In vitro*/ *in vivo* (mice)	(Zachek 2010),
Glassy Carbon from pyrolyzed photoresist	Serotonin/ FSCV	*In vitro*	(Hirabayashi, 2017)
Carbon Fiber MEA	Dopamine/ FSCV	In situ	(Koehne, 2011)
Carbon Fiber	Neurotransmitter (Dopamine, Norepinephrine, Serotonin)/ FSCV	*In vivo* (rats)	(Robinson, 2003)
Carbon Fiber	Dopamine/ FSCV	*In vivo* (non-human primate)	(Schwerdt, 2003)
Carbon Fiber	Adenosine/FSCV	*In vitro*	(Swamy 2007)
Carbon Fiber	Epinephrine/FSCV and chronoamperometry	*In vitro*	(Taleat, 2017)
Carbon Fiber with 'graphene blossoms'	Dopamine/ CV and DPV	*In vitro*	(Du, 2014)
Trimethyl Ammonium Bromide Functionalized Graphene Oxide and MWCNT on glassy carbon	Dopamine/ CV and DPV	*In vitro*	(Yang, 2014)

1.3 Coupled Electrophysiology and Neurotransmitter Detection

Monitoring the electrical signals produced by neurons in biological systems, electrophysiology, has been a common method of attempting to understand how the central nervous system (CNS) works. Methods used to investigate the trends from bundles of neurons, such as EEG (electro encephalography) that records electrical signals attenuated through the various layers of tissue that cover the brain and even the skull, or methods that investigate single cells like patch-clamp studies that use an aspiration pipette to record the ionic movement across individual cells, have been implemented in an attempt to understand our brain. While these electrical signals can give us insight through correlation, there are limits to this technology. This is because the electrical signal described as electrophysiology is not a pure electrical signal; it is one of electrochemical nature where the movement of charged ions or molecules induces electrical gradients that can be transduced into an electron signal and read out as a voltage. But how much information do we lose by just looking at charge rather than the chemical? This very question has prompted researchers to invest in the FSCV methods described. With both electrophysiological and electrochemical methods becoming standard in neuroscience studies, some investigators have begun to look at how the two modalities are related. Does the neurotransmitter signal give us more insight into the electrophysiological signal? Can the two be coupled? These questions inspired researchers such as Hu et. Al. and Patel et. Al. to look at how cell cultures respond to changes in concentrations in neurotransmitters and how this change affects the electrophysiological signal (Hu, 2015; Patel, 2013). Hu and colleges found that at higher concentration of 5-HT, more hippocampal nerve cells were inhibited causing a drop in the electrophysiological recording. Patel's group was able to establish a simultaneous change in

electrophysiological response and dopamine concentrations in response to a tetanic electrical stimulus (Hu, 2015). In an in-situ brain slice study, Suzuki et. Al. was able to simultaneous detect changes in concentrations of dopamine using a CNT based microelectrode array. Similar studies were done by Song *et al.* with dopamine in situ but with a platinum microelectrode array (Song, 2012). Some coupled detection has also been done *in vivo* (Roberts, 2017). Belle *et al.* used a 2-electrode system, FSCV and electrophysiological spike detection to determine the effects of drugs applied to medium spiny neurons *in vivo*. Dopamine concentration release and firing rate were successfully monitored to determine the effectiveness of the drug (Belle, 2013). Kirkpatrick *et al.* were able to correlate dopamine oxidation with firing of neuron when dopamine concentrations reached current levels large enough (30nA) for the neuron to generate an action potential; these experiments also showed that using patch clamp method to detect neural spiking and the fast scan cv did not influence one another and thus could be reliably use together (Kirkpatrick, 2016).

Table 3: Coupled Electrophysiology and Electrochemistry

Electrode Type	***Neurotransmitter***	***In situ/ In vivo***	***Electrophysiology***	***Electrochemistry***	***Reference***
Palatium MEA	Serotonin	Cells grown directly on MEA	Local field potential	FSCV	(Hu, 2015)
Gold MEA	Dopamine	Neuron grown across electrodes	Sharp electrode (not part of MAE) was used for intracellular voltage recording	Amperometry	(Patel, 2013)
CNT MEA	Dopamine	Brain Slice	Local field potentials	Amperometry	(Suzuki, 2013)
Platinum MAE	Dopamine	*In vitro*	Local Field potential	Voltammetry	(Song, 2012)
Carbon Fiber	Dopamine	*In vivo*	Local Field potential	FSCV	(Belle, 2013)
Carbon Fiber	Dopamine	*In vivo*	Patch Clamp	FSCV	(Kirkpatrick, 2016)

CHAPTER 2

Materials and Methods

2.1 Design of Multi-Modal Neural Probe Arrays

The following section covers the various designs of the platform used to characterize glassy carbon (GC) microelectrodes, the glassy carbon/polyimide interface, or the feasibility for using the technology for *in vivo* studies

2.1.1 Penetrating Probe Design

Surface microelectrodes can be placed on top of the neural tissue and be used to detect electrophysiological signal and/or stimulate neurons from the surface. However, these microelectrodes have a difficult time detecting electrical neural spikes or electrochemically detecting neurotransmitters. Thus, a vital consideration in the development an electrode capable of neurotransmitter detection, electrophysical signal detection, and stimulation, was how to design a probe capable of penetrating neural tissue. The first requirement was to make the probe small enough as to not cause too much tissue damage. While less than 10 μm (10 μm being about the size of a neural body), would cause less damage during the penetration process, reliable implants used *in vivo*, such as those penetrating probes design by NeuroNexus ®, are 50 microns in thickness. Thus, a design constraint of a maximum of 50 microns in width and thickness. However, to make a probe resistant to delamination, the width of each layer needed to be carefully considered. First, to maximize the bonding of the carbon with the polyimide layer, the width of carbon electrode needed to be smaller than the width of both the base and top insulation. Next the width of the trace was determined. Since the top layer of metal was platinum, and because platinum does not adhere well to polyimide without an adhesion layer like

titanium (Ohuchi, 1986), the trace was made as small as possible to maximize the contact between the top and base insulation. However, how small the trace could be made was limited by the smallest via that could be reliably opened in the polyimide base layer. Thus, since a 15 micron via was determined to be the smallest via that could be reliably fabricated in the SDSU Microfabrication facility, the design was made to have a trace 20 μm in width, allowing for full coverage of the via, and a base insulation of 40 microns in width. The probe design and dimensions are diagramed in Figure 2. In Figure 3, a probe is shown with the top insulation of 50 microns in width. This allows for 10 microns of polyimide to polyimide contact, and 10 microns to encapsulate all the layers with the final base insulation. If the top insulation was made thick enough, then the probe would be capable of penetrating neural tissue despite the small size of the probe. However, to decrease the width without changing fabrication parameters, a stiffener was added. This allows for the stiffener to contribute to the final thickness of 40 microns, as shown in the cross-section in Figure 3 (c), without contributing to the total thickness. In this case, the base and top insulation are thin enough to curl up thereby reducing the total width of the probe to 40 microns or less. The length of the stiffener was then also modified to the penetration depth necessary, in this case 1mm. This probe design became the basis for all designs of microelectrode arrays.

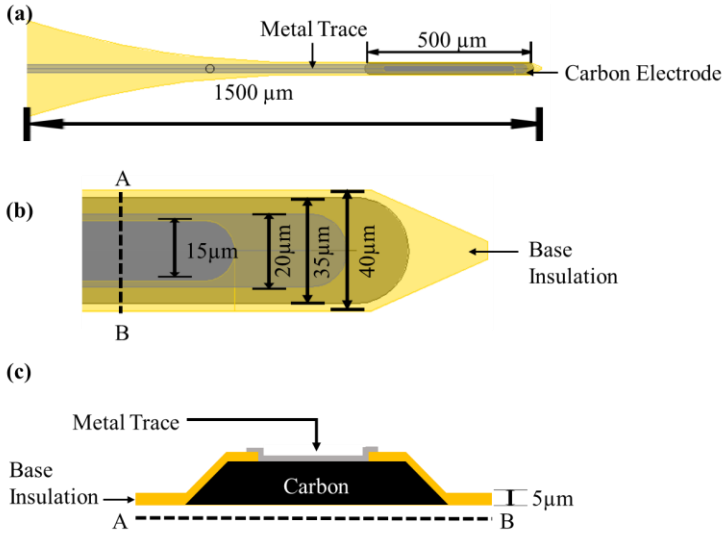

Figure 2: Probe dimension (carbon, trace, base insulation)

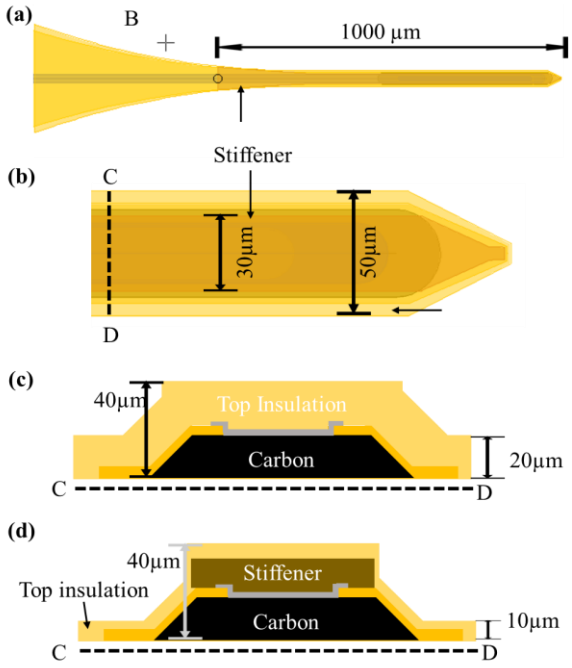

Figure 3: Probe Dimension (top insulation and stiffener)

2.1.2 Fully Implantable Neural Probe Array

While the probe design was kept constant, the body design was modified for the application. The first array “Penetrating Glassy carbon Electrode for Sensing and Stimulation” (PeGESaS) was designed with 12 probes, six on each side of the device head, and an additional large platinum electrode that could be used as a reference electrode. The PeGESaS design is shown in detail Figure 4. The benefit of this electrode design is that the probes can be bent to the side allowing the rest of the design to be fully implanted for long term *in vivo* studies.

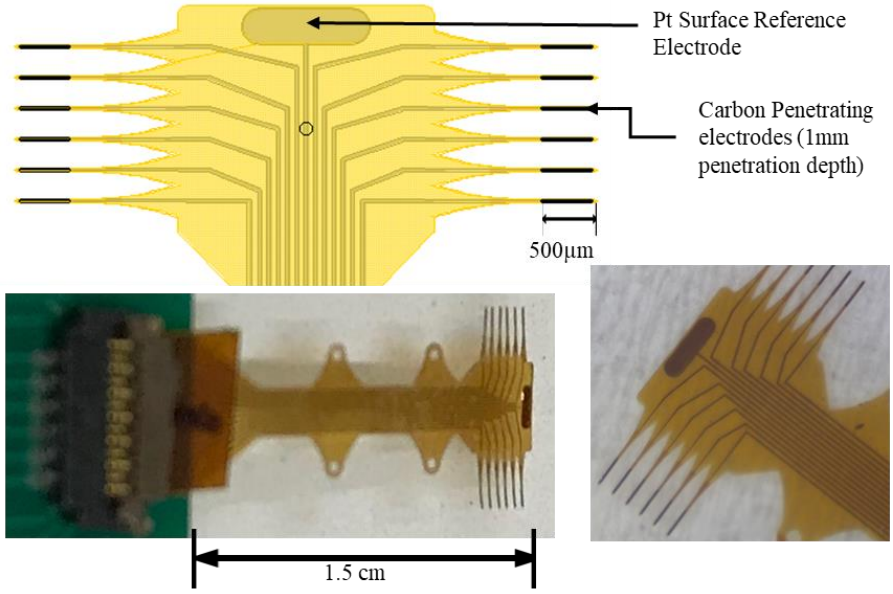

Figure 4: 12-Channel PeGESaS Design

While the initial PeGESaS device was successful, other designs were developed to test the feasibility of incorporation of surface microelectrodes onto the head of the probe. Figure 5 shows the layout of PeGESaS Lun, a modification of the original PeGESaS design with 8 penetrating microelectrodes, 2 platinum surface microelectrodes, and 2 glassy carbon

microelectrodes. PeGESaS Sol, shown in Figure 6, also has 8 penetrating microelectrodes with a 1mm penetrating depth and 4 glassy carbon microelectrodes.

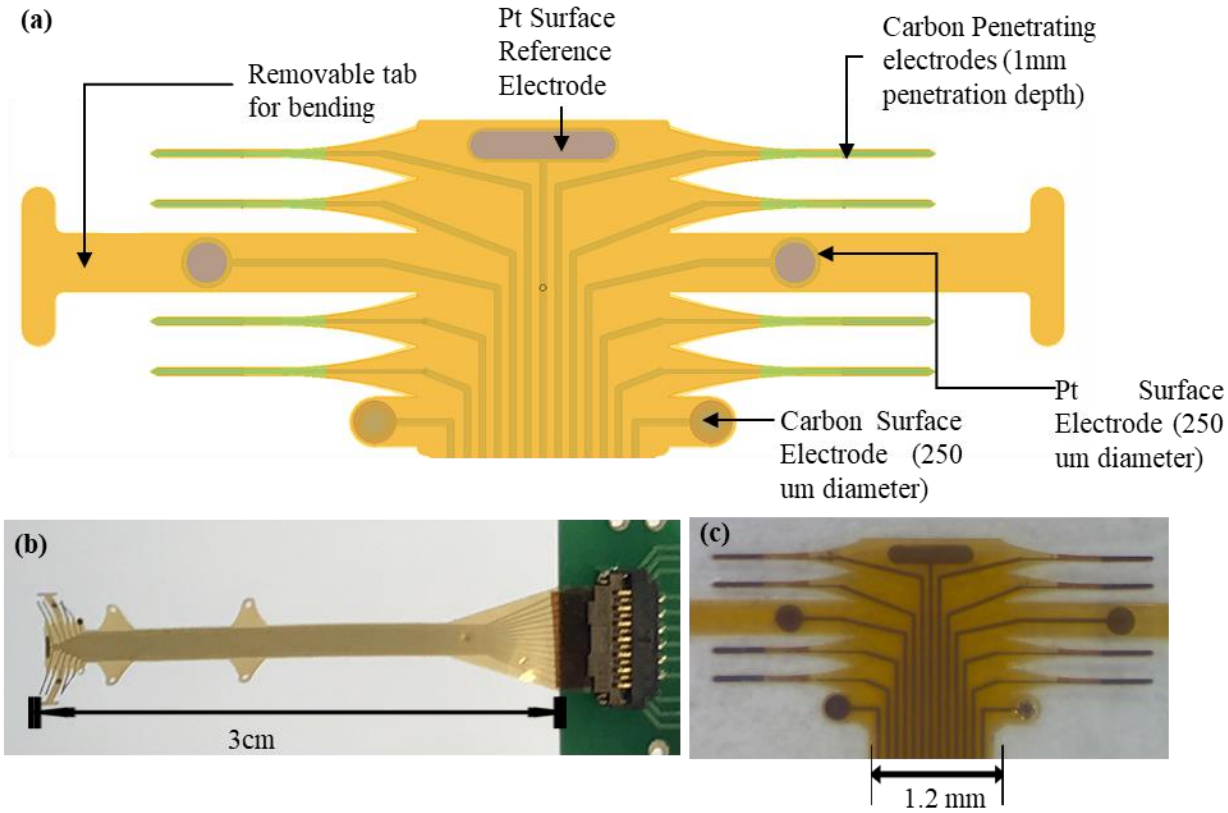

Figure 5: PeGESaS Lun Design

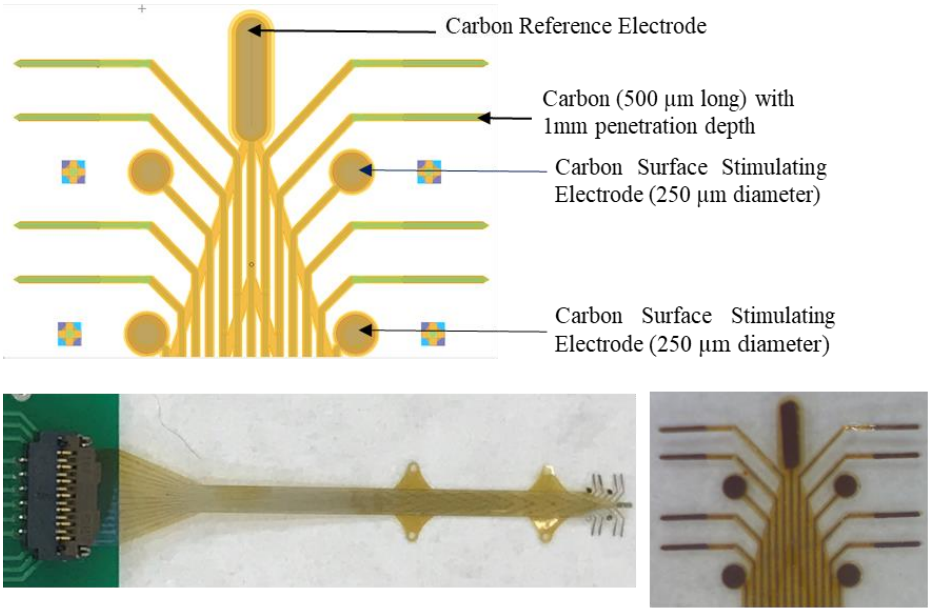

Figure 6:PeGESaS Sol

2.1.3 Design for Acute Implantation

While the 12 channel PeGESaS device was designed to allow for full implantation in either the spinal cord or the brain, a simpler design was fabricated to demonstrate that the probes would be suitable for an acute implant. In this PeGESaS Acute design, shown in Figure 7, the need for bending is eliminated, simplifying the fabrication process. This could be penetrated directly into the tissue and then held in place by an external bar or bone of the animal, making the probe suitable for most cortical applications and any acute application where the animal can remain anesthetized.

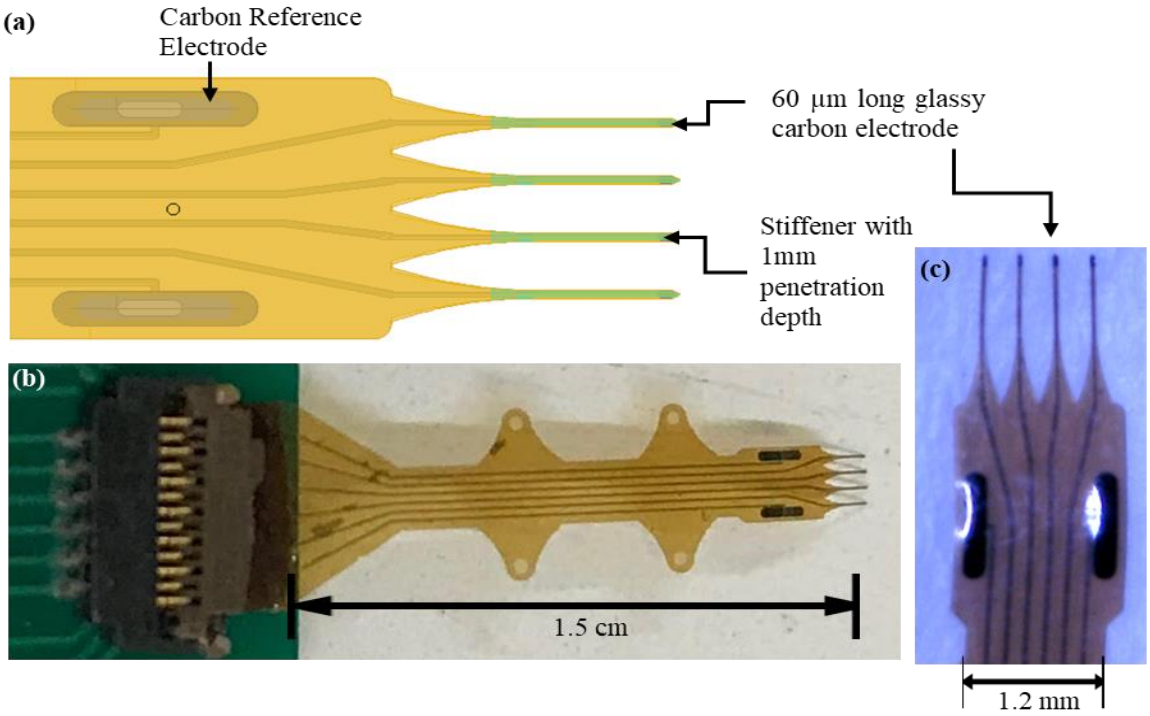

Figure 7: PeGESaS Acute Design

Table 4: Summary of Neural Probe Array Designs

Design Name	***Type of Electrodes***	***Reference Electrode***
PeGESaS	Penetrating (0.15 mm^2)	Platinum
PeGESaS Lun	Penetrating (0.15 mm^2) and Surface (0.05 mm^2)	Platinum
PeGESaS Sol	Penetrating (0.15 mm^2) and Surface (0.05 mm^2)	Carbon
PeGESaS Acute	Penetrating (180 μm^2)	Carbon

2.2 Fabrication and Cleanroom Processes

2.2.1 Photolithography

Photolithography is the process of building structures using light to polymerize or depolymerize polymers. The first step of the process involves starting off with a rigid substrate, the most common one being a silicon wafer. This wafer is then cleaned using acids, solvents, and/or oxygen plasma etching to remove organic and inorganic residues on the surface. The next step involves deposition of a polymer onto the substrate, then using a spin coater to generate a uniform film with a desired thickness based on the velocity of the spin and the viscosity of the polymer. The polymer is then heated to remove any solvents in a process referred to pre-bake or soft-bake. After soft-bake, a mask design is applied to the surface of the polymer and UV light is exposed to desired section of the polymer. The UV light causes the crosslinking or breakdown of the polymer. In the case of crosslinking polymer, a post-bake follows UV exposure. Non-crosslinked polymer is then chemically removed using a developer specific to the polymer.

In this research the standard photolithography process, shown in Figure 8, was used to generate various structures in multiple layers. The details of each process are descried in the following sections.

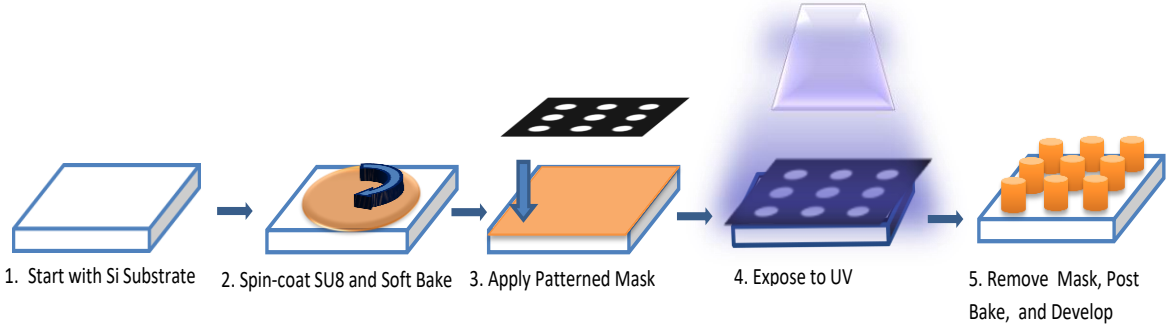

Figure 8: General Photolithography Process

2.2.2 Pyrolysis

Pyrolysis is process of carbonizing polymers by heating polymer up to high temperatures in an inert environment. In this research, pyrolysis was done in a nitrogen (N_2) environment in an MTI tube furnace (Figure 9). SU-8 (*Microchem, Boston, MA*), a photosensitive epoxy, was used as the polymer precursor, and prepared on a silicon substrate as described in section 2.1.1.

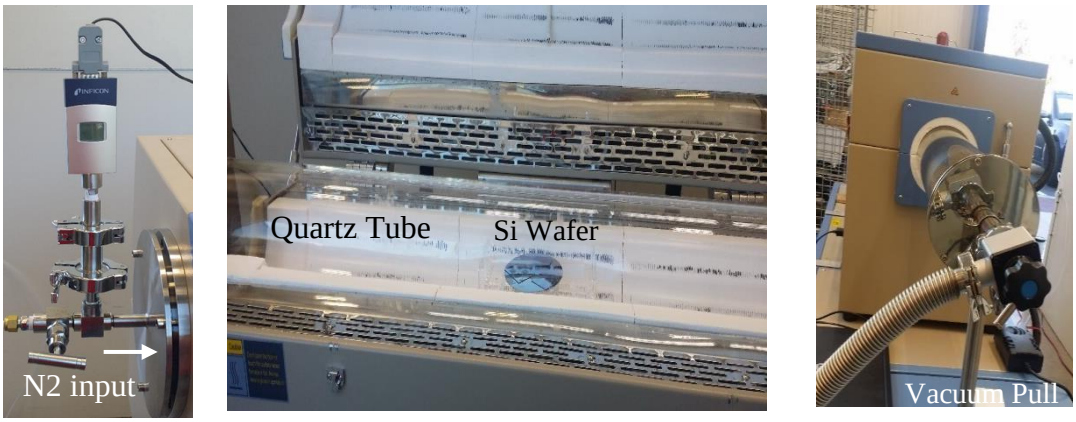

Figure 9: MTI Furnace used for pyrolysis

The standard protocol for heating, shown in Figure 10, involved a slow ramp-up to a max temperature of 1000ºC and a subsequent hold for one hour at the maximum temperature before cooling. The standard flow rate for N_2 was 15 sccm while the chamber was under vacuum. Deviations from the standard were tested to determine optimal conditions for pyrolysis.

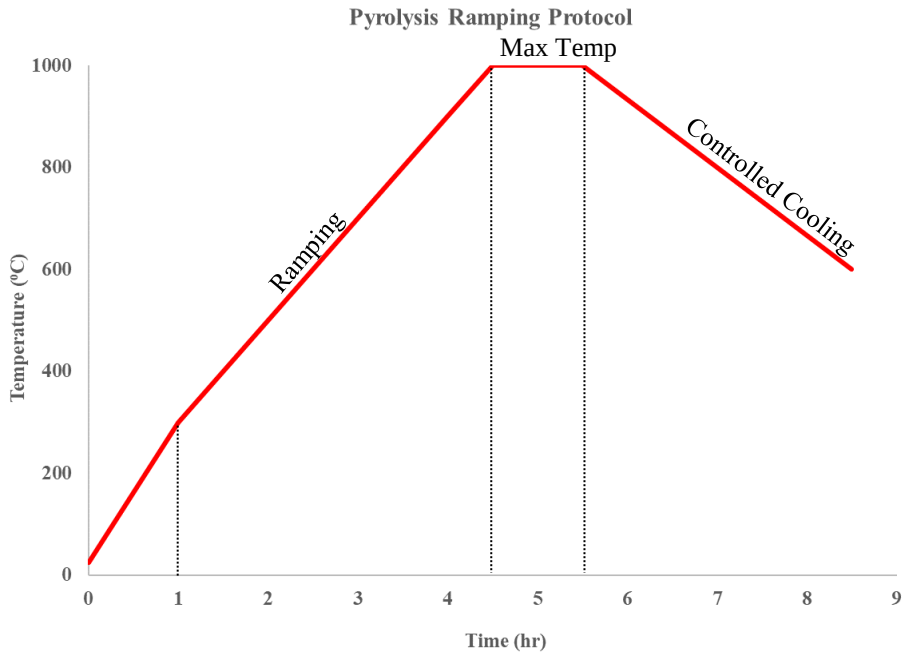

Figure 10: Pyrolysis heating protocol

2.2.3 Interface Test Devices

A 50% dilution of SU-8 (10) (*MicroChem*) in acetone was spun at 4000 rpm onto a silicon wafer and patterned as shown in Figure 11. These samples were then pyrolyzed at 1000ºC to generate glassy carbon (GC) microstructures thin enough (< 2 um) that the interface between the GC and silicon could be probed by FTIR-ATR spectroscopy. Each sample was then plasma etched for 30 or 120 seconds, at a pressure of 500, 600, or 750 mTorr. Some control samples

were not plasma etched. After plasma etching, HD4100 photosensitive polyimide (*Hitachi Chemical, DuPont, MicroSystems)* was applied immediately to the surface of the sample and spin coated on at 3000 rpm. Pre-baking was done for 1 min at 90°C, and then 1 min at 120°C. Ultra-violet light exposure at 350 mJ/cm^2 was used to crosslink the polyimide, and then each sample was post-baked at 80°C for 1 minute. After post-baking, each sample was cured at 1 of 4 temperatures: 150°C, 200°C, 300°C, or 375°C. The samples were then lifted off the silicon substrate using buffered hydrofluoric acid. A total of 29 samples were prepared, using all possible combinations of plasma etching time, plasma etching pressure, and curing temperature.

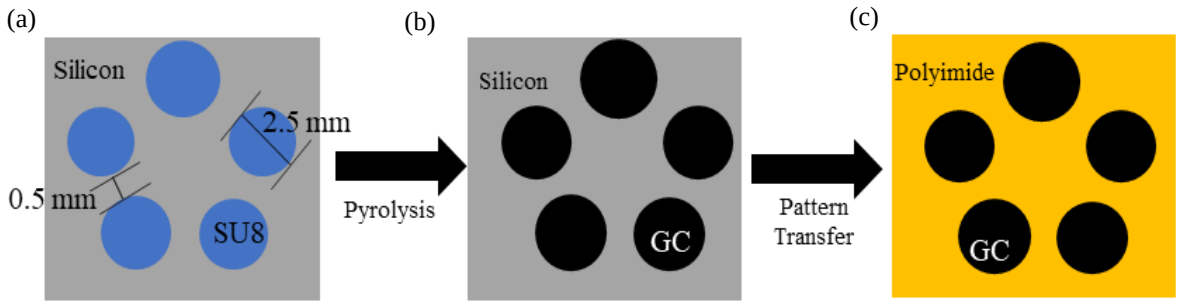

Figure 11: Sample Generation and Design: 2.5 mm diameter electrodes arranged in a circular pattern with equal spacing on a 1 cm by 1cm (a) before pyrolysis on silicon (b) after pyrolysis on silicon (c) after lift-off and pattern transfer to polyimide

2.2.4 Glassy Carbon and Polyimide Devices

Since the particular glassy carbon used in this research must be generated on a silicon substrate that can withstand the pyrolysis temperature of 1000°C, a new method needed to be developed in order to use this material as an electrode in implantable devices that require flexibly. The new method involves two key steps: (1) transfer of the glassy carbon onto a

flexible polymeric substrate, and (2) the use of metal traces to conduct the signal to an outer bump pad for electronic access. All GC-MEMS devices were fabricated using multiple layers of the standard method described in section 2.1.1. Figure 12 below outlines the steps for each part of the fabrication.

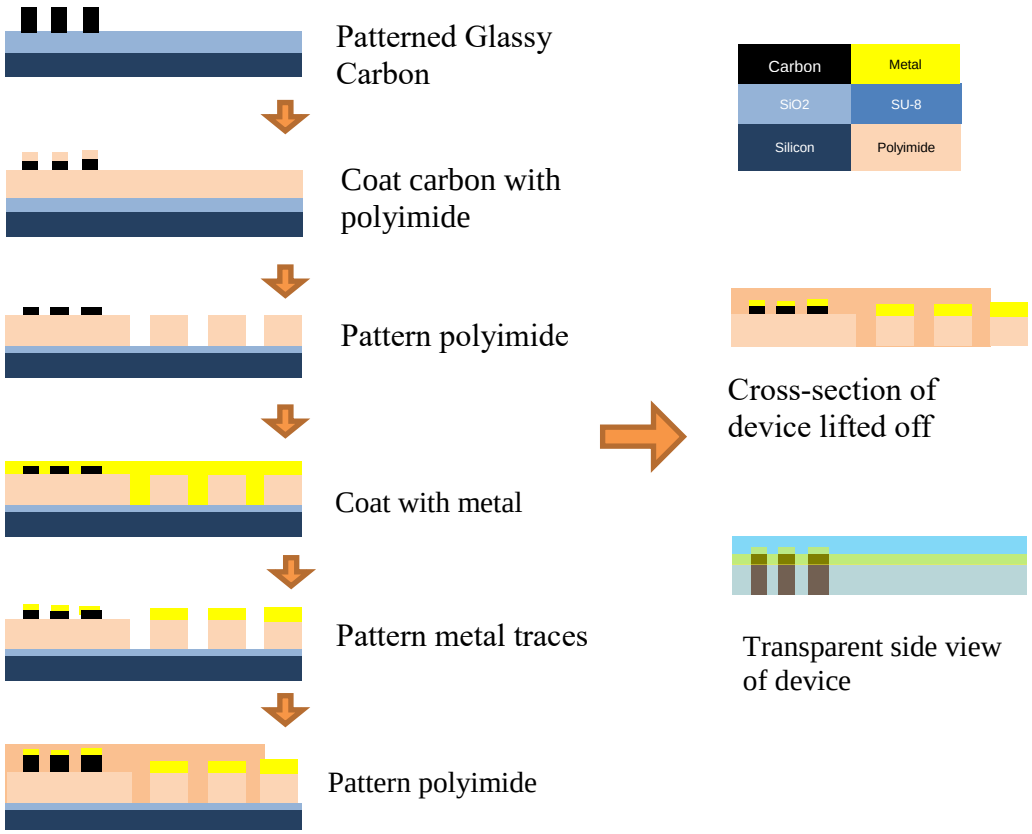

Figure 12: Pattern Transfer protocol used to place glassy carbon structures on a flexible polyimide substrate

2.2.5 Penetrating Electrode

While surface microelectrodes can be made easily with the process described in section 2.1.5, making a device that can penetrate neural tissue takes a few more steps. One consideration

is how to make the device such that it stays rigid enough to pierce neural tissue, but flexible enough to be fully implanted *in vivo*. To do this, each penetrating probe contains an extra layer of polyimide, thickened to allow for penetration into neural tissue.

The devices were each fabricated using the protocol outlined in section 2.1.5 but with an additional polyimide layer added to the top to thicken the probe and allow for penetration. Table 5 below outlines the polymers and parameters used in each layer.

Table 5: Photolithography Protocols used for each layer

Polymer	***Layer***	***Spin (rpm)***	***Soft Bake***	***Exposure (mJ/cm²)***	***Post Bake***	***Hard Bake/Cure****
SU-8 (10)	Carbon	1000	3 min 65ºC 7 min 95 ºC	375	1 min 65 ºC 3 min 95 ºC	30 min, 150ºC
SU-8 (100)	Carbon	3750	10 min 65 ºC 25 min 95 ºC	400	3 min 65 ºC 7 min 95 ºC	30 min, 150ºC
Durimide 7520	Stiffener	1800	3 min 85 ºC 7 min 100 ºC	150	30 min Ambient	Cure: 350ºC
HD4100	Insulation /Base	1000-3000	3 min 90 ºC 3-6 min 110 ºC	375	11 min 65 ºC	Cure: 375 ºC
HD4100	Stiffener	400	3 min 90 ºC 15 min 110 ºC	400	15 min 75 ºC	Cure: 375 ºC
Futurrex	Trace	400	3 min 150 ºC	360	7 min 100 ºC	

* Curing was done in a laminar flow tube furnace under nitrogen at a flow of 25 sccm. Polyimides were cured by first ramping to 200ºC holding at 200ºC for 1 hour, ramping to max temperature, and holding at max temperature for 1 hour.

2.3 Electrochemical Methods

Electrochemical testing allows for the characterization of an analyte or of a working electrode. In this research, the electrochemical testing was used to characterize the glassy carbon working electrode or its response to specific analytes, such as 5-HT. In the three probe set-ups, a large platinum mesh electrode (*Ametek, San Diego, CA*) was used as the counter electrode, a Ag/AgCl reference electrode (*Ametek, San Diego, CA*) was used as the reference, and the glassy carbon (GC) microelectrode being tested was used as the working electrode. Three probe set-ups were done in 100mL of phosphate buffer solution (0.01 M PBS) on either Solartron Analytical (*Solarton Analytical, Ametek, San Diego, CA*). or Gamry.

2.3.1 Electrochemical Impedance Spectroscopy

Electrochemical Impedance Spectroscopy (EIS) was done with a 3-probe set-up. Frequency sweeps were done at 10 mV (galvanostatic) amplitude and swept from 1 MHz to 1Hz.

2.3.2 Cyclic Voltammetry

Cyclic voltammetry (CV) had a variety of applications in this research, including conditioning, electrochemical window testing, nafion deposition, and serotonin (5-Hydroxytryptamine or 5-HT) detection. CVs run at scan rates below 10 V/s (not fast scan) were always run on either the Gamry or Solarton potentiostat with a 3-probe set-up in a 100 mL beaker.

After fabrication, an electrode may have some residue or dirt on the surface. To clean the surface, cyclic voltammetry was run using a conditioning protocol. In this protocol the electrode

was scanned from -0.6 to 1.2 V at a rate of 300 mV/s for at least 60 cycles or until the electrode was stable enough to produce the same CV for subsequent runs.

Electrochemical windows were run on microelectrodes to test if a change in fabrication parameters altered the stability of the electrode. Electrochemical window was run at 100mV/s from -3 V to 2V for 2 or 3 cycles.

Nafion deposition was done with the standard 3 probe set-up with an additional 1 mL of 5% Nafion solution (*Fuel Cell Earth, Woburn, MA*) added to the PBS. On a single device, all glassy carbon microelectrodes were connected to one another. First Nafion was deposited by holding the glassy carbon electrodes at 1.1V relative to the reference. Then the microelectrodes were cycled from -0.6 to1.2V at least 100 times until stabilized.

2.3.3 Fast Scan Cyclic Voltammetry

Fast scan cyclic voltammetry is a common method used to detect the presence of analytes *in vivo*. Scan rates in FSCV are usually in the range of 100 V/s-2 kV/s. This fast scan rate has the advantage of giving better temporal resolution needed in *in vivo* experiments, especially when looking for the release of a neurotransmitter in response to an action potential which happens on the order of 1 ms.

The Solarton potentiostat was used as a proof of concept: given a fast scan rate, glassy carbon can still detect small volumes of a neurotransmitter, in this case serotonin (5-HT). In these experiments, the waveform was continuously scanned from 0V to 1V to -0.4V to 0 for 100 cycles at 1 kHz and 1.5 kHz at concentrations ranging from 25 nM-10 µM of 5-HT (5-Hydroxt

tryptamine hydro chloride) (*Sigma Aldrich, St. Louis, MO*). The voltammogram obtained from each molarity was then subtracted from a 0M scan using Matlab (*Mathworks*).

The WaveNeuro (*Pine Research, Durham, NC*) system is a potentiostat built for use *in vivo*. This system uses a 2-probe set-up. For these experiments a silver wire coated in silver chloride was used as both the counter and reference electrode. The glassy carbon electrode was used as a working electrode. For each experiment, the best range, waveform, and scan rate was chosen based on the current response of the electrode. Scan rates ranged from 400V/s- 1kV/s. Waveforms were either chosen as a triangular waveform that ran from -0.6V-1.2V or an N-shape waveform ran from 0.2V to -0.6 V to 1.2 V and back to 0.2 V. A high current response could cause clipping of the signal, in which case the scan rate was lowered to as low as 400V/s and waveform rage was decreed to 0.2V to -0.4V to 1V. For each calibration, 5-HT was added at various molarities ranging from 10 nM-100 nM. after at least 10 seconds of background had been collected. HDCV software (*University of North Carolina, Department of Chemistry*) was used for background subtraction and analysis.

2.4 Fourier Transform Infrared Spectroscopy

FTIR-ATR spectroscopy was done using a Nicolet iS50 FT-IR Spectrometer equipped with a Smart iTR diamond ATR cell (*Thermo Scientific, Court Vernon Hills, IL*). For each sample, a spectrum of the glassy carbon (GC) microelectrodes on silicon was taken before the GC electrodes were plasma etched and transferred to the polyimide. To achieve this, three of the five GC electrodes (the three that were most intact per sample) were washed with methanol, dried, and placed on the diamond cell. 128 spectral scans were recorded, which was sufficient to

achieve good resolution within a reasonable timeframe. The scans for each electrode were then complied, and all 102 discreet GC spectra averaged, resulting in a single original GC spectrum. Once the GC electrodes were transferred to the polyimide, the same three electrodes originally scanned for each sample were again washed with methanol, dried, and placed on the diamond for the optimal 128 scans. The 3 spectra per sample were averaged to produce the interface spectrum for that parameter.

Polyimide spectra were taken at the edge and at the center of each assembled sample, and again 128 spectral scans were performed and complied. The spectra of each sample cured at the same temperature were then averaged.

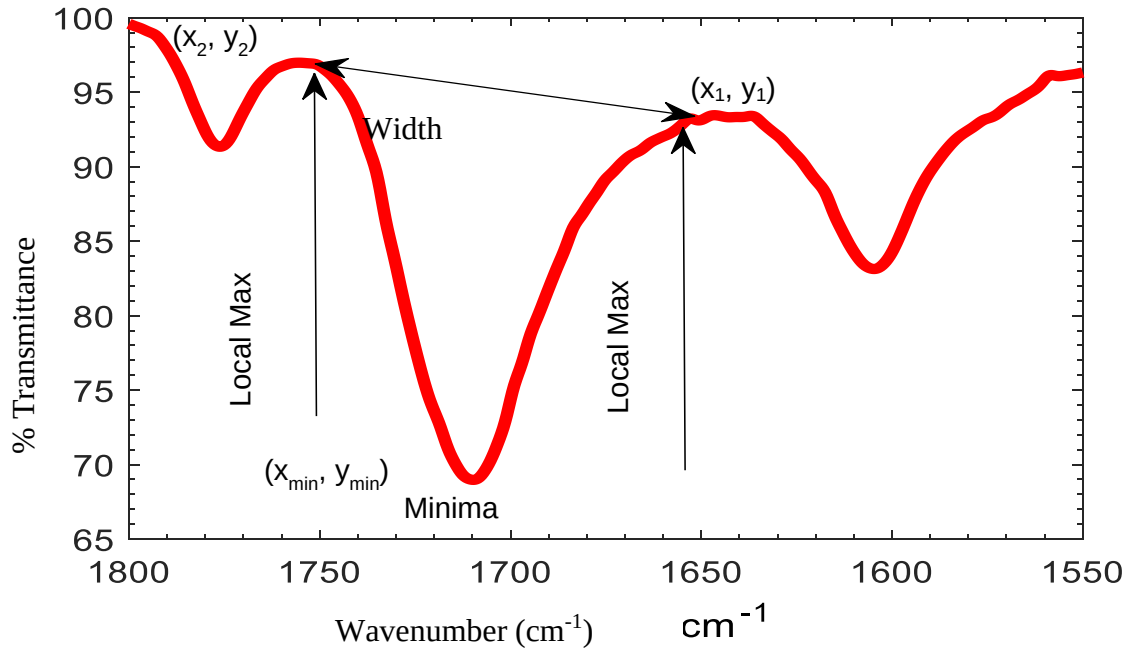

Figure 13: Example of peak measurements for FTIR spectra. For each peak, a region for the peak of interest was designated. Within that area, the local minima were found and designated at (xmin, ymin). xmin was referred at the minima for the peak. To find the width and midpoint, the local maxima in each direction encountered outside of the minima were defined and designated as (x1, y1) and (x2, y2). The distance between these coordinates was designated as the width. For asymmetric peaks or broad peaks wher0e xmin and ymin were difficult to determine, the midpoint was calculated as the average between x1 and x2.

Once FTIR spectra were obtained, Matlab was used for analysis of the vibrational peaks in the raw data. The scatter plots generated display error bars corresponding to twice the standard deviation (2σ) in order to reflect a 95% confidence. In order to pick up small changes in the peaks, data was collected from the baseline corrected FTIR signal, an example of which is shown in Figure 13.

Distinguishing small changes in bond conformation can be challenging in FTIR (Colthup, 1950). Therefore, a robust and statistically relevant approach is required to analyze the data and confirm the presence of bonds and statistically significant changes in the peak and, therefore, the

bond) with 95% confidence. For this analysis, the width, minima, and midpoint of the peaks of interest were chosen as metrics to characterize the bonds present for each parameter. For this study, the three metrics, width, minima, and midpoint, were defined as follows:

1. The local maxima, or zero slope locations (defined by 3 consecutive points of the same value), within the region of interest were taken to be the outer limits of the peak ((x_1, y_1) and (x_2, y_2) in Figure 13). The distance between these points was defined as the width. This metric is commonly used is FTIR analysis to detect a change in the chemical bonding either at full-width or full-width-half-the-maximum (Silverstein, 2007). In this study, the full-width was used in place of the full-width-half-the-maximum to ensure the capture of very slight changes in width due to overlapping of peaks that may not show up at half the maximum (Colthup, 1950). The width allows for insight into the range of vibrational modes for a given bond type; the wider the peak, the more types of vibrational modes, and thus the less consistent the conformation (Colthup, 1950; Silverstein, 2007).

2. Minima were defined as the *wavenumber* at which the peaks of interest reached their minimum transmittance (shown in Figure 13 as (x_{min})). While the y values are often used to determine concentration, variability in the fabrication process and thus the amount of sample present make y_{min} an unreliable metric. However, x_{min}, sometimes referred to as the frequency band, is not dependent on the amount of sample, and is, therefore, used to determine the most likely bond (the dominate vibrational mode) and its degree of stability (Colthup, 1950; Silverstein, 2007). Downshift in minima (i.e. a slight shift in the location on the x axis from

where it is expected) indicates a dominant lower frequency vibration of the bond, implying better stability and thus stronger bonding (Colthup, 1950)

3. Midpoint is defined as the average of x_1 and x_2. While this metric is not commonly used in FTIR, we submit that it is especially useful when width and minima alone are not enough to describe the peak. For symmetric peaks, midpoint and minima will have the same wavenumber. For asymmetric peaks, however, the wavenumber of the midpoint differs from that of the minima, implying a significant change in bond organization has occurred, but not enough to shift the local minima all together.

Each of the above three metrices describes distinct characteristics of the material being imaged. Thus, if a statistically significant difference between GC, polyimide, and the interface is observed in any one of the metrics, it is reasonable to conclude a unique bond has formed at the interface.

Section 2.4, in full, is a reprint of some of the material as it appears in *Journal of the Electrochemical Society:* Hirabayashi, Mieko, Nha Uyen Huynh, Shane Witsell, Alberto Perez, Laura Sandoval, Naoya Yamada, and Sam Kassegne, 164, no. 5 (2017): B3113-B3121. The dissertation author was the primary investigator and author of this paper.

2.5 Scanning Electron Microscopy

Scanning Electron Microscopy (SEM) was done using an FEI Quanta 450 FEG Scanning Electron Microscope (*ThermoFisher Scientific, Waltham, MA*). 15-20 kV accelerating voltage was used for images of carbon and polyimide.

2.6 Simulation

Molecular simulations were done using Spartan v7 molecular modeling software. Bond angles were determined using energy minimization. Electrostatic potentials were generated using the emended density functional theory (DFT) module.

CHAPTER 3

Investigation of Glassy Carbon/ Polyimide Interface

The following chapter is an investigation of the polyimide and glassy carbon (GC) interface that is generated as a result of using microfabrication methods used to generated glassy carbon structures on a flexible polyimide substrate, an example of which is shown in Figure 14 (a). Understanding how this interface, diagramed in Figure 14 (b) and (c), is formed is essential to developing robust microelectrode arrays suitable for *in vivo* applications. Investigation was carried out by first developing test structures as described in section 2.2.3 and then analyzing the samples using Fourier Transform Infrared Spectroscopy, as described in section 2.3.

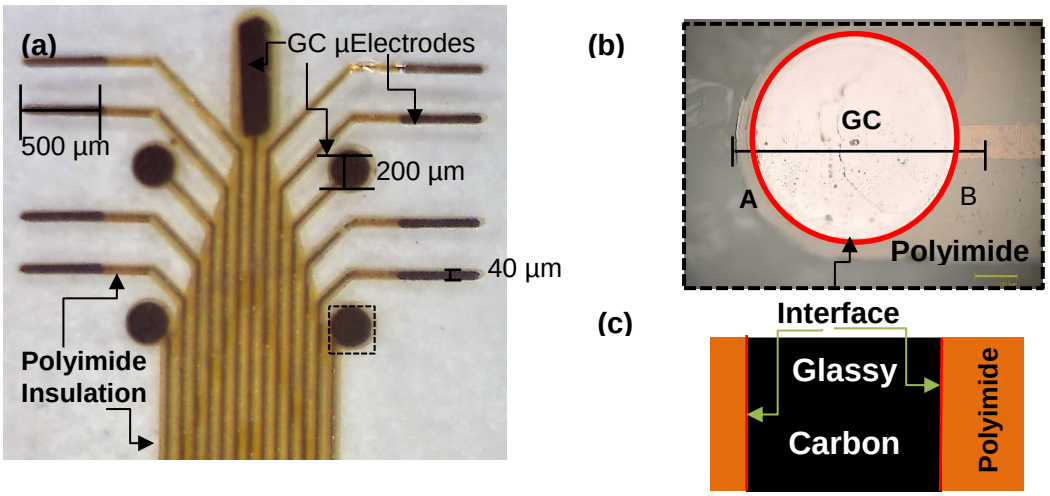

Figure 14: (a) MEMS fabricated glassy carbon/polyimide device (b) zoom of one of the circular electrodes (c) vertical cross section A-B

In the following sections, both the complete FTIR spectrum and the microstructures visualized with SEM are reviewed. In the FTIR spectra (shown in Figure 15), the boxed areas indicate the areas of interest: hydroxyl peaks, carbonyl peaks, and ether or anhydride peaks. Hydroxyl peaks and carbonyl peaks were analyzed to determine the presence of hydroxyls,

carbonyls, or carboxylic acids. The presence of hydroxyls or carboxylic acid dimers would imply participation in hydrogen bonding at the interface. Additionally, carbonyl and ether/anhydride peaks were used to determine the presence of anhydride bonds at the interface. Table 6 summarizes the peaks of interest and the corresponding spectrums investigated. Figures 16 through 19 show the average interface spectrum, polyimide spectrum, GC spectrum, and the interface spectrum of the control (no plasma etching) cured at 375^{o}C. Arrows on plotted spectra indicate measured minima in sharp peaks; in broad peaks, arrows indicate zero slope points used to calculate width and midpoint.

Table 6: Summary of types of peaks of interest, bonding group, and algorithm for determination of their presence. Ambient energy corresponds to pre- and post-baking treatments and UV exposure during lithography

Peaks of Interest	**Spectrum**	**Bonding Group**	**Enabling Condition**	**Metric Used**
Hydroxyl	GC Polyimide Interface Control Interface	Carboxylic Acids	Ambient energy	Width
Carbonyl	GC Polyimide Interface Control Interface	Carboxylic Acids Anhydride	Ambient energy	Not Significant Difference between samples
Ether	GC Polyimide Interface Control Interface	Cyclic Anhydride	Ambient energy	Minima, Width
Ether	GC Polyimide Interface	Non-Cyclic Anhydride	Annealing > 200^{o}C & O_2 plasma etching	Midpoint, Width

In Figure 15, the first panel showing the polyimide spectra demonstrates that the polyimide contains an amine (peak at 3300 cm^{-1} that decrease in amplitude with increased curing temperature and the C—N peak at 1610 cm^{-1}), carboxylic acids (1777 cm^{-1} and 1710 cm^{-1}), and

ethers (1070 cm^{-1} and 1240 cm^{-1}) (Colthup, 1950; Li, 1998 ; Silverstein, 2007,). The presence of an aromatic backbone is suggested by the characteristic tetra-substituted benzene peaks at 1970 cm^{-1}, 1650 cm^{-1} (overtones), and 800 cm^{-1} (Colthup, 1950). These peaks are consistent with those found in pyromellitic dianhydride (PMDA)-oxydianiline (ODA), a common form of photosensitive polyimide (Li, 1998). Thus, throughout the rest of this study, we assume the PMDA-ODA configuration of polyimide.

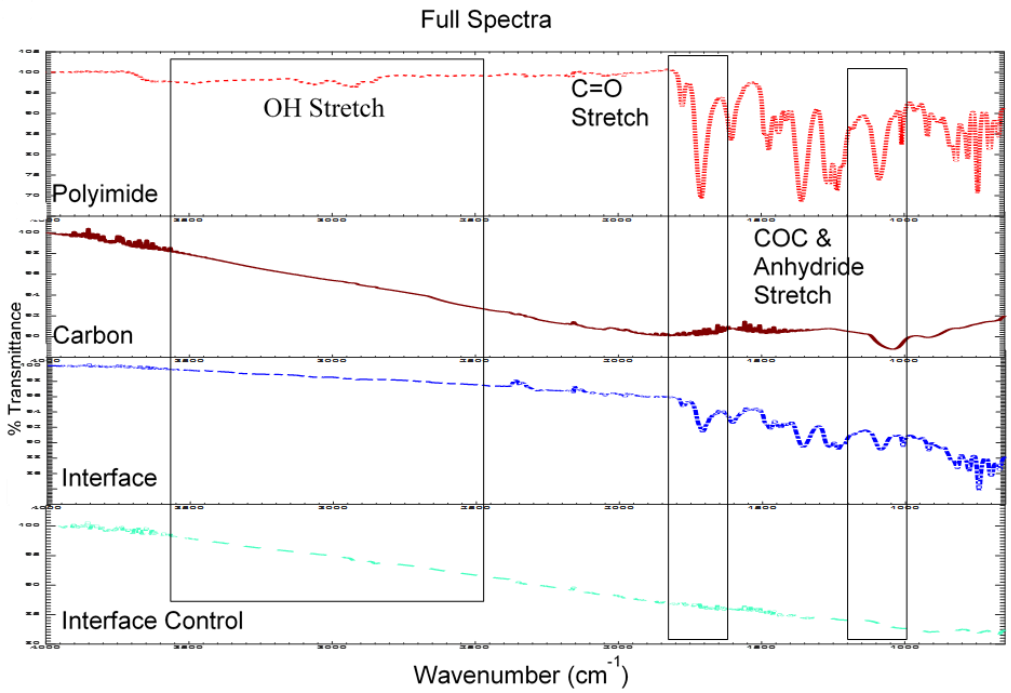

Figure 15: Full Spectra Average of all glassy carbon on silicon spectra before plasma etching and pattern transfer (GC), Average of all polyimide spectra taken (cured a at 375ºC) (Polyimide 375ºC), Average of all interface spectra with polyimide cured at 375 ºC and plasma etched (Interface 375ºC) and Average of all non-plasma etched interface spectra cured at 375 (Control Interface 375ºC)

Figure 15 also outlines the functional groups that are likely to participate in bonding: hydroxyl, carbonyl, and ether groups. The presence of strong carbonyl peaks in the plasma

etched interface, as shown in Figure 16, that are not present in the control interface samples suggests that plasma etching increases the number of carbonyls on the surface. In Figure 17, three broad hydroxyl peaks are shown. While these peaks are broader than the traditional hydroxyl peaks, the broadness can be explained by the high level of conjugation in the glassy carbon structure. From Figure 17, it can be seen that hydroxyl peaks are only more prominent in the plasma etched interface spectrum, indicating that hydroxyl groups are likely generated by plasma etching. In Figure 18, a peak consistent with that of ethers part of a non-cyclic anhydride is shown. Because this peak was not detectable in the GC samples nor in the non-plasma etched interface samples (but was clearly present in both the plasma etched interface samples and the polyimide), we argue that anhydrides are likely generated as a result of both plasma etching and polyimide curing. Figure 19 shows a peak that could be indicative of a cyclic anhydride or of ethers that are not part of an anhydride. The peak can be seen in the interface controls but is more prominent in the plasma etched interface. This suggests that the application of the polyimide or the fabrication process itself aided in the development of cyclic anhydrides. While many peaks shown in the polyimide are also seen in the interface, there are small differences between the two that distinguish one from the other. However, without statistical analysis, the significance of the differences seen in Figures 16 through 19 are difficult to determine. Thus, the averages and standard deviations of each peak's characterizing metrics were calculated, as described in Section 2.3, and plotted in scatter plots.

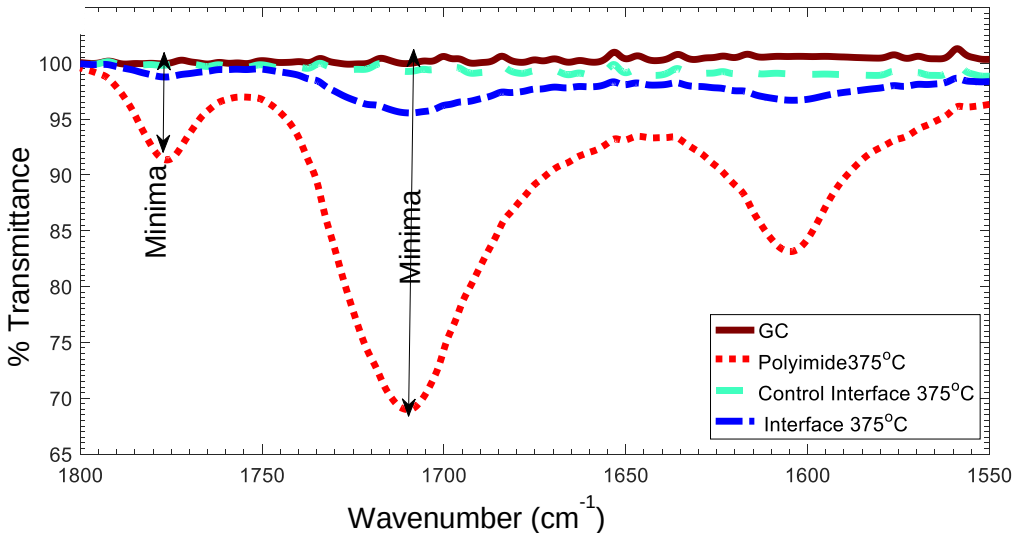

Figure 16: Results show the interface control looks much like the bare glassy carbon spectra. However, after plasma etching the carbonyl peaks look much stronger overall, indicating an increase in carbonyl groups as a result of plasma etching.

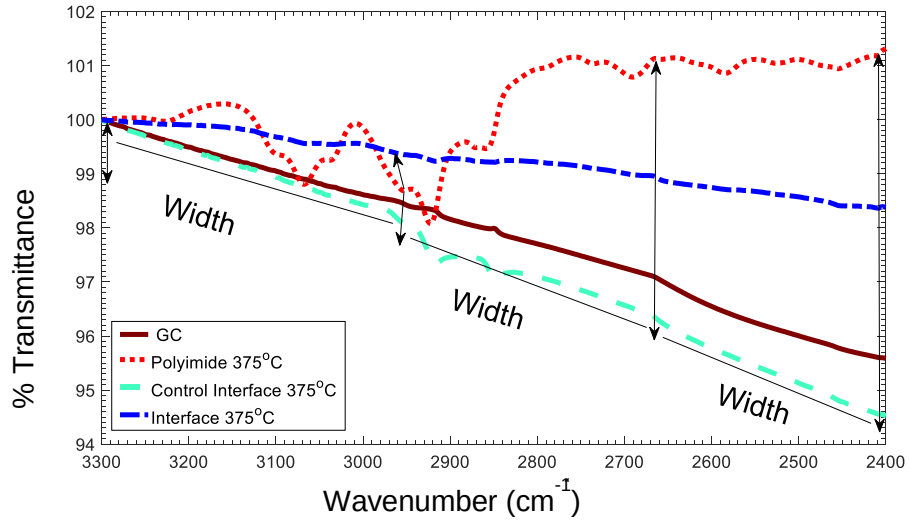

Figure 17: Hydroxyl Peaks: Three distinct peaks can be seen here in the interface and bare glassy carbon. Arrows show the 'Zero slope' areas used to define the width of the broad hydroxyl peaks. Lower frequency (wavenumber) hydroxyl peaks can be representative of carboxylic acids and/or carboxylic acid dimers. The plasma etched interface has more defined peaks than the bare GC or the interface, indicating plasma etching generates more hydroxyl groups, and possibly carboxylic acids, on the surface.

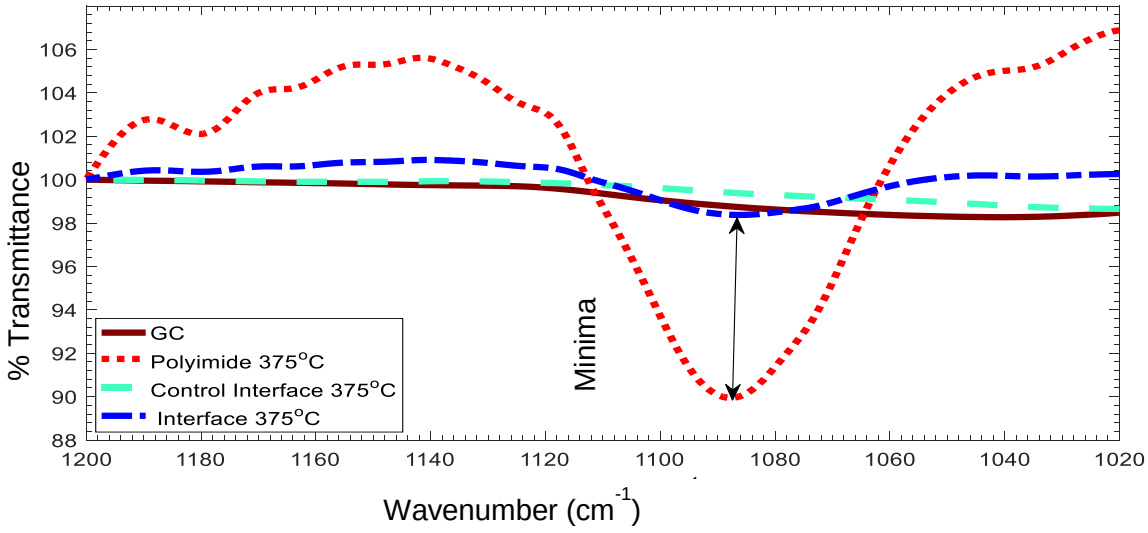

Figure 18: Non-Cyclic Anhydride Peaks: Anhydride existence at the interface is likely a result of plasma etching, since this peak is not seen in either the glassy carbon or the non-plasma etched interface.

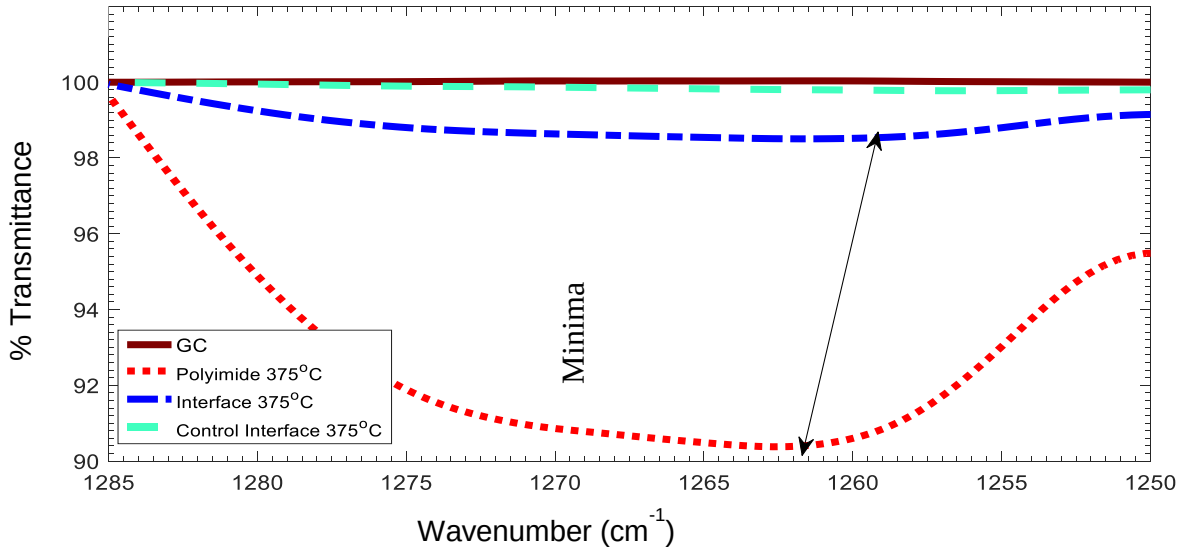

Figure 19: Cyclic Anhydride Peak: The change between the plasma etched and non-plasma etched interface suggests that cyclic anhydrides were formed from functional groups generated by plasma etching.

3.1 Effects of Oxygen Plasma Etching

Oxygen plasma etching is known to induce acyl groups onto graphitic surfaces through radical chemistry (Hirabayashi, 2013). Among these are carboxylic acids, hydroxyls, esters, or even epoxides, which can interact with functional groups intrinsic to many polyimide monomers. It is hypothesized that one possible mechanism for polyimide bonding to GC is through the interaction between carboxylic acids on the polyimide and on GC, which can form covalent anhydride linkages. Thus, plasma etching GC and then transferring it onto polyimide is likely to form these strong covalent bonds. The proposed mechanism for polyimide-GC bonding can be

seen in Figure 20. Figure 20 (a) shows a graphitic island (black -C) with a carboxylic acid functional group. If a polyimide precursor (green-C) were to come into close contact with the carboxylic acid (red-C), hydrogen bonding through carboxylic acid dimers could form at the interface as shown in Figure 20 (b). With enough energy input, the interaction between the carboxylic acids would allow the formation of anhydride bonds at the surface (red in Figure 20 (c) and (d)).

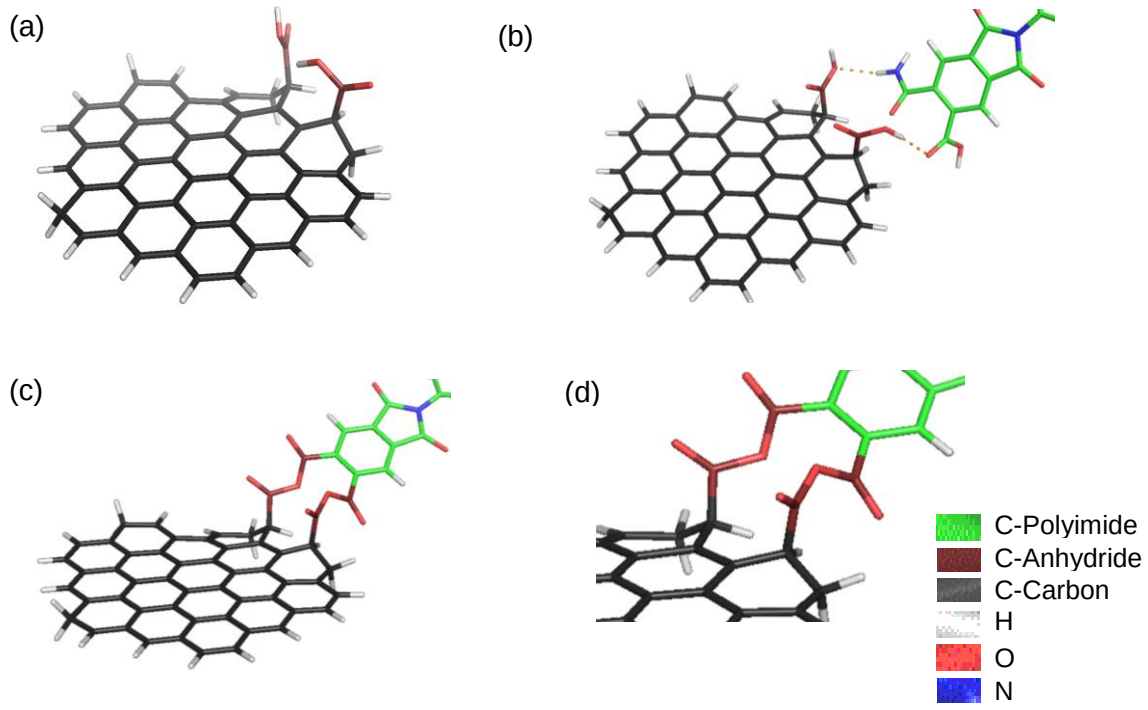

Figure 20: (a) Glassy carbon with carboxylic acid functional group(b) Hydrogen bonding between polyimide carboxylic acids and glassy carbon carboxylic acids (c) dianhydride model between glassy carbon and polyimide (d) zoom of (c)

3.1.1 Plasma Etching and Hydroxyl Peak

Significant changes due to plasma etching were seen in hydroxyl-carboxylic acid peak as well as hydroxyl-carboxylic acid dimer peak. The hydroxyl-carboxylic acid dimer can be seen in Figure 21. In IR spectra, these dimers are seen as a downshifted hydroxyl peak somewhere between 3300 cm^{-1} and 2400 cm^{-1} , as well as a carbonyl peak between 1780 cm^{-1} and 1720 cm^{-1} (Silverstein, 2007). Because various types of carbonyl peaks exist the around 1700 cm^{-1}, the presence of the carbonyl peak alone cannot definitively prove the presence of carboxylic acid dimers. Thus, to confirm the presence of carboxylic acid dimers at the polyimide/GC interface, as well as any influence of oxygen plasma etching, the downshifted hydroxyl peak was used as the primary indicator.

Figure 21 shows that the hydroxyl-carboxylic acid peak exists on the bare GC before pattern transfer onto polyimide but has a much larger width when compared to the any interface sample, implying that these carboxylic acids are distinct from those at the interface. This type of clear distinction, however, is not present when comparing the non-plasma etched and plasma etched interfaces. Interface samples etched at 750 mTorr and 120 secs have a larger width, up to 300 wavenumbers larger than the rest. This large increase in width is likely due to the unsteady plasma; at higher pressures, particularly those above 700 mTorr for the equipment and power used, the plasma generation is less stable. The variability in the plasma would then translate into variability in conformation of groups generated at the surface by the plasma. Since the width of the peak represents the degree of variability in the conformations of the functional groups, an increase in width with an increase in plasma variability is expected. Overall, there is no discernible trend with pressure or time, suggesting that plasma etching has a relatively uniform

effect regardless of parameter within the range tested, and that this effect is not significantly different from samples with no plasma etching at all.

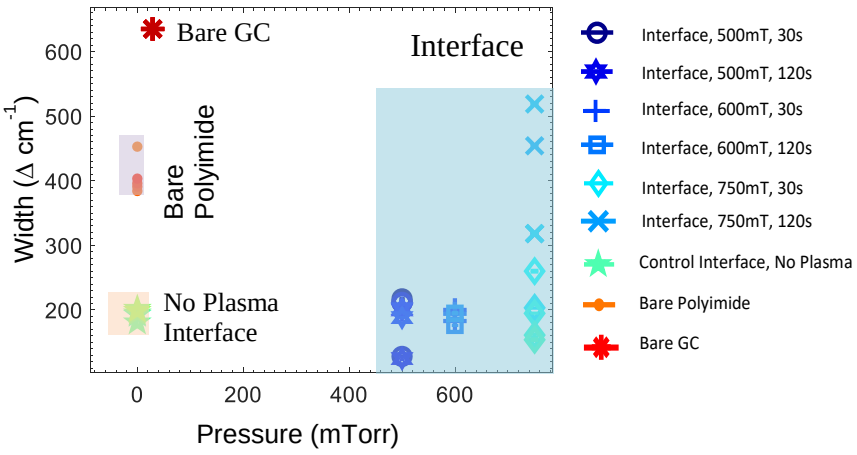

Figure 21: Hydroxyl-Carboxylic Acid Peak: The width of the OH peak is not detectable in the bare glassy carbon spectra and significantly different in the polyimide. Thus, even without plasma etching, unique carboxylic dimers are forming between the glassy carbon

Since a previous work has demonstrated that oxygen plasma etching of GC does induce carboxylic acids (Chen, 2009; Hirabayshi, 2013), it would be expected that the non-plasma etched interface sample would display the same hydroxyl-carboxylic acid peak as the bare GC. The substantially smaller peak width in non-plasma etched interfaces could be explained by the interface fabrication process itself using up carboxylic acids, thus decreasing the width. If this were the case, however, then some statistical difference between the plasma etched and non-plasma etched interface samples would still be expected. The nearly negligible statistical difference implies that either (a) the effects of plasma etching on the surface are less significant than other changes due to the fabrication process, or (b) the functional groups induced by plasma etching are immediately used up in another reaction when combined with polyimide. For

example, the carboxylic acids generated during plasma etching could interact with the carboxylic acids native to the polyimide to create an anhydride.

3.1.2 Plasma Etching and Anhydride Peaks

The non-cyclic anhydride ether peak (formed from 1 carboxylic acid rather than the 2 used in the cyclic form) is not present at all in the GC before plasma etching nor in the non-plasma treated interface samples. Since anhydrides cannot be created by plasma etching process alone (Chen, 2009; Zschoerper, 2009), their unexpected presence after plasma etching suggests that the functional groups (namely carboxylic acids) created on the GC allowed for the formation of anhydride bonds when polyimide was added. This chain of reactions further supports the hypothesis that plasma etching generates carboxylic acids that are then immediately used.
The high variability within the plasma etching samples effectively removes any trend with pressure or time. However, while some of the peak widths of the interface samples lie within the 2σ range (Figure 22) of the polyimide, the difference of at least 20 wavenumbers between the interface minima (Figure 22 (b)) and the polyimide minima confirms that the non-cyclic anhydrides present at the interface are distinct from those in the polyimide, and that they are formed through plasma etching.

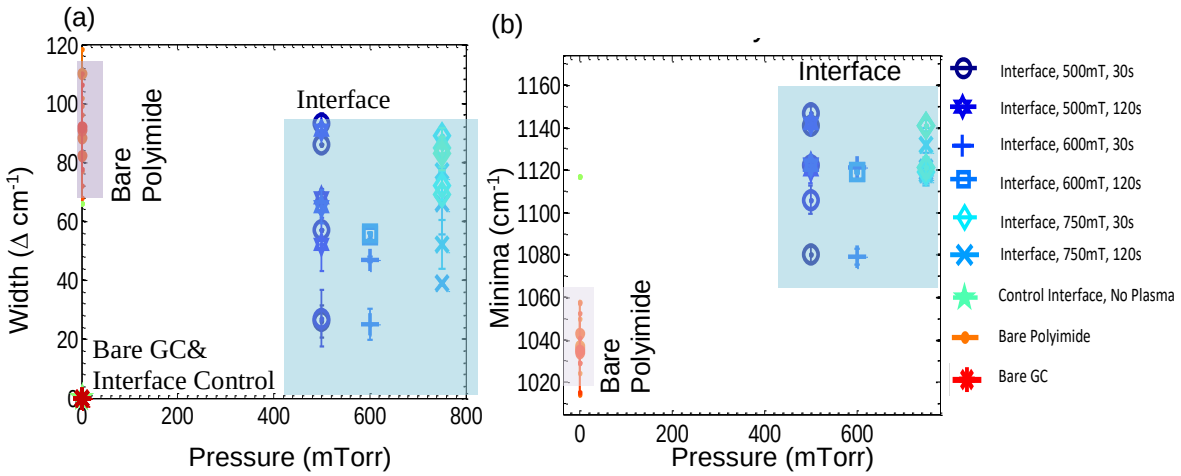

Figure 22: Non-cyclic anhydrides: Bare GC and the non-plasma etched interface control spectra had no peaks associated with non-cyclic anhydride region. The interface, however, clearly has these peaks, which differ from the polyimide peaks in width (a) and minima (b), indicating that plasma etching allowed for the generation of cyclic anhydrides. Higher variability in the midpoint in plasma etched samples is due to the randomness of the plasma etching process. '0 Torr' on the plot indicates no plasma etching.

3.2 Effects of Curing Temperature

Once the glassy carbon (GC) is plasma etched, as discussed in Section 3.1 and shown in detail in our previous work (Hirabayashi, 2013), the GC microstructure has many acyl functional groups, including carboxylic acids, carbonyls, ethers, and hydroxyls at the termination of the graphitic sheet. At these functional groups, the carbon is able to interact with polyimide. When polyimide is added to the plasma etched GC at room temperature, hydrogen bonding between available polyimide and GC dicarboxylate occurs, creating favorable conditions for dianhydride formation. Anhydride formation from carboxylic acids also becomes more likely with higher input energy, and thus with increasing temperature (Gillingham, 1999; Zschoerper, 2009). The results presented in Section 3.1 demonstrate that samples etched at 500 mTorr had more

consistent results; thus, the Figures in the following section only show the interface samples etched at 500 mTorr or not etched at all.

3.2.1 Temperature and Hydroxyl Peak

In Figure 23, the hydroxyl peak around 2500 cm^{-1} is shown. There is a clear difference between the polyimide, glassy carbon, and interface samples, in both width and midpoint, across all curing temperatures. While GC, polyimide and interface samples all do display a carboxylic acid dimer peak, the significant difference in width (~200 cm^{-1}) between the polyimide and interface and between the bare GC and interface samples (>100 cm^{-1}, ~400 cm^{-1} for most data points) and width suggests that the carboxylic acids at the interface are not the same as those native to the polyimide. Additionally, the overlap of the non-plasma etched and plasma etched samples implies that the presence of the dimers is not a function of plasma etching, but rather that of the interaction of the polyimide and GC at the interface. Since a decrease in width implies increased uniform bond conformations, the decrease in width at the interface implies that the bond between the GC and the polyimide includes carboxylic acid dimers with a very specific conformation.

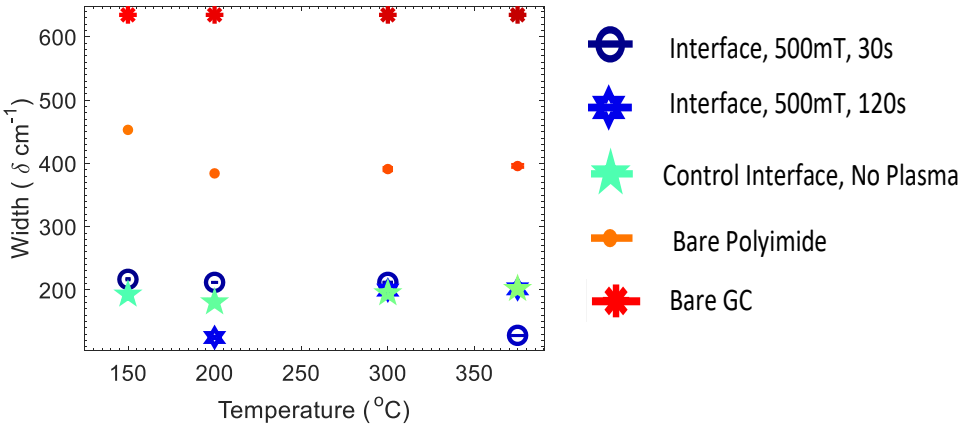

Figure 23: Carboxylic Acid Measurements: Width prove carboxylic acids at the interface are distinct from polyimide and glassy carbon.

3.2.2 Temperature and Carbonyl Peak

Figure 24 (a) shows that the minima of all plasma etched interface samples at all temperatures considered match the minima displayed by the polyimide alone, whereas the minima of the non-plasma etched interface samples aligns with that of the bare GC alone. In contrast, Figure 24 (b) shows that the width of the both the plasma etched and non-plasma etched samples aligns with that of the bare GC. The alignment of the non-plasma etched samples to the bare GC in both minima and width makes it challenging to distinguish clearly between bonds present at the interface and bonds native to the GC. However, the contrast of the plasma-etched samples (alignment with polyimide in minima and GC in width) is sufficient to indicate that a unique bond exists at the plasma etched interface that is not displayed in either the bare GC or the polyimide.

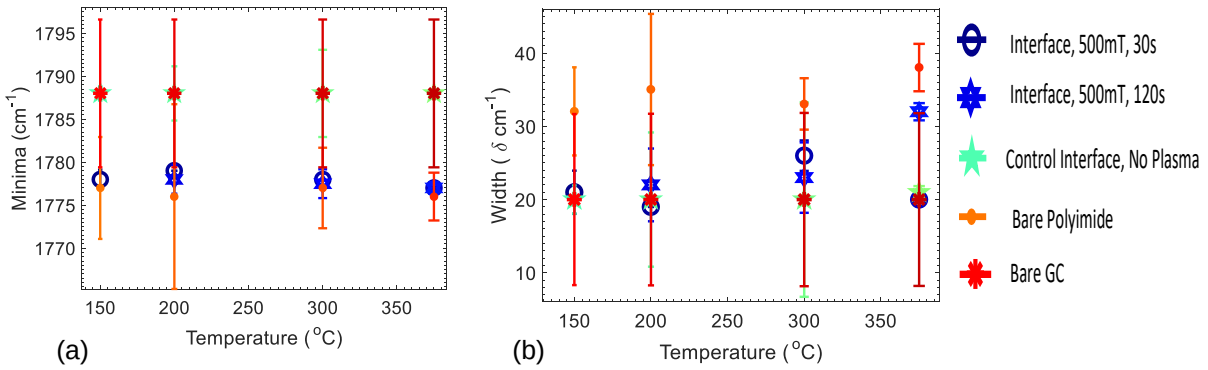

Figure 24: Carbonyl Peak Measurements: Measurements at 1777 are indicative of an asymmetric carbonyl peak which can be part of an anhydride bond. Differences are not conclusive without the presence of an anhydride peak.

It is known that for polyimide, a minimum at 1777 cm^{-1} can be the result of a carbonyl that is indicative of a dianhydride bond (Silverstein, 2007). The match of the plasma etched interface samples' minima to that value thus suggests the presence of an anhydride at the interface as well. Additionally, the increasing width of the carbonyl peak with increasing temperature in the plasma etched samples is a trend that suggests formation of anhydrides is more significant at higher curing temperatures, provided the sample has been plasma etched.

3.2.3 Temperature and Anhydride Peaks

Unlike carbonyls, which are present in bare glassy carbon (GC), polyimide, and at the interface, anhydride peaks are only detectable in the polyimide and at the interface. Additionally, there is a clear statistical difference between those anhydrides native to the polyimide and those at the interface. Figure 25 (a) shows that the peaks measured at the interface have a minimum about 20 cm^{-1} smaller in wavenumber than the polyimide minima at temperatures higher than 200°C. While the width and the midpoint do not differ significantly, the change in the minima is enough to show that the interface has a different anhydride vibration in the 1275 cm^{-1} region.

Moreover, the fact that the interface samples are more discreet from the polyimide with increasing temperature is itself significant. The downshift in minima of the plasma etched samples indicates that some reaction occurs to form more stable bonds. The observed downshift begins at 200°C temperature at which anhydrides form from carboxylic acids (Gillingham, 1999) which implicates new anhydride formation at the interface as the cause of the downshift at higher temperatures.

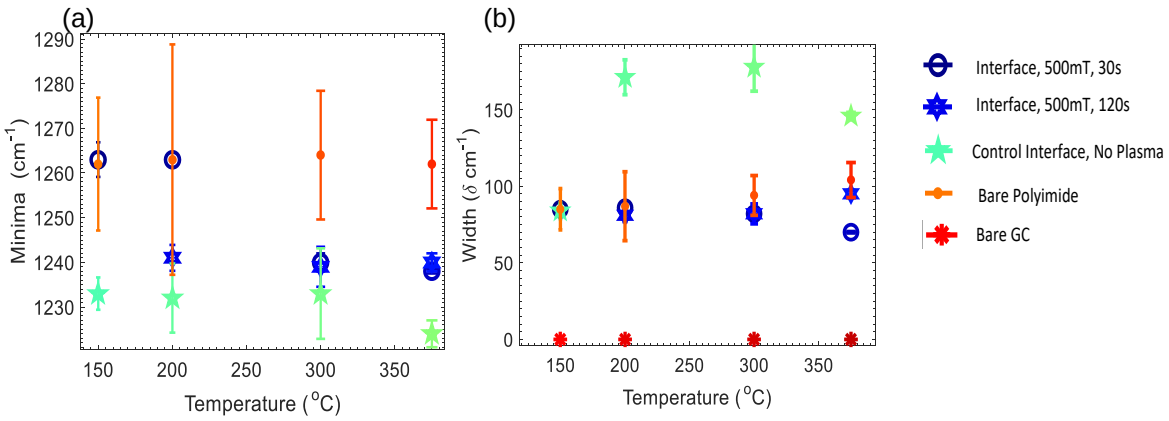

Figure 25: Cyclic anhydride: The minima shows that the interface does change significantly at temperatures above 200°C, high enough to imply anhydride formation. The width shows that there are no carbon-native anhydrides, and again at higher temperatures the trend supports the distinction between the polyimide anhydride and the plasma etched interface anhydride. It is therefore likely that a combination of higher curing temperature and plasma etching is required for unique anhydride generation at the interface.

Unlike the cyclic anhydrides, the minima of the non-cyclic anhydrides (Figure 26) show a clear difference from the polyimide samples. However, though there is no clear trend in the plasma etched interface samples, there is a statistically significant change in variability between different plasma etch parameters as the curing temperature increases. In the non-cyclic anhydride region, the plasma etched samples reach minimum variability in width at 200°C. This suggests that the bonds become more organized and take on the same or similar conformations that

vibrate at the same frequency. Because the temperature at which the variability converges is close to the temperature for anhydride formation between two carboxylic acids, we can conclude that at least some the bonds generated at the interface are anhydrides.

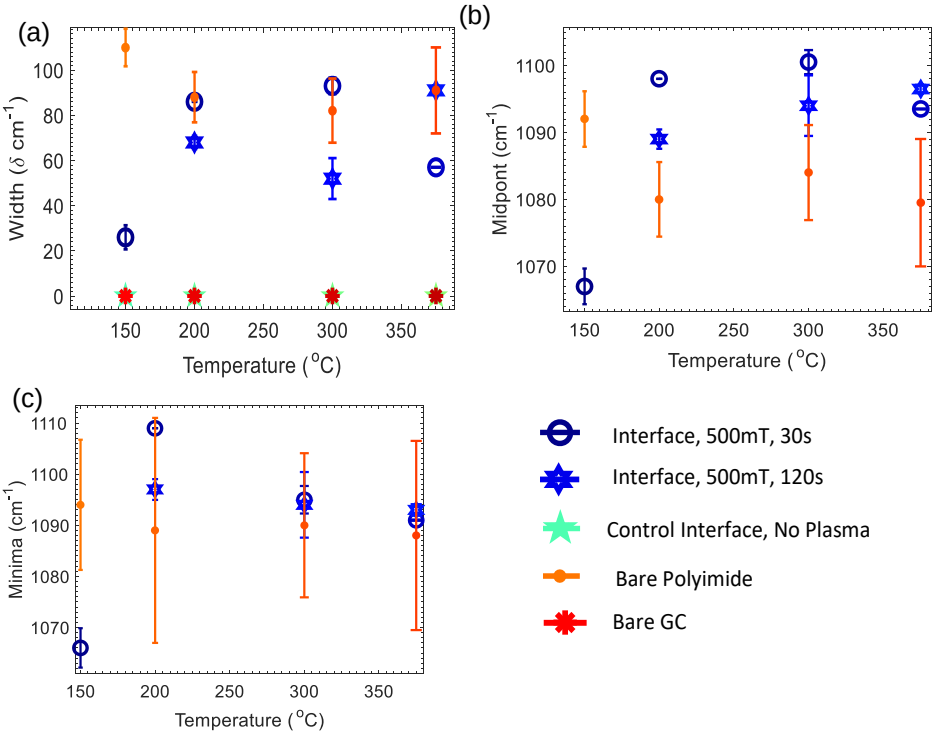

Figure 26: Non-cyclic anhydride region: The midpoint shows the most significant difference between the polyimide (orange) and the interface (blue). Minimum variability is at 200oC or higher for all metrics, implying reactions taking place to form more anhydrides with similar conformations.

3.3 Scanning Electron Microscopy Images

Scanning Electron Microscopy (SEM) was used to visually support the findings that plasma etching and higher curing temperatures create strong bonding between GC electrodes and polyimide substrate. Samples that were plasma etched at 600 mTorr for 120 seconds and cured at 375ºC were first coated with 6 nm of platinum to increase conductivity and minimize charging of the surface during imaging. They were then loaded onto a stage tilted at 45º and imaged at 20 kV

using secondary electron detection. Images were taken at magnification levels ranging from 100x to 75,000x to provide a thorough visual representation of the microstructures of the interface between the GC electrodes and the polyimide base.

Figure 27 (a) shows the topography of a GC electrode and polyimide at 100 times magnification; the bright line across the images indicates a clearly formed interface between the two materials. In Figure 27 (b), the interface is shown again at 17,000 times magnification. In this image, the GC and polyimide microstructures can be seen more clearly. The GC, farther from the interface, has both smooth and porous areas; the smooth areas are likely the areas where the oxygen plasma did not interact with the surface. In the GC porous areas, the oxygen plasma was able to break through the smooth surface and expose the more porous interior portions of the electrode. The polyimide structure, visible at the bottom of the image, appears rough but not porous. However, closer to the interface, the topographic differences between the two materials blends together, suggesting local material dispersal across the GC/polyimide boundary.

Figure 27 (c) and (d) show a further magnified view of this stretch of interface at 50,000 times magnification and 75,000 times magnification respectively. The dashed interface lines in 19 (c) and (d) delineate where the glassy carbon meets the polyimide. Here, the high magnification shows the sheets of glassy carbon interlacing with the chains of polyimide. The linking between the chains and sheets supports the findings that the two materials form new and unique intermolecular bonds at the interface.

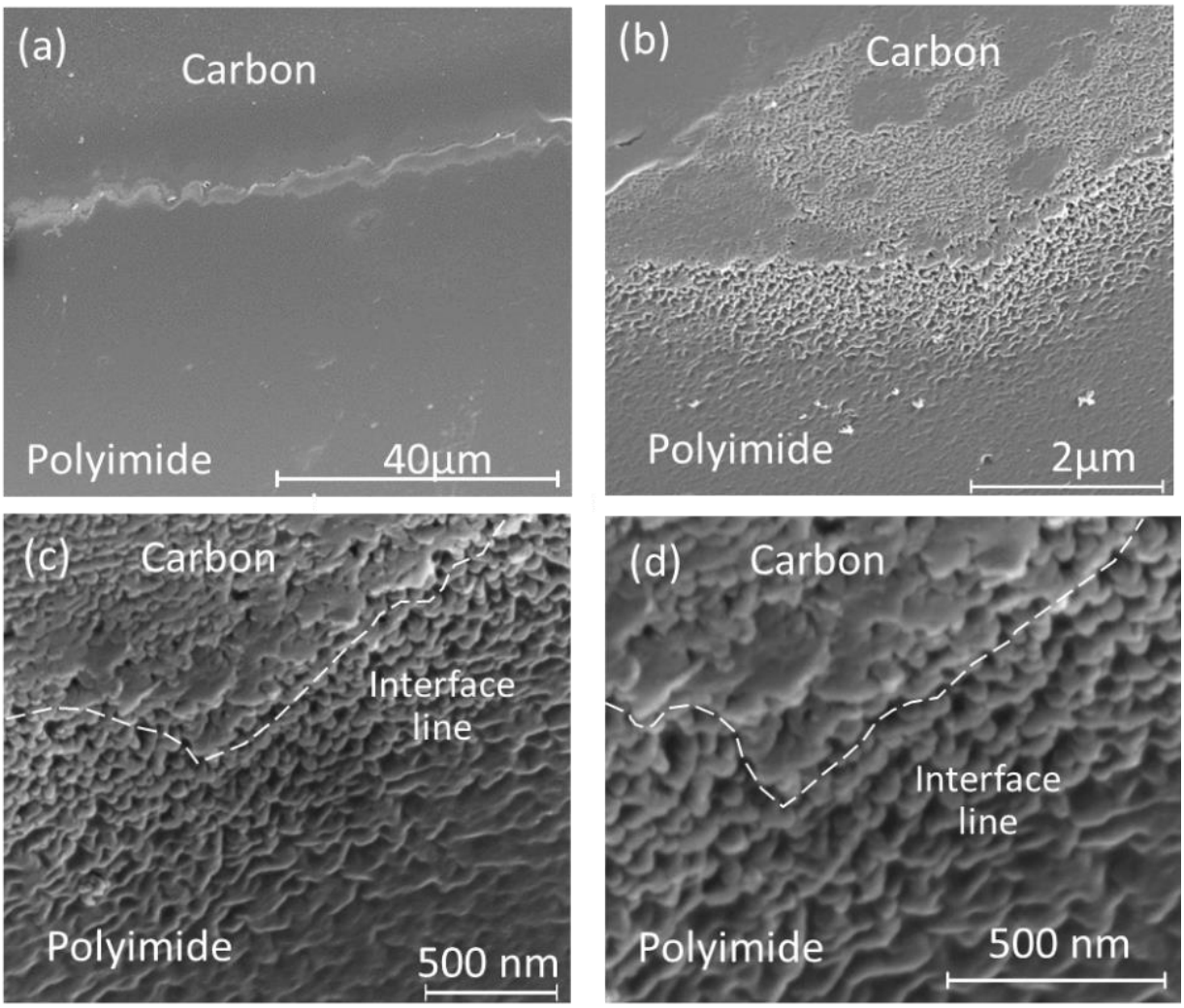

Figure 27: SEM of Glassy Carbon/Polyimide interface. Microstructures of the interface are pictured at 100x magnification (a), 15,000x magnification (b), 50,000x magnification (c), and 75,000x magnification (d). Similar microstructures across the interface line provide visual indication of material dissemination caused by inter-material bond formation.

Chapter 3, in full, is a reprint of the material as it appears in *Journal of the Electrochemical Society:* Hirabayashi, Mieko**,** Kyle Logan, Christopher Deutschman, Thomas McDowell, Martha Torres, David Pullman, and Sam Kassenge. 165, no. 8 (2018): B3060-B3070. The dissertation author was the primary investigator and author of this paper.

CHAPTER 4

Coupled Detection of Electrophysiological and Electrochemical Signals

This chapter investigates the ability to record electrophysiological signals and electrochemical signals *in vitro* using a glassy carbon array. To do this, first a microelectrode array, detailed in Figure 28, was fabricated as discussed in section 2.2.5 and then treated with Nafion. Calibration techniques were carried out using fast scan cyclic voltammetry, as discussed in section 2.3.3, using the Solarton potentiostat. Finally, a simulated coupled recorded was generated using a breadboard potentiostat and a previously recorded ECoG signal.

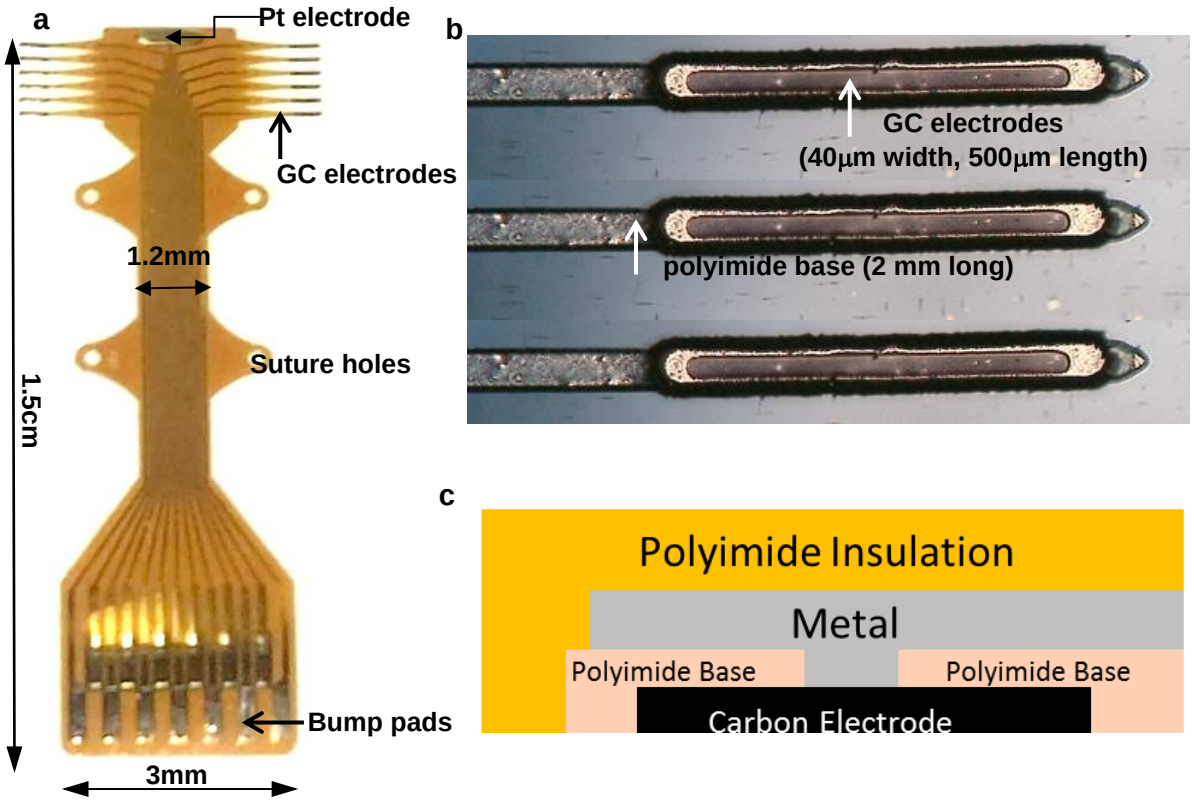

Figure 28: Penetrating Electrode Device: (a) Whole Device (b) Zoom of probes with carbon electrodes (c) Horizontal cross section of probe (Hirabayashi, 2017)

4.1 Calibration with Serotonin

Calibration of peak current vs concentration was done with on-device glassy carbon microelectrodes. To predict how this would change the electrochemical interaction, impedance readings between GC-to-GC microelectrode (working electrode – GC; counter electrode – GC) were compared with traditional large platinum counter electrode to GC reading. Figure 29 shows that the difference in impedance is very small and statistically negligible. However, the Nyquist plot shows higher imaginary impedance, especially at lower frequencies, indicating a more capacitive effect in GC microelectrodes. These differences are most likely due to decreased distance between the counter and the working electrode and an additional capacitive effect on the GC-to-GC readings from the GC and the Nafion.

After conditioning, GC-to-GC readings were used to calibrate the probes. As described in detail in Section 2.5, cyclic voltammograms were taken at various 5-HT concentrations. The background current was subtracted from these cyclic voltammograms and the measurement of the peak current density at the oxidation voltage of 5-HT (~0.7V) was plotted against the concentration as shown in Figure 30. 715 Hz was calculated from a scan rate of 1kV/s and a range of -0.6 to 1.2V per cycle. This gave a reasonable sensitivity but only a lower detection limit of about 2.5μM, which may be useful in some cases like human (Griessenauer, 2010), but not low enough for serotonin (5-HT) concentrations in the rat (John, 2007). Thus, the scan rate was then increased to 1.5kV/s; this only slightly increased the sensitivity. However, decreasing the voltage range to -0.4 to 1V per cycle while running a scan rate of 1.5 kV/s lowered the detection limit to about 25 nM. Working with a scan rate at this higher frequency not only enables detection at lower limits but also allows for a more direct method of separating the

electrophysiological signal from the, usually in the range below 100 Hz, from the FSCV signal through frequency analysis.

Though we could detect 25 nM, the difference between 25 nM and 50 nM was very small and did not follow a linear trend. Thus, despite the linear regression predicting better sensitivity, in practice, the background subtraction only resolves a difference of 25 nM. While having the sensitivity be close to the lower detection limit is not ideal, these results are still comparable to the detection limits reported by others in literature. The Mayo Clinic's WINCS device meant for human intraoperative cortical neurotransmitter detection reported detection of concentration of 5-HT from 250 µM-10 µM in-situ (Griessenauer, 2010). Other in situ experiments reported a lower detection limit of 0.1 µM in mouse brain tissue (John, 2007). *In vitro* experiments by Swamy et. al. reported detection of 130nM *in vitro* with single carbon fiber electrodes with in a coating of single walled carbon nanotubes (Swamy, 2007). Zachek et. al. reported *in vitro* results in 2008, 5 µM detection of 5-HT with pyrolyzed carbon electrodes (Zachek, 2008); in 2014 this same group was able to detect 500 nM of 5-HT in the rat cortex (Hashemi, 2012). Since the rat brain tissue and rat brain 5-HT concentrations were detected between 100 nM and 500nM, concentrations much higher than our lower detection limit, we expect that our microelectrode array will still sufficiently detect 5-HT *in vivo*.

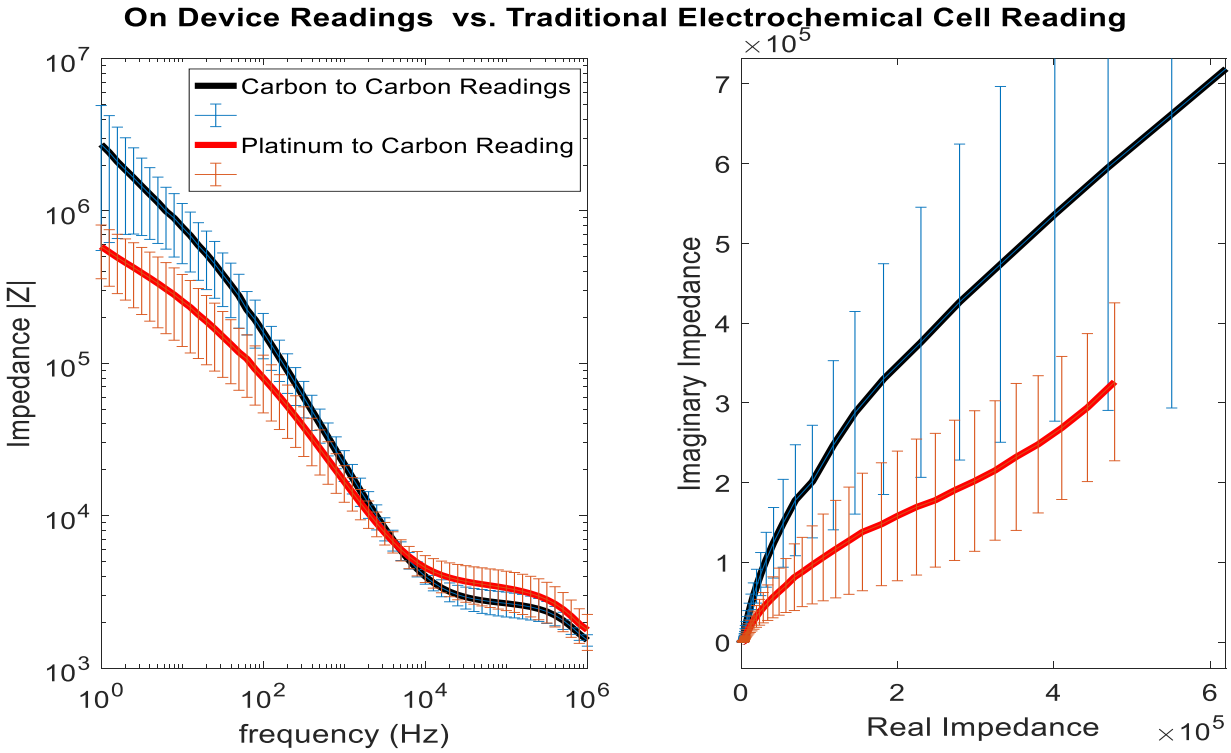

Figure 29: Bode and Nyquist plots show that carbon to carbon readings have little effect on the impedance. (n = 12)

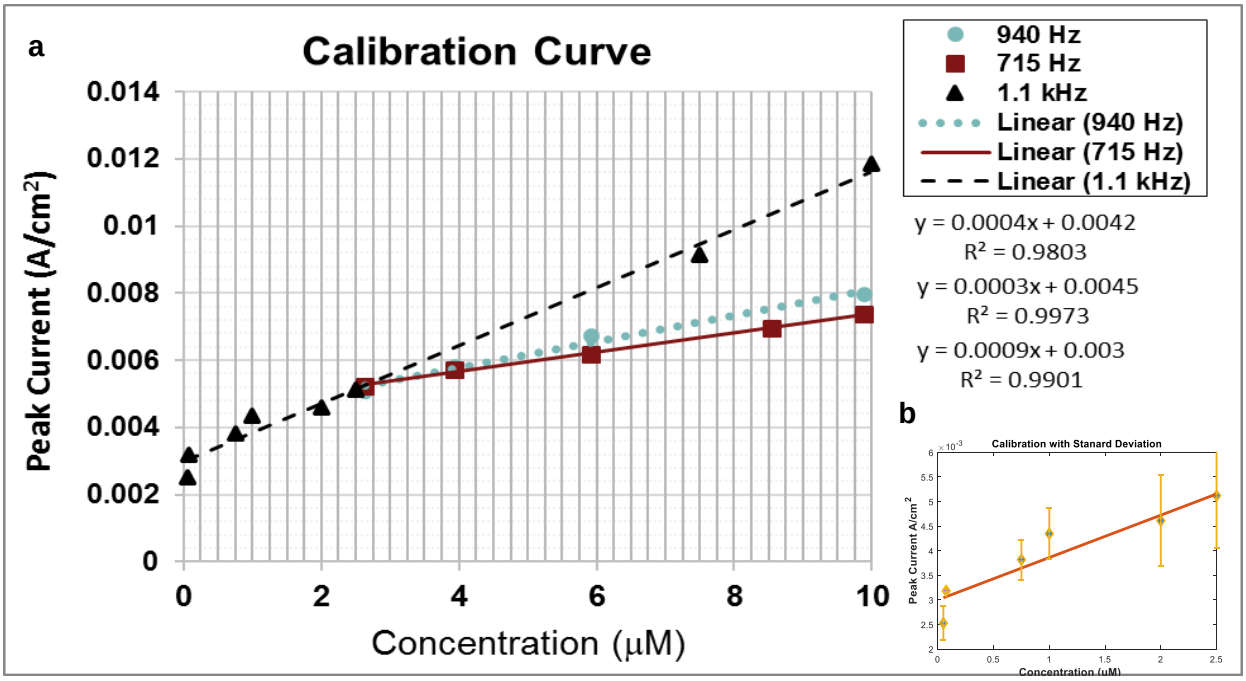

Figure 30: (a)Calibration at different input frequencies shows higher frequency yields better sensitivity and lower detection limit. (b) zoom of 1.1 kHz data points taken below 2.5 µM with standard deviation shown (n=100)

4.2Effects of Nafion Coating

When Nafion was applied electrochemically, an oxidation peak due to the Nafion oxidation appears at 1.1V and reduction peaks appear at 0.4 and -0.4 V. After about 100 scans, as shown in pink in Figure 31, the oxidation and reduction peaks reach maximum amplitude. At this point the impedance, as shown in Figure 32, reaches a minimum. Figure 32 also shows that at the minimum impedance Nafion generates a larger phase with a phase shift, indicating a large capacitive effect. At 100 scans, we expect the coating to be more uniform and homogeneous; however, the large capacitance implies a presence of significant space between the Nafion and the carbon that creates extra capacitance. In this case, the unbalanced oxidation and reduction peaks in Figure 31 imply an unstable coating which would result in Nafion degradation and,

hence, an unstable electrode. Thus, to ensure that only reversible oxidation and reduction reactions were occurring at the surface of the electrode, scans were continued until oxidation and reduction peaks disappeared. For most microelectrodes, this occurred at about 350 scans. This increased the impedance slightly but decreased the phase indicating closer contact between Nafion and the carbon electrode. Figure 33 shows how the Nafion coating changes the sensitivity and charge storage capacity of the electrode. Before Nafion coating (red) the area of the curve is small, indicating a small charge storage capacity of 14 mC/(cm^2), and the oxidation peak of 5-HT at about 0.7 V cannot be seen without background subtraction. However, with the Nafion coating, after 350 scans, area of the green curve is much larger, giving a charge storage capacity of 119.4 mC/(cm^2) resulting in better sensitivity to the 5-HT oxidation which can be seen as a small inflection can be seen at 0.7 V even without background subtraction.

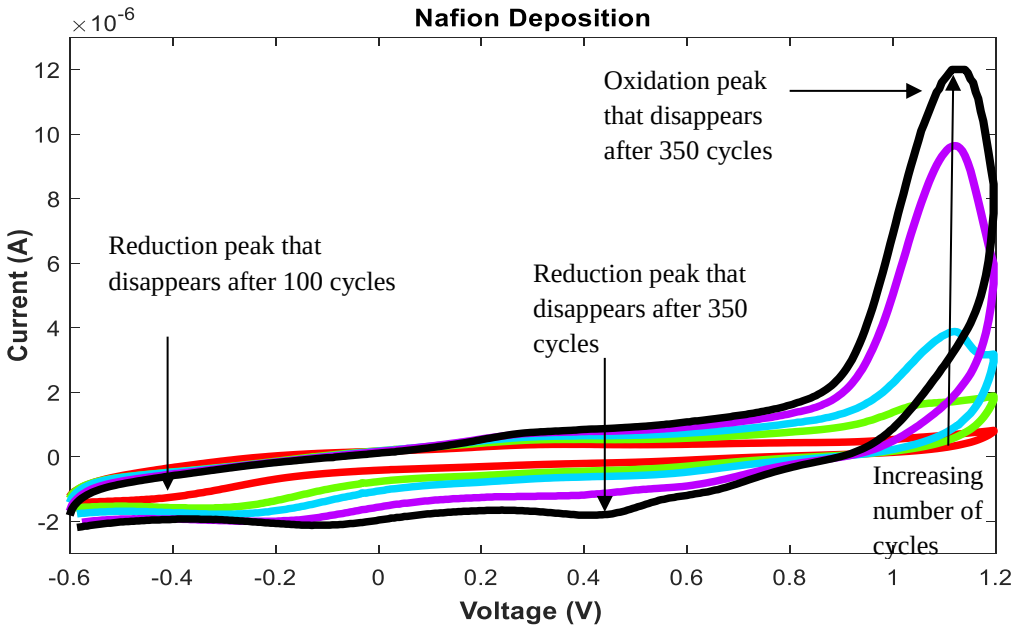

Figure 31: Cyclic voltammetry showing increase in Nafion oxidation peaks with increasing number of scans

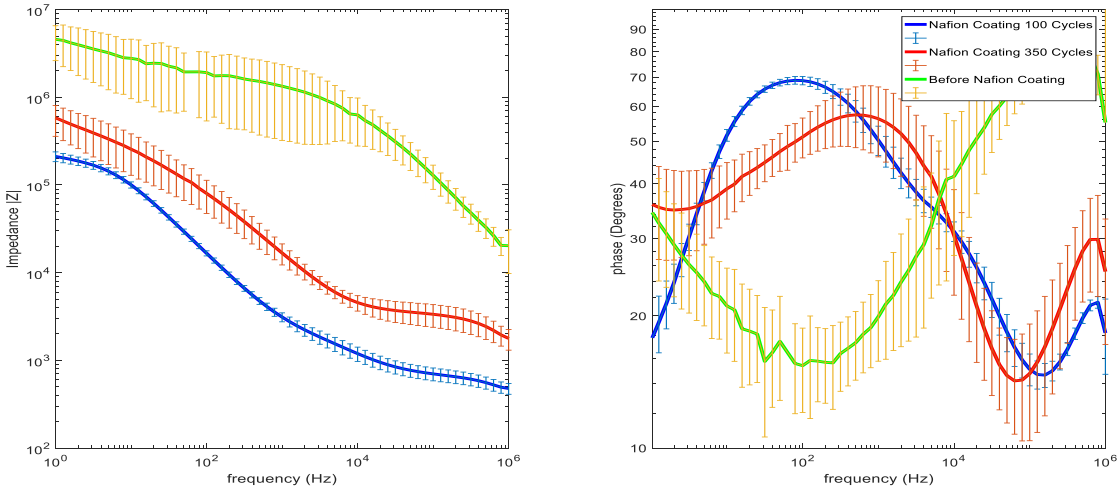

Figure 32: Bode & phase plots of electrodes before Nafion deposition, after 100 scans of cyclic voltammetry, and after 350 scans of cyclic voltammetry. At 100 scans, the impedance decreases but the phase shift is large. At 350 scans the phase shift decreases & impedance increases due to less capacitance between the Nafion and the carbon electrode. At this point, the Nafion coat is stable and does not disintegrate under fast scan cyclic voltammetry. *60Hz noise interfered with signal collection so the point at 60Hz impedance and phase was extrapolated. (n = 12)

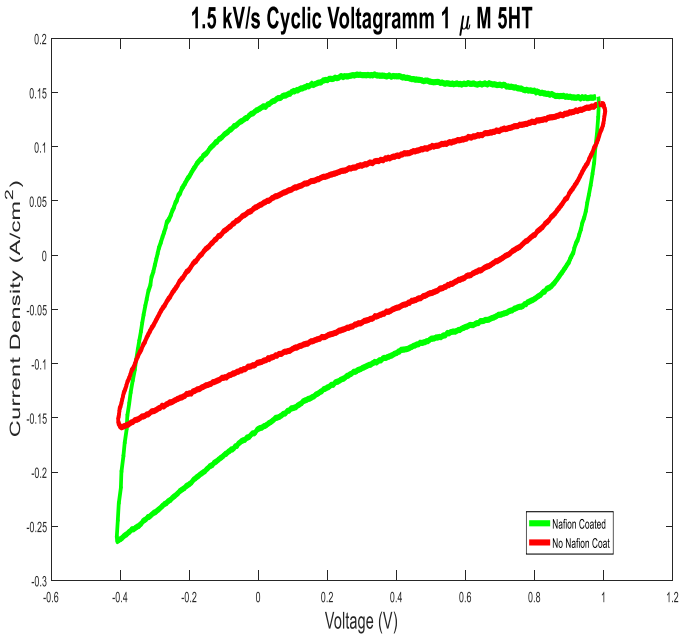

Figure 33: shows two additional effects of Nafion. One is an increase in charge storage capacity, from 14 $\frac{mC}{(cm^2)}$ to 119.4 $\frac{mC}{(cm^2)}$. The other is an increase in serotonin oxidation sensitivity; the red graph, before Nafion, shows no oxidation peak when scanned at 1.5 kV/s, while the Nafion coated electrodes show a slight inflection at about 0.7 volts, the oxidation of 5-HT was extrapolated.

1.3 Coupled Detection

Raw ECoG data previously collected with cortical glassy carbon electrodes under the dura was used as an input signal into an electrochemical cell. In this same cell was an array in which one electrode was used for reading and one was used for stimulating as shown in Figure 34 below.

A breadboard potentiostat was assembled to properly input the ECoG data into the electrochemical cell. This potentiostat consists of three operation amplifiers, the control amplified, the I/E converter, and electrometer (Economou, 2002). The control amplifier and I/E converter are the standard portions of a potentiostat that allow the signal from the working and

counter electrodes to be read relative to the reference electrode. The electrometer works to adjust the input signal to high frequency and low amplitude ranges (5 kHz and 200 nV) making it more suitable for FSCV (Nazari, 2009).

When coupling the ECoG signal with the 5-HT input, the same electrode was used as the working (reading) electrode in both electrochemical circuits, while two separate electrodes, one adjacent to the working for 5-HT input signal and one on the opposite side of the device for the ECoG input signal (Figure 34). 5-HT detection was done using the FSCV protocol described in 2.2.3.

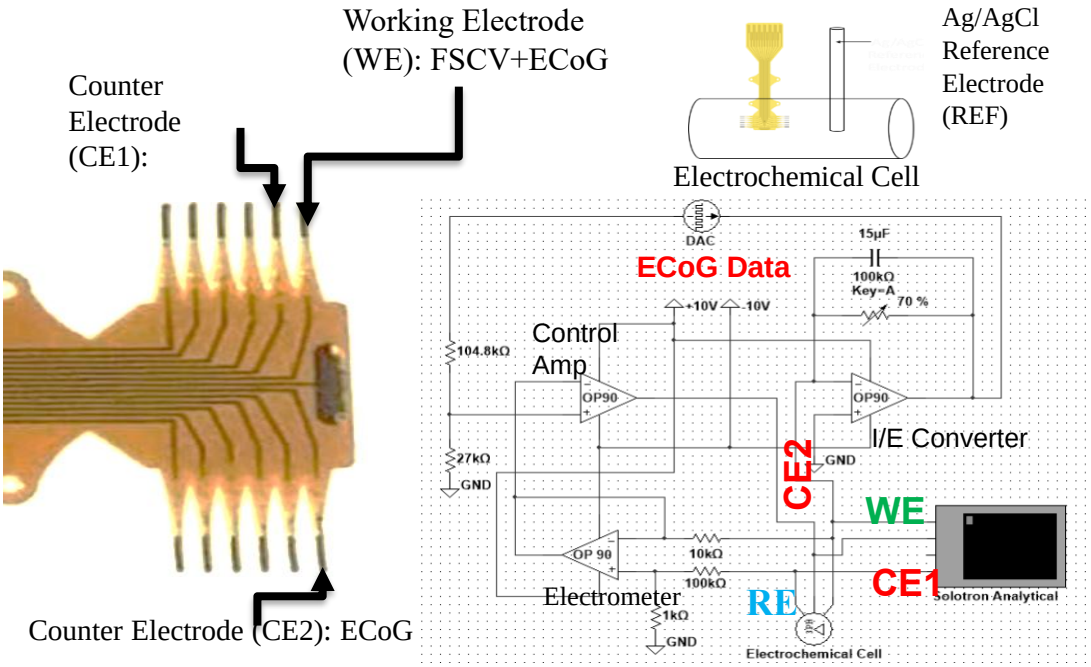

Figure 34: Coupled Detection Setup

ECoG alpha and beta signals occur below 100Hz. However, in this time, only a small amount could be seen in the 1 ms FSCV that was run. Thus, about 100 cycles of FSCV were run at 1.5 kV/s with ECoG input. The data extracted from the working electrode was filtered with a

lowpass filter at 30 Hz, the range for alpha and beta waves. At low frequency, the impedance is nearly linear, so the current density was multiplied by the area and impedance to obtain the voltage (Figure 35). To show that the FSCV could be filtered out of the ECoG data and still maintain the integrity of the signal, the same filter was applied to the ECoG data and focused on the 1 second collected during FSCV. The waveforms shown in Figure 35 were similar indicating the FSCV did not inhibit the capture of the ECoG data. However, some small artifacts from the raw CV data (labeled a and b) show up in the filtered ECoG data. These artifacts are due to small drifts in the electrochemical cell, but on such a small timescale, the analysis of the ECoG would likely not be altered. Additionally, a 10-fold increase in amplitude did occur due to the amplifier settings in the electrometer potentiostat (the raw ECoG data was multiplied by 10 to show a better comparison); this makes the data noisier than what we would expect *in vivo* but does not change the ECoG signal. Furthermore, *in vivo*, we do not expect to continuously run the FSCV, so drifts in the electrochemical signal would be much small and can be extrapolated from time data if necessary. While this filtering processes was performed on only one concentration, the effect of the FSCV on the ECoG signal is so small that we would expect no change from lower concentrations and negligible change in higher concentrations.

Figure 35 shows clearly that electrochemical data and electrophysiological data can be obtained with the same electrode. While some refinement in the filtering may be needed, the data still shows that these two signals can be collected and discerned from one another. While not done in this experimental set-u, the electrode design allows for at least 6 sets of electrochemical data to be obtained. If every other electrode is used as a counter electrode, then each adjacent electrode can be used to detect 5-HT and electrophysiological data giving spatial and temporal

data about the 5-HT and its effect on the electrophysiological signal. Rather than obtaining purely 5-HT data, this device, because of the surface chemistry of the glassy carbon, has the ability to immobilize enzymes through hydrogen or covalent bonding functional groups in the surface (Hirabayashi, 2013). These enzymes, such as glutamate dehydrogenase (Hashemi, 2012), can detect non-electroactive species of interest through amperometry. In this case, selective immobilization can be done on different probes, allowing for detection of multiple neurochemicals and offering much more insight into the electrophysiological signal.

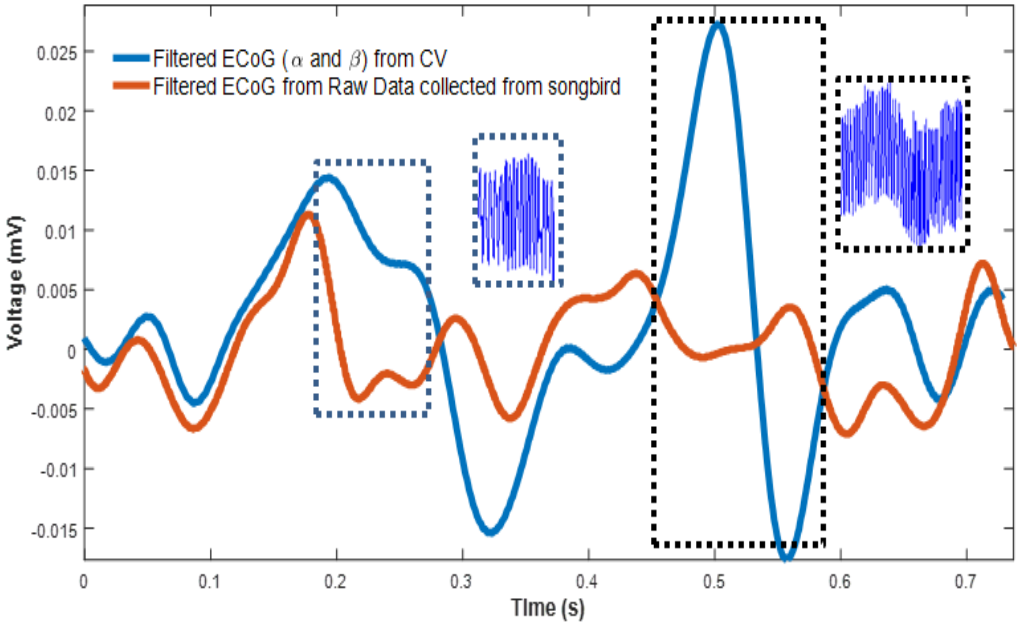

Figure 35: ECoG extrapolated from Coupled ECoG and FSCV

Chapter 4, in full, is a reprint of the material as it appears in *Journal of the Electrochemical Society:* Hirabayashi, Mieko, Nha Uyen Huynh, Shane Witsell, Alberto Perez,

Laura Sandoval, Naoya Yamada, and Sam Kassegne, 164, no. 5 (2017): B3113-B3121. The dissertation author was the primary investigator and author of this paper.

CHAPTER 5

Glassy Carbon and Neurotransmitter Detection

Serotonin, or 5-Hyrodytryptamine (5-HT), is a neurochemical linked to a variety of neural signal processes such as memory, vasodilation, long-term potentiation, cardiovascular and gastrointestinal function. In the central nervous system, 5-HT's involvements in mood disorders (depression and anxiety) as well as neuroplasticity are suspected but not well understood (Hudspeth, 2013). Part of the reason for this lack in understanding is the difficulty in measuring levels of 5-HT in real-time experiments using electrochemical methods like fast scan cyclic voltammetry (FSCV). Dopamine detection using FSCV is fairly straight forward reaction that oxidizes the amine and deprotonates the hydroxyls on the dopamine to produce dopamine-o-quinone (Chen, 2003). 5-HT on the other hand, can have various oxidation by-products resulting in secondary oxidation peaks, dimerization, and irreversible reactions (Wrona, 1987). The following chapter investigates the mechanisms behind electro-oxidation of 5-HT to determine the best protocols for FSCV detection of 5-HT.

5.1 Charge Transfer and Oxidation Mechanisms

5.1.1 Electrostatic Interactions between Glassy Carbon and Neurotransmitters

Figure 36 demonstrates the most basic mechanism used to describe electrochemical oxidation of serotonin (5-HT) or dopamine (DA): a voltage applied between glassy carbon and another electrode causes a 2 proton and 2 electron loss from 5-HT or dopamine to generate quinone-imine or dopamine-o-quinone. However, this simplified version does not inform the reason 'activated' carbon (Bath, 2000) is needed for detection, why carbon tends to be more sensitive to neurotransmitter detection than metal electrodes, nor why electrodes tend to be more

sensitive to dopamine than 5-HT (Zachek, 2008). To understand this, the interaction between the carbon and the neurotransmitter need to be considered.

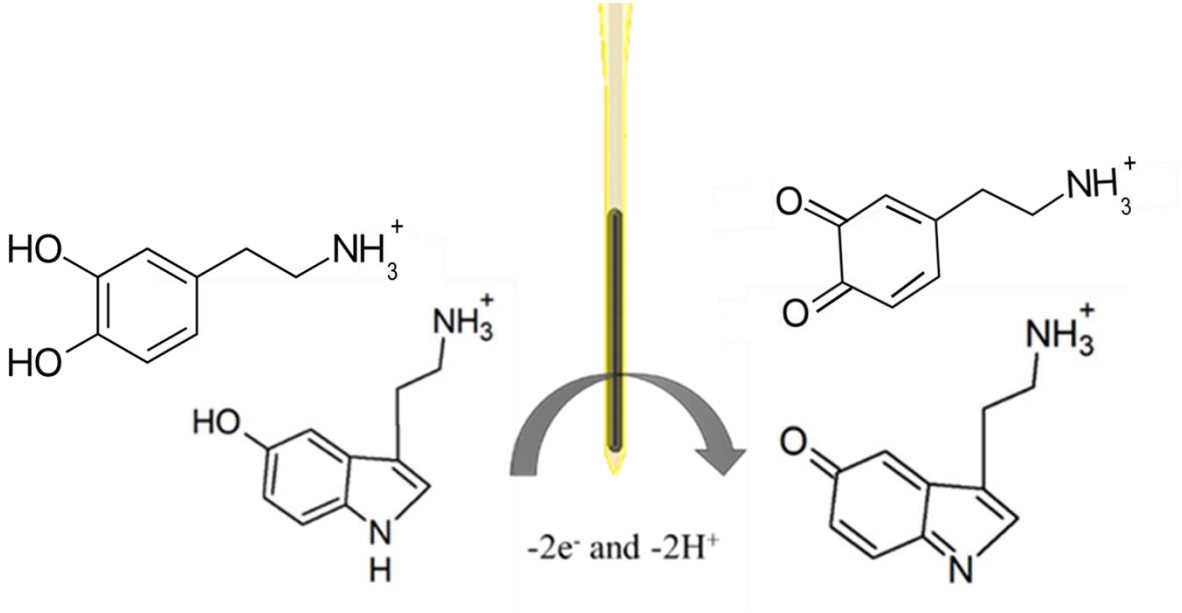

Figure 36: Electrochemical Oxidation of 5-HT at a glassy carbon electrode by loss of 2 electrons and 2 protons to a quinone imine.

Figure 37 shows the structure and the electrostatic potential of 5-HT at physiological pH. Because of its high pKa, the amine on the 5-HT and dopamine are always protonated at physiological pH. This proton's positive charge is distributed mostly over the amine, but also give the majority of the molecule a positive charge. Thus, ideally, a working electrode in an electrochemical system would have a net negative charge to attract the neurotransmitter close to the surface even before a potential is applied.

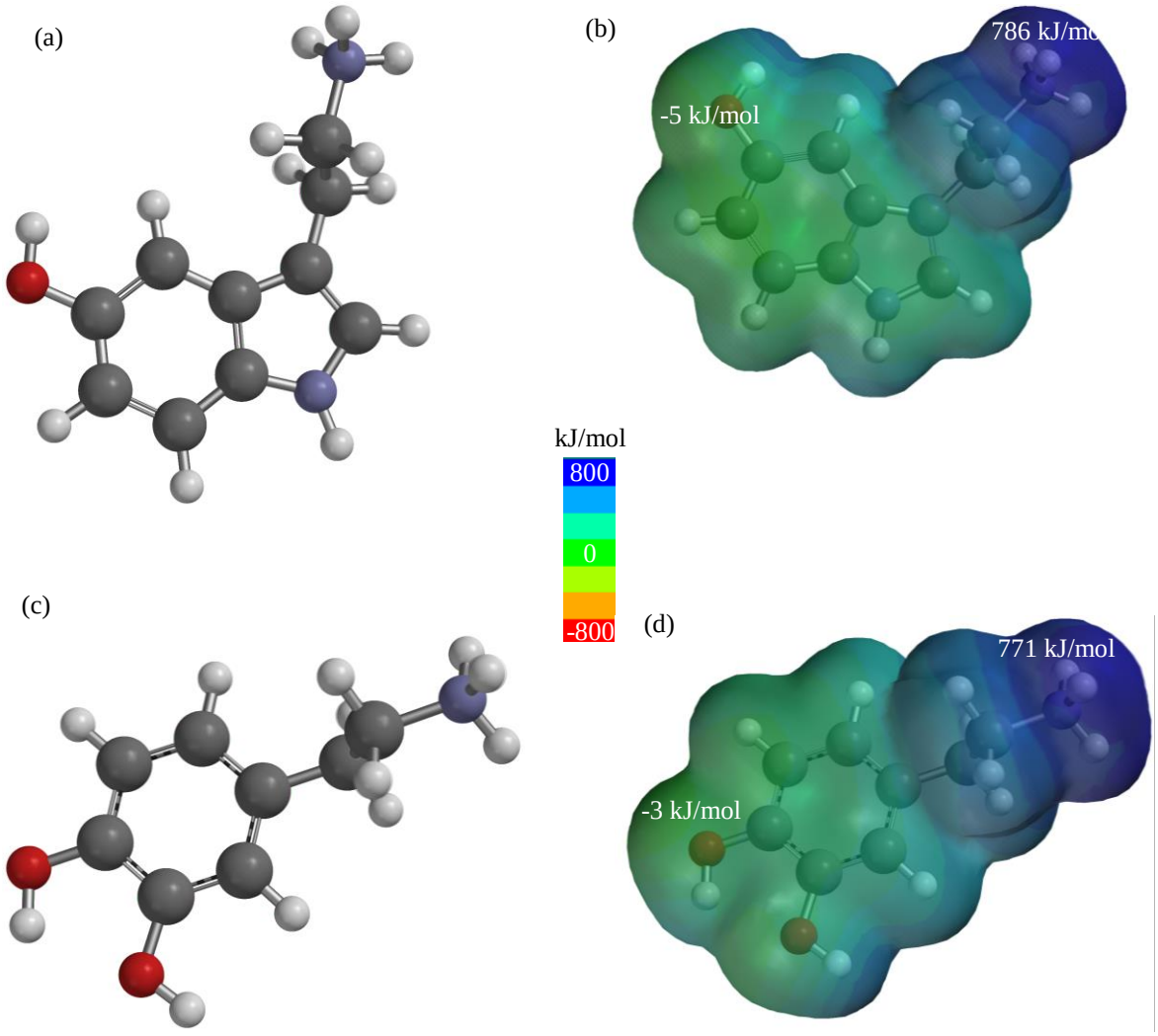

Figure 37: Serotonin (5-HT) (a) Ball and Stick model (b) Electrostatic Potential Map

Figure 38 (a) shows an example of a 4-ring aromatic system. Because the ring system allows for hybridization of electron orbitals, the negative charge is concentrated above and below the atoms in the center of the ring. This gives the majority of the surface of an aromatic system like glassy carbon a slight net negative charge. However, this charge can be altered depending on how functional groups change the geometry and delocalization of electrons. Figure 38 (b) through (d) shows just a single hydroxyl changes the overall surface charge. First the hydroxyl

always induces a large positive charge near the hydrogen and negative charge near the oxygen. Secondly, the degree of the effect is dependent on the location. A hydroxyl on a central atom, as shown in Figure 38 (b) distributes the positive and negative charge more evenly, while a hydroxyl on a terminating carbon (Figure 38 (c) and (d)) has a stronger positive and negative change in a much more localized area. While the wider area of negative charge is more beneficial for holding the 5-HT or dopamine cation in place, the total attraction is more important to pull the cation to the surface of the carbon; this magnitude of attraction is given by the dipole moment (denoted DM in figures). Interestingly, while configurations (b) and (d) have a stronger dipole moment than the unfunctionalized aromatic system, as expected, configuration (c) has a lower dipole moment. This is most likely because the angle of the oxygen happens to cause the hydrogen from the hydroxyl to line up with the other terminal hydrogens, stabilizing the molecule, and bringing down the dipole moment. In this case, the functionalization is having the exact opposite effect intended. Luckily, this will only happen if the aromatic system stays completely flat, which is impossible with multiple functional groups, so cases shown, such as (c), are possible, but less likely to happen.

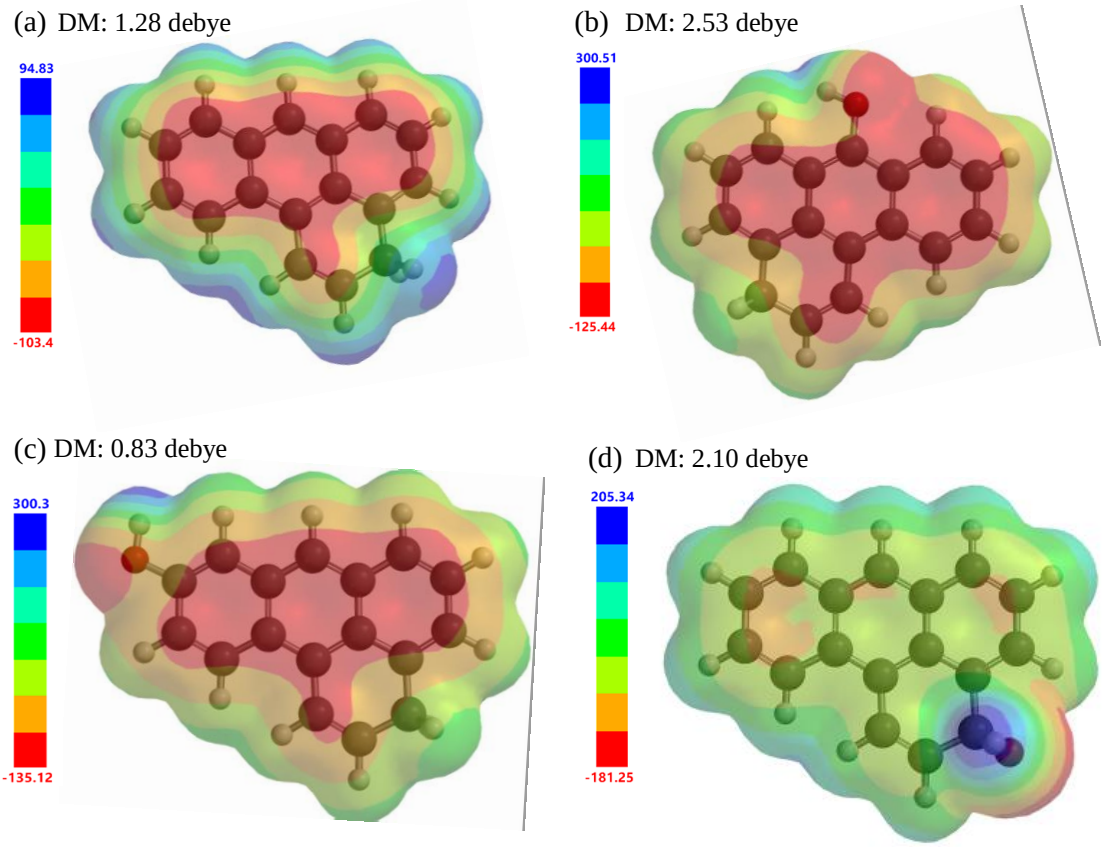

Figure 38: Effects of adding hydroxyl functional groups on aromatic systems (a) aromatic system with no hydroxyl groups. (b) Aromatic system with a hydroxyls group on a central ring (c) aromatic structure with hydroxyl on a terminating carbon with 1 hydrogen (d) aromatic structure with hydroxyl on a terminating carbon with 2 hydrogens

Methyl groups, hydroxyls, and carboxylic acids are among some of the more commonly formed functional groups on a carbon surface (Chen, 2009; Hirabayashi, 2013). These groups are diagramed in Figure 39 on a simplified 2 ring aromatic system. While methyl groups do not induce a huge change in the electrostatic potential (Figure 39 (a)), the overall area does become less positive, making the terminal groups less likely to repel a 5-HT or dopamine cation. Hydroxyls and carboxylic acids seems to have similar effects with the oxygen pulling in electrons generating a very negative area near the oxygen and a positive region along the proton

associated with the functional group. Carboxylic acids, with a dipole moment of 2.59 debye, would be more effective at pulling in a 5-HT cation than methyl (DM= 0.45 debye) or hydroxyl (DM=1.99 debye) groups alone, but together, these functional groups not only generate a large dipole moment (DM=3.27 debye), but as seen in Figure 39 (d), a combination of the functional groups generates a larger area of more negative potential along the surface. Thus, by increasing the amount of functionalization, the probability of electrostatic interaction between the carbon and 5-HT cation increases.

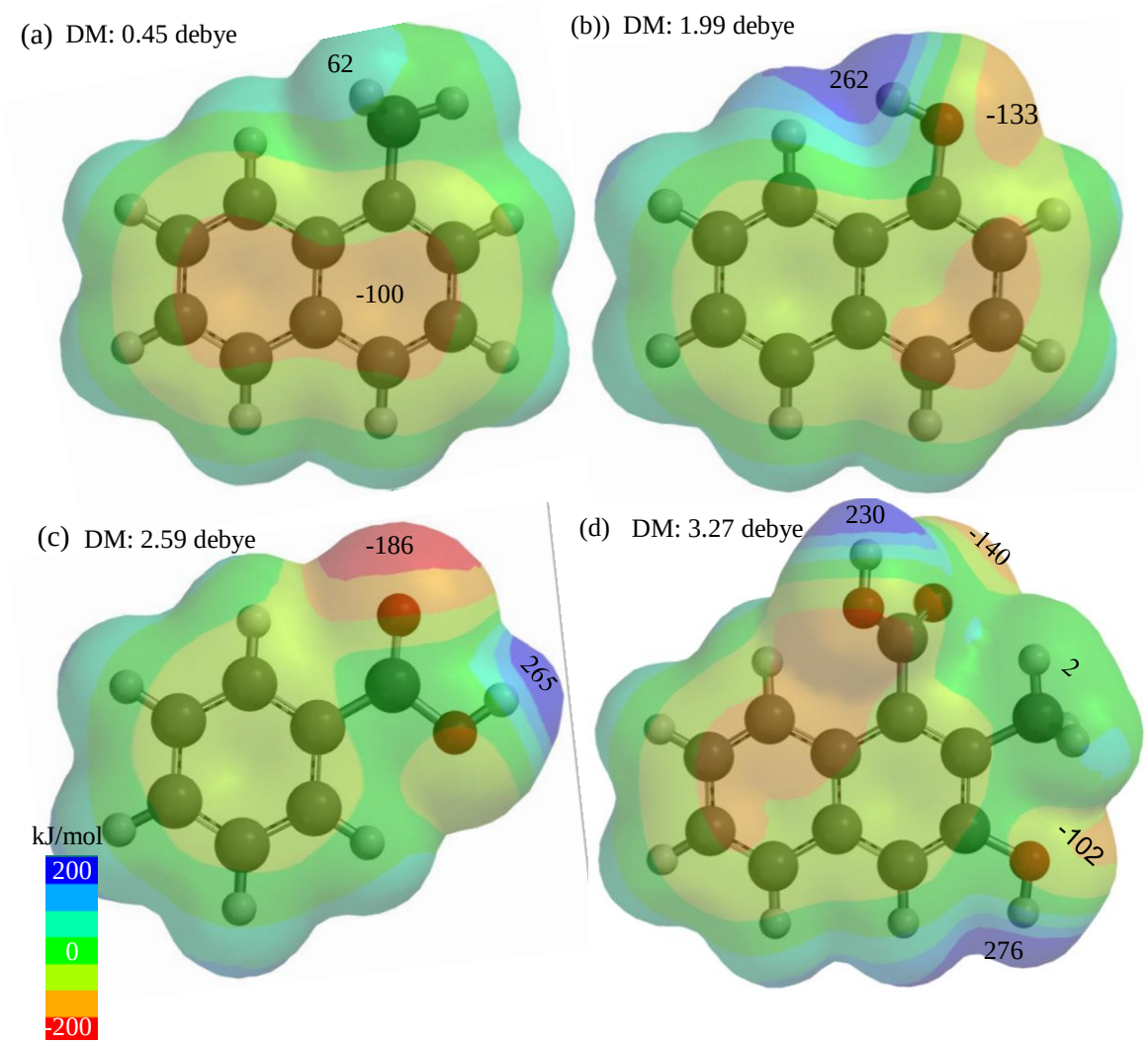

Figure 39: Effect of various functional groups on aromatic systems (a) Methyl (b) Hydroxyl (c) Carboxylic acid (d) Methyl, hydroxyl, and carboxylic acid

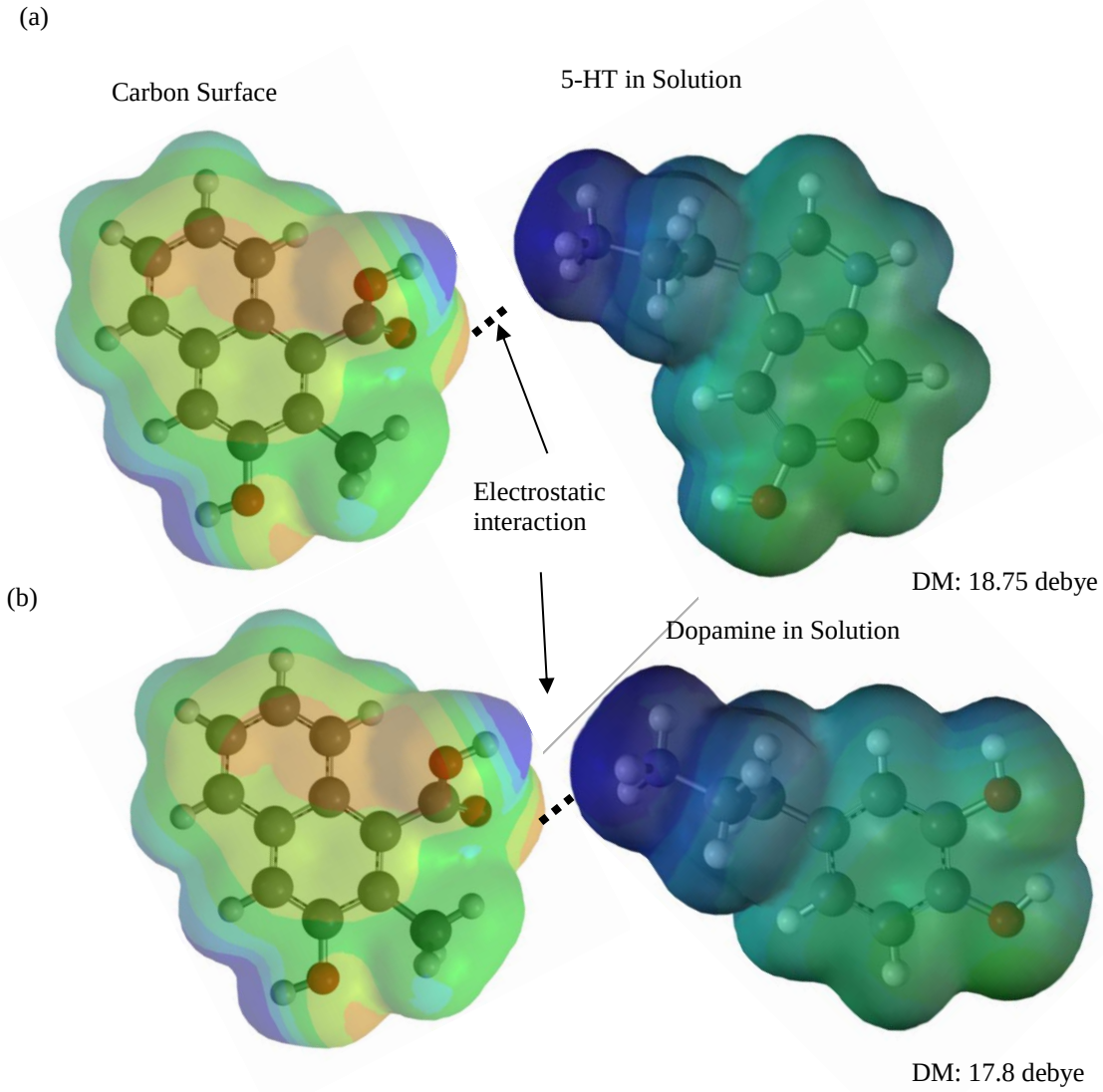

Figure 40: Most likely electrostatic interaction of 5-HT and dopamine with a functionalized surface

Figure 40 shows the most likely interaction between 5-HT or dopamine with a functionalized carbon surface. This pull caused by the differences in the dipole moments helps to explain why carbon is more efficient at oxidizing neurotransmitters but does nothing to elucidate why 5-HT is more difficult to detect. In fact, if it were just the dipole moments to consider, the

dipole moment of 5-HT is slightly higher which could make the initial electrostatic pull stronger thus easier to oxidized and detect. In experiments, however, sensitivity to dopamine is consistently higher than that seen in 5-HT (Fang 2013; Griessenauer, 2010; Jackson, 1995; Van Gompel, 2010). Perhaps then it is the oxidation by-products that have an effect? Figure 41 shows the electro-oxidation byproducts of 5-HT and dopamine generated by a 2 electron, 2 proton loss to form quinones. These maps little difference in the quinones suggesting that there should be little difference between the ability to reverse the reaction back to 5-HT or dopamine. This suggests that there are is more to the 5-HT oxidation than just the simple oxidation to quinone imine. Thus, the following sections further investigates the reactions between 5-HT and glassy carbon.

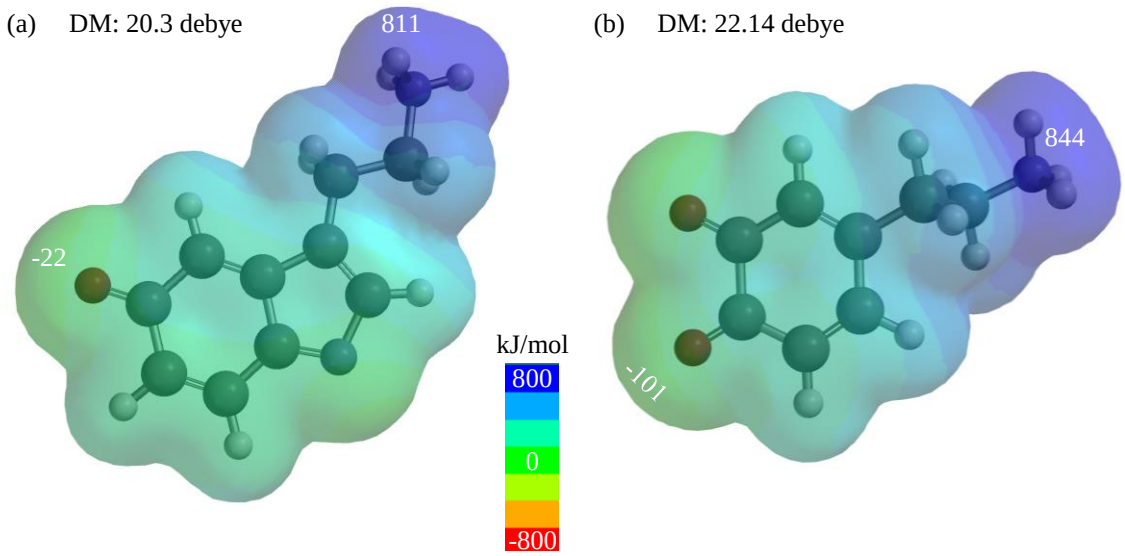

Figure 41: Electrostatic Potential Maps of quinone byproducts of (a) serotonin (quinone imine) and (b) dopamine (dopamine-o-quinone)

Table 7: Summary of findings from Electrostatic Potential Simulations

Model	***Dipole Moment (Debye)***	***Minimum Potential (kJ/mol)***	***Maximum Potential (kJ/mol)***
5-HT	18.75	-5	786
DA	17.8	-3	771
Quinone-Imine	20.3	-22	811
Dopamine-o-quinone	22.14	-101	844
2-ring functionalized Aromatic	3.27	-140	230

5.1.3 Electro-oxidation of Serotonin and its Byproducts

The electrochemical reactants oxidized serotonin (5-HT) were extensively studied by Wrona et. Al under acidic (Wrona, 1987) and physiological conditions (Wrona, 1990). From these studies, they found that 5-HT did not just produce quinone-imine, but rather 15 other byproducts. They proposed that the oxidation happens in a series of steps. First 5-HT is oxidized to its carbocation and then further oxidation to a quinone imine, as shown in Figure 42. Since this is reaction dominates at faster scan rates (Wrona, 1990), more recent literature using FSCV to detect 5-HT assume that this is the primary reaction occurring at scan rates 300 V/s-1kV/s (Güell, 2014; Griessenauer, 2010; Lama, 2012; Patel, 2013). However, subsequent reactions of the carbocation, diagramed in Figure 42, with 5-HT produce dimers, 5,5'-Dihydroxy-4,4'-bitryptamine (**Dimer 1**), 3-(2-Aminoethyl)-3-[3'-(2-aminoethyl)-indol-5-one-4'-yl]-5-hydroxyindolenine (**Dimer 2**), and 5-[[3-(2-Aminoethyl)-1H-indol-4-yl]oxy]-3-(2-aminoeythyl)-

1H-indole (**Dimer 3**) (Wrona, 1990a). When the reaction is sufficiently slowed, the carbocation can react with water allowing the formation of tryptamine -4,5-dione and its oxidized form 4,5-dihydroxytryptamine (Wrona, 1990 a; Wrona, 1990b). All of these reactions are diagramed in Figure 43.

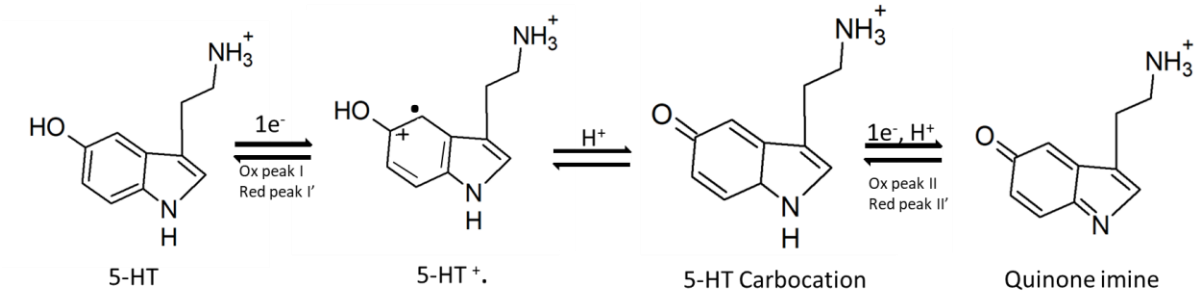

Figure 42: 2 step oxidations proposed and proven experimentally by Wrona et. Al (Wrona 1990a, Wrona 1987)

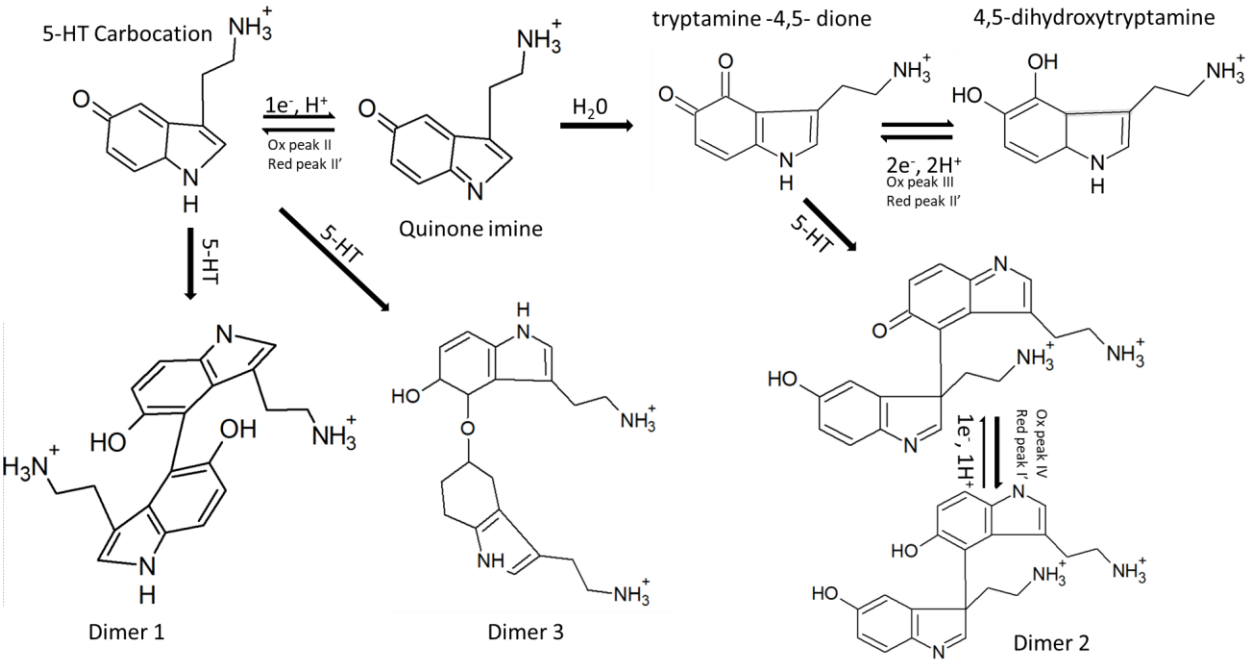

Figure 43: Various reactions that occur as a result of electro-oxidation of 5-HT

Figure 44 shows a cyclic voltammogram performed by Wrona *et al*. of 11.47 mM of 5-HT in PBS (pH=2) taken at 200 mV/s (Wrona 1990b). Similar oxidation peaks were seen at physiological pH, with voltages just slightly shifted to the left (Wrona 1990a). Figure 44 shows four separate oxidation peaks. Peak I appear first during the first scan starting at 0V, with peak II following quickly after. Reduction peaks 1' and II' appear after the initial oxidation and then subsequent runs show peaks III and IV then followed again by I, II, I' and II'. Peaks I and II appear as a result of the two-step oxidation process of 5-HT to the 5-HT carbocation as shown in Figure 42. After 5-HT has been oxidized to the carbocation, some of it is converted to quinone imide, some of it is immediately reduced back into 5-HT contributing to reduction peak I'. Some of the carbocation is converted into dimers. The dimers most often formed, 5,5'-Dihydroxy-4,4'-bitryptamine (Dimer 1), 3-(2-Aminoethyl)-3-[3'-(2-aminoethyl)-indol-5-one-4'-yl]-5-hydroxyindolenine (Dimer 2), and 5-[[3-(2-Aminoethyl)-1H-indol-4-yl] oxy]-3-(2-aminoeythyl)-1H-indole (Dimer 3) (Wrona, 1990a). If the scan is slow enough, the quinone imide reacts with water to produce 4,5-dihydroxytryptamine, which can be reduced to tryptamine -4,5- dione, producing reduction peak II'; since this reaction is reversible, tryptamine -4,5- dione is oxidized to generate peak III and then reduced again producing peak II'. Dimer 2 can be reversibly oxidation causing oxidation peak IV after the initial oxidation; the reduction of this dimer will produce peak II (Wrona, 1990a, Wrona, 1990b).

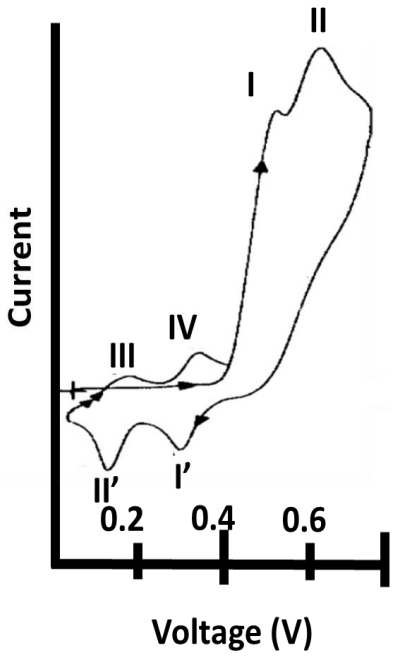

Figure 44: Cyclic voltammogram of 11.47 mM of 5-HT in PBS (pH=2) taken by Wrona et. Al. at 200 mV/s. Original from Figure 1 in Wrona, J. *Electroanal. Chem* (1990) 256. Figure was flipped and annotated for comparison purposes.

5.2 Effect of Scan Rate and Oxidation By-Products on Voltammogram

With the findings made by Wrona et. Al in mind, effects of the scan rate on the oxidation were observed more closely. Figure 45 shows background subtracted voltammograms of 1.0 uM 5-HT in PBS (pH=7.2) taken at 400 V/s, a scan rate commonly used for FSCV using the protocol described in section 2.2.3 on the *WaveNeuro* potentiostat. Panel (a) shows the first detection of 5-HT with a single oxidation peak at 0.7 V reduction at -0.2 V. Panel (b) shows the scan after 800 ms (8 scans), which shows the appearance of 2 more oxidation peaks at 0.1 and 0.4 V. Panel (c), taken after 5.2 seconds (52 scans) shows the same peaks as panel (b) but with the peak at 0.4 V having an amplitude comparable to the peak at 0.7 V. When compared to Wrona's findings in Figure 44, the fast scan voltammogram oxidation and reduction peaks in Figure 45 are farther

apart; this is expected because of the drastic difference in scan rate which tends to increase the difference between the voltage seen at oxidation and the voltage seen at reduction. The loss in the oxidation peak I and reduction I' is likely due to the merger of peak I and II at the faster scan rates. Thus, the initial peak seen in Figure 45 panel (a) is likely due to peaks I and II in Wrona's findings, the initial two step oxidation process. Because all the subsequent reaction either require the 5-HT carbocation to react with another 5-HT molecule or water, it is not surprising that oxidation peaks III and IV do not show up until after several scans are performed. After a few more seconds in scanning peak IV becomes much larger while peak I deigns to decrease in size; this is also expected since peak IV is produced by the oxidation of a dimer which uses up 5-HT that would be seen in peak I+II. Thus, while the reaction in Figure 42 is the most likely reaction to occur at fast scan rates, subsequent reactions of the same fluid can produce the other by-products.

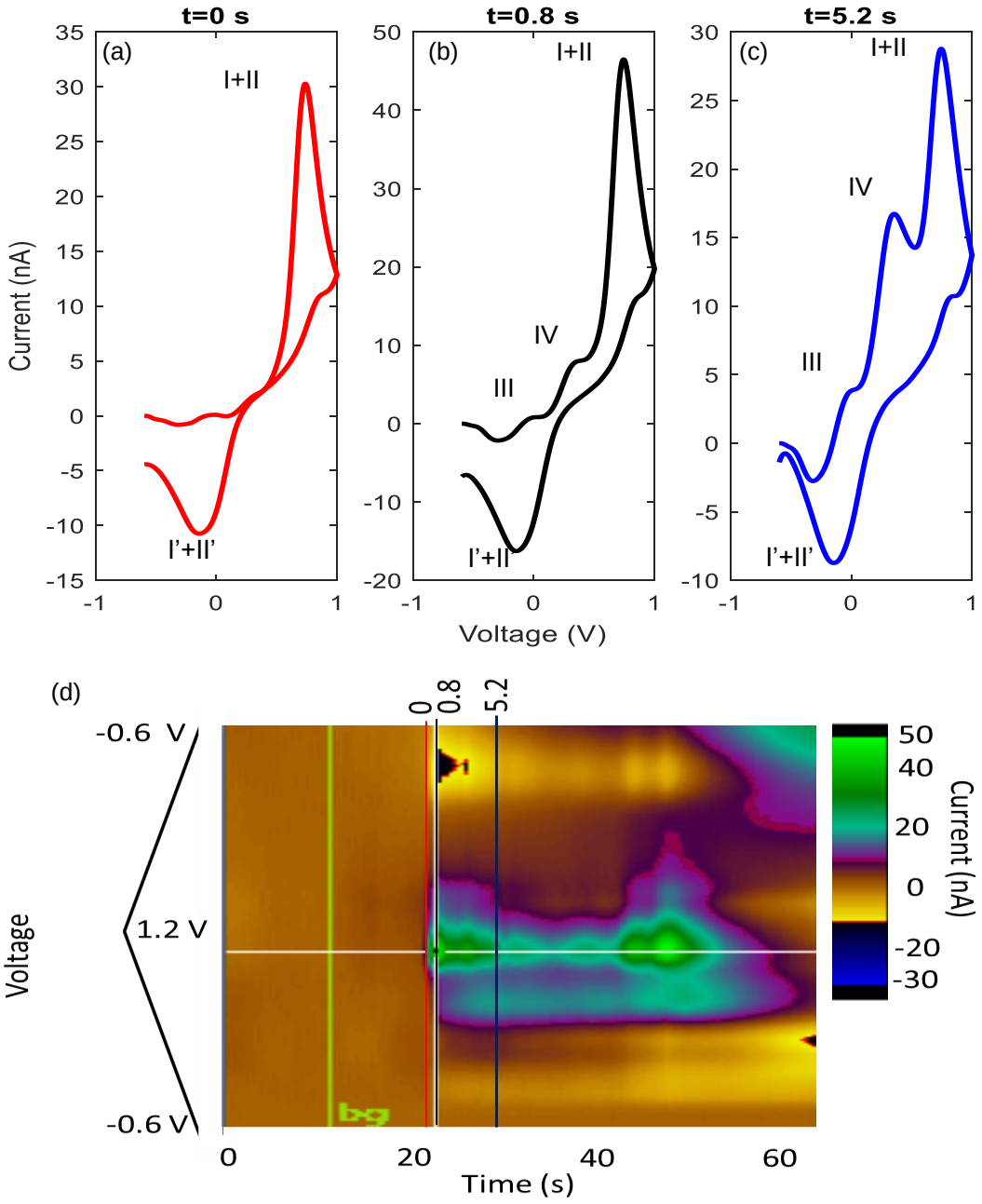

Figure 45: Background subtracted voltammogram of 1.0 µM 5-HT in PBS (pH=7.2) taken at 400 V/s

5.3 Adsorption

Adsorption is the phenomenon of molecules electrostatically interacting with the surface. As discussed in detection 5.1.1, some adsorption and desorption is required for electron transfer and oxidation of the analyte. However, if only adsorption occurs, and no desorption, then, at best, electro-kinetics of the system change. If too much adsorption occurs with no desorption, then these adsorbed molecules can prevent any further oxidation averting any further detection.

5.3.1 Input Waveform

One of the reasons for the limited *in vivo* research of serotonin (5-HT) is due to the difficulty in obtaining repeatable calibration curves due to adsorption of the 5-HT and its by-products onto the surface of the electrode (Güell, 2014; Patel, 2013). This adsorption not only prevents newly present 5-HT from being detected but can also skew concentration if the adsorbed species can be reversibly oxidized and reduced. These types of complications result in difficulty in obtaining a reliable and repeatable calibration curve, which is necessary for determining concentration *in vivo*. As a result, researchers have modified methods for detection by either changing the input waveform or adding coatings to the surface to prevent adsorption.

The traditional 'Dopamine Waveform' has been a triangle waveform that scans at 400 V/s and a frequency of 10 Hz. However, when testing 5-HT, researchers have found that increasing the scan rate could give higher sensitivity without increasing the signal to noise ratio (Bath, 2000). Researchers also found that changing the waveform to start and end at positive voltages increased sensitivity by preventing the adsorption of the positively charged by-products of 5-HT oxidation (Jackson,1995). The traditional waveform used for dopamine, triangle input form from -0.6 V to 1.1 V at 400V/s scan rate pulsing at 10 Hz, was compared to the suggested

waveform for 5-HT detection, a N shape input that ran from 0.2 V to 1.2V to -0.6V back to 0.2V at 800 V/s scan rate pulsing at 10 Hz. This was done using the *WaveNeuro* potentiostat and protocols for FSCV described in section 2.2.3. Figure 46 shows that the triangle waveform produced a secondary oxidation peak implying the formation of dimers and possibly adsorption of these dimers. However, using the N-type waveform showed electrophysiological signal sensing no secondary oxidation peak initially or even after reaching the max current. These results suggest that the N-type waveform and fast scan rate can be used to prevent adsorption and/or formation of dimers that skew the calibration process.

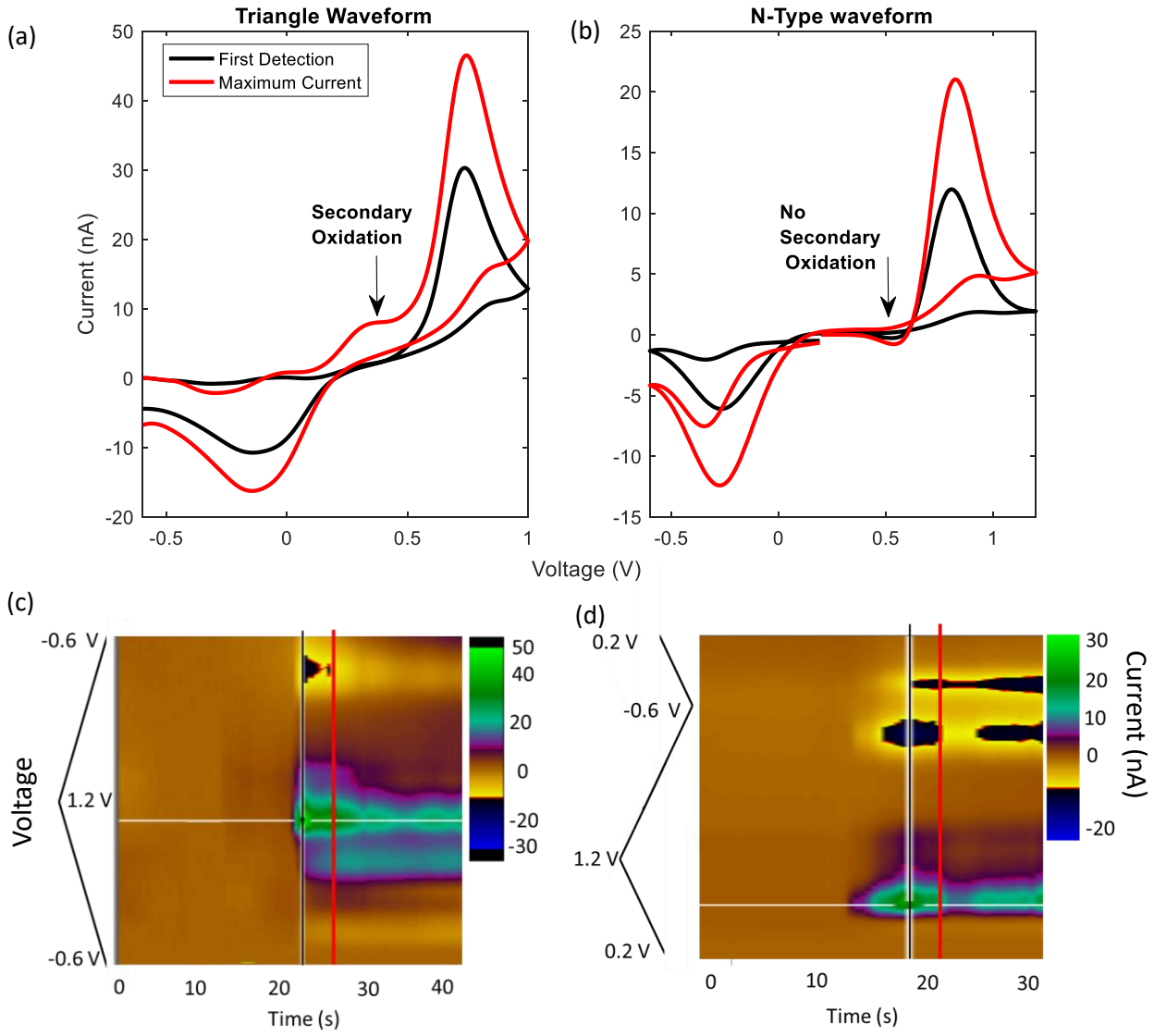

Figure 46: Difference in response to triangle waveform versus a N-type waveform

5.3.2 Nafion coating

Nafion is a perfluorinated polymer with negatively charged sulfonate side chains (Schmidt-Rohr, 2008) that can be coated on an electrode and used as a protective layer to prevent adsorption of positively charged molecules (Jackson, 1995). This polymer has been successfully

used to coat electrodes to prevent the adsorption of 5-HT oxidation by-products (Hashemi, 2009; Jackson, 1995). By preventing adsorption, the polymer can increase the sensitivity to 5-HT by 50 or even 2000 percent (Hashemi, 2009; Jackson, 1995; Phiel, 1996). Figure 47 shows SEM of an electrode that was coated using the protocol described in section 2.2.2. The SEM, taken at 20kV shows that the Nafion coating not only fully covers the electrode surface, but also increases the overall surface area.

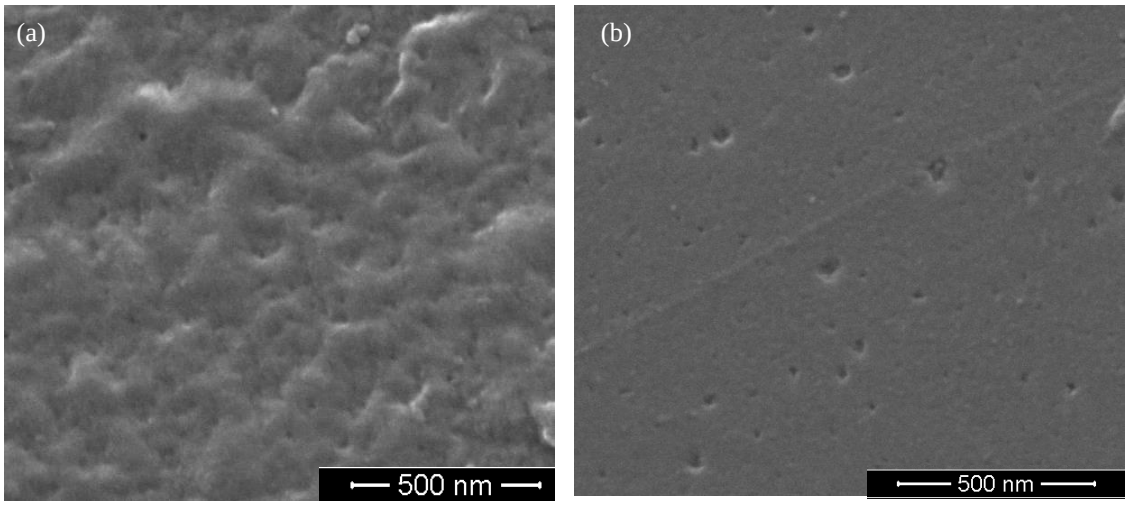

Figure 47: (a) SEM of Nafion Coated Electrode. (b) Same electrode with no Nafion coating

Using the *NeuroWave* potentiostat and protocols for FSCV discussed in section 2.2.3, the FSCV of Nafion coated and bare glassy carbon electrodes were taken at 800 V/s using the N type waveform in a solution of PBS and 1 µM of 5-HT.

Figure 48 shows that the Nafion deposition did slightly increase the sensitivity to the 5-HT. Furthermore, from the voltammograms, a shift in the voltage of the peak current is apparent. While a shift in the whole curve (oxidation and reduction voltage) can be caused by changes in scan rate, reference electrode, or pH changes, in this case the shift only affects the oxidation

voltage implying that the shift in the peak is actually the addition of the primary oxidation and the secondary oxidation peak discussed in the previous section. Therefore, even though the presence of secondary oxidation peak is not completely apparent, the shift in the oxidation voltage implies that the bare glassy carbon is more susceptible to secondary oxidation and thus adsorption.

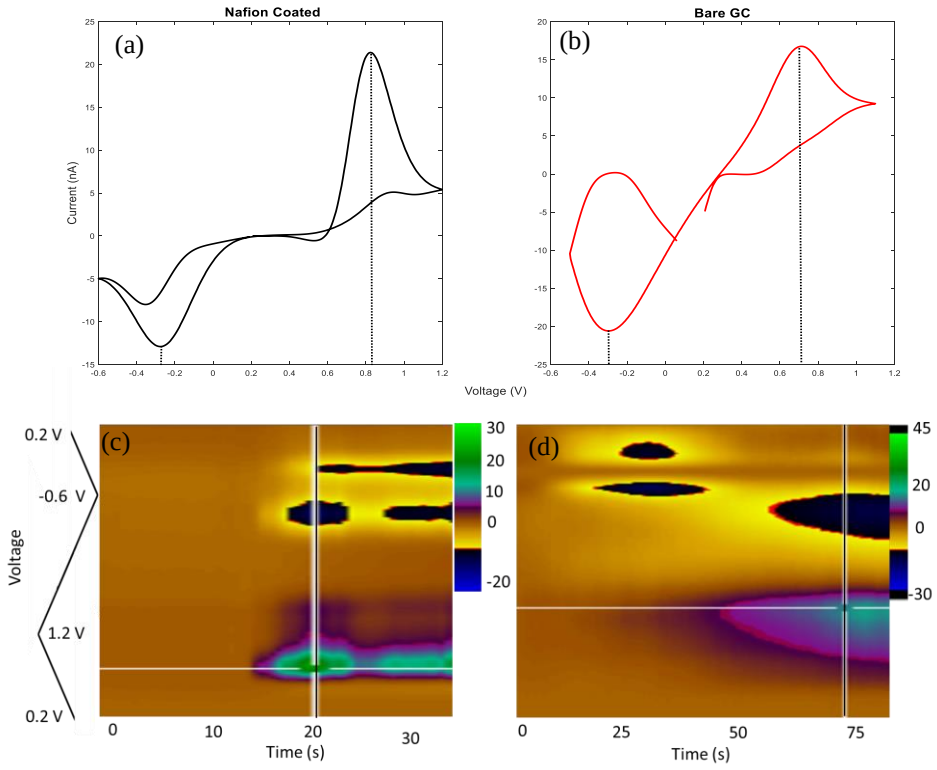

Figure 48: Background subtracted Voltammograms of (a) Nafion coated and (b) bare GC electrodes and false color plot of (c) Nafion coated and (d) bare GC electrodes

It is important to note that Nafion has other advantages. As discussed in chapter 4, Nafion can also decreases impedance and increases charge storage capacity. Furthermore, this coating also has the ability to prevent fouling by extracellular metabolites like 5-hydroxyindole acetic acid (5-HIAA) by preventing direct interaction with the metabolites (Hashemi, 2009). However,

other researchers have noted disadvantages to Nafion coating electrodes. For example, by adding this extra barrier, the charge transfer becomes a function of the coating rather than the electrode; if the polymer is applied too thick, a diffusional barrier is created decreasing the response time of the electrode (Pihel, 1996). While these affects were not seen in our experiments, it is possible that the thickness of the Nafion deposited using the methods described in section 2.32 just was thin enough to have no noticeable effect on the temporal response.

5.4 Surface modification for increasing sensitivity to neurotransmitters

In preparation of *in vivo* testing, the characteristics of the carbon surface was modified in hopes of increasing the electrochemical sensitivity to neurotransmitters (such as 5-HT). Since the sensitivity of the carbon electrode has much to do with its ability to electrostatically interact with the 5-HT cation, as described in section 5.1.1, adding more functional groups could increase the electrode's sensitivity the neurotransmitter. By increasing surface porosity, the number of terminating graphitic planes is increased; since each terminus has at least one functional group, increasing porosity should effectively increase sensitivity to 5-HT.

5.4.1 Pyrolysis Nitrogen Flow rate

One method for increasing porosity is by modifying the pyrolysis parameters such as gas flow rate. Increasing the flow of the inert gas during pyrolysis seems to have the effect of increasing the porosity on the surface of the electrode without impacting electrical impedance (Huynh, 2017). Thus, the sensitivity to 5-HT was compare on electrodes pyrolyzed with a gas (nitrogen) flow rate at 15 sccm and 40 sccm. First glassy carbon electrode arrays were fabricated using the pyrolysis processes described in 2.1.1 and fabrication protocol as described in section

2.2.5. After Nafion coating was completed on each device as described in section 2.3.2, calibration curves were generated using the *WaveNeuro* potentiostat and protocols described in section 2.3.3.

Results show that by increasing the gas flow rate, sensitivity of the carbon electrode can be increased. Figure 49 has SEM of two electrodes before Nafion coating. These images show that the change in pyrolysis flow rate was able to alter the surface roughness substantially. Figure 50 shows that sensitivity increased from 0.009 nA/nM for carbon generated under 15 scmm to 0.019 nA/nM for carbon generated under 40 sccm.

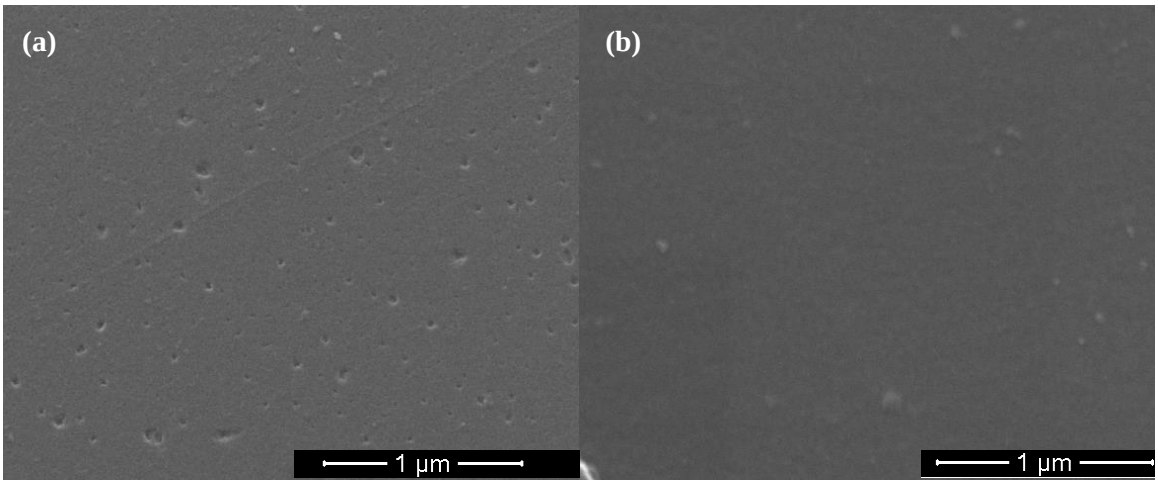

Figure 49: SEM of Glassy Carbon pyrolyzed at (a) 40 sccm (b) and 15 sccm

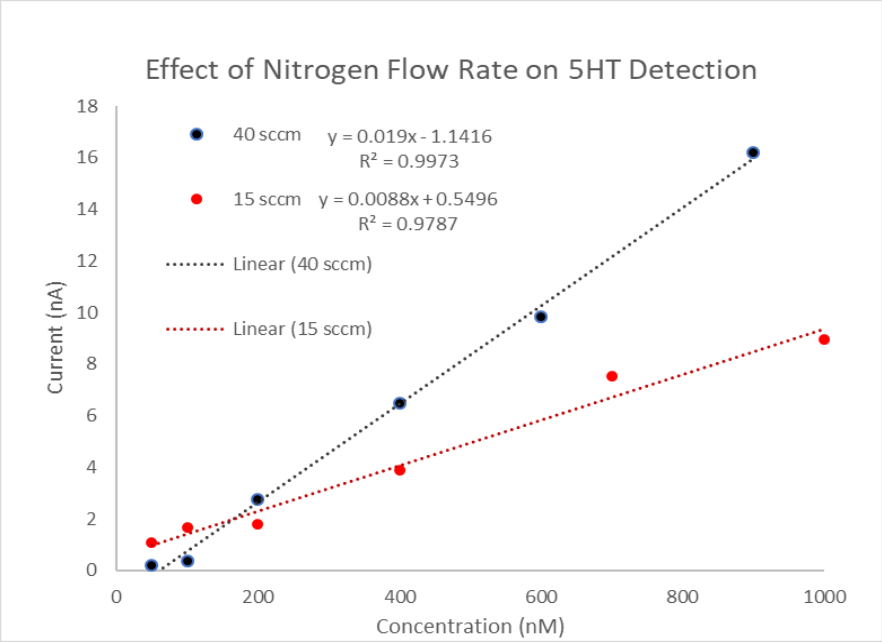

Figure 50: Calibration Curve for 5-HT Detection on GC electrodes pyrolyzed at 15 sccm and 40 scmm nitrogen flow are

5.4.2 Oxygen Plasma etching

Oxygen plasma etching has been known to increase oxygen containing functional groups by inducing defects onto the surface. The physical change in the surface can be seen clearly in the SEM images in Figure 51. Figure 51 (a) shows the microelectrode after oxygen plasma

etching and Figure 51 (b) shows another microelectrode without oxygen plasma etching.

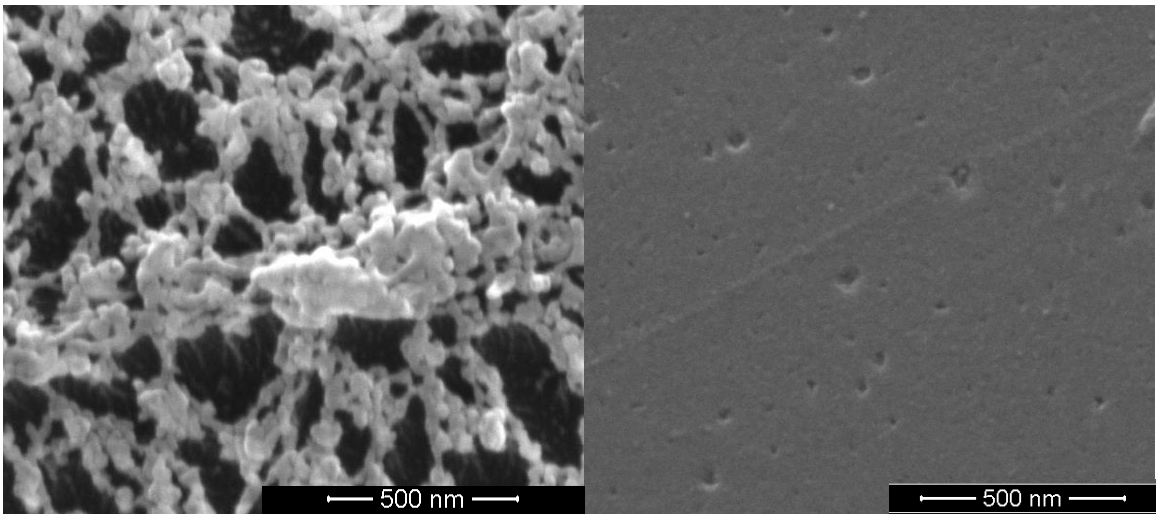

Figure 51: SEM of (a) Plasma Etched (at 100W for 5 min) Glassy Carbon and (b) Non-Plasma Etched Glassy Carbon

Microelectrodes were calibrated using the *WaveNeuro* potentiostat and calibration methods described in section 2.2.3. After the initial calibration curve was generated, the same electrode was oxygen plasma etched at 100 mW for 120 s. After plasma etching, another calibration was performed. Figure 52 shows an example of how the calibration parameters changed after plasma etching. While the change in the slope of the linear fit suggests an increase in sensitivity after oxygen plasma etching, the dramatic drop in the R^2 value suggests that this linear fit may not be reliable; this is most likely caused by the oxygen plasma etching damaging the polyimide insulation. Once the polyimide insultation is damaged, the polyimide is more likely to uptake water which would allow more access of the electrolyte to the insulated carbon and metal trace. This would give the appearance of higher sensitivity but would make the measurements less reliable. Another possibility is that the plasma etching increased the porosity to a point where even though adsorption happened more readily, desorption became difficult,

resulting in less surface area for oxidation and electron transfer and a non-linear fit. Thus, while oxygen plasma etching the surface may increase sensitivity, further testing is needed to determine whether or not adjusting the etching parameters can produce a more sensitive and still a reliable electrode.

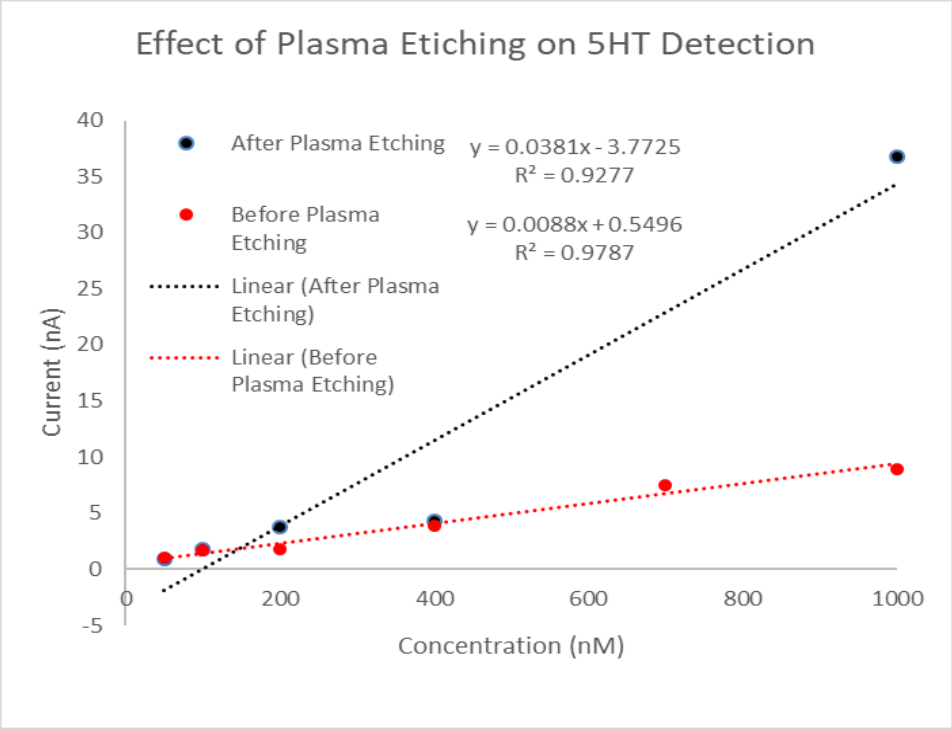

Figure 52: Effect of plasma etching

Investigation into the fundamental mechanisms behind neurotransmitter detection using fast scan cyclic voltammetry gives great insight into ways to improve sensitivity to electrochemical oxidation of neurotransmitters. By looking at the electrostatic potential map, it is clear that inducing functional groups greatly changes the dipole moment of the surface and would theoretically improve the reversible adsorption required to oxidized the analyte. Therefore, by introducing changes into the surface properties of the carbon through pyrolysis

protocol modification and post-fabrication oxygen plasma etching, the phenomena behind the reversible adsorption can be increased thus increasing sensitivity to electro-oxidation of neurotransmitters. The electrostatic potential simulations, however, do not show why electrodes tend to be less sensitive to 5-HT oxidation than dopamine oxidation. This is elucidated by looking at the various irreversible reactions that happen after 5-HT oxidation, leading to the formation of byproducts that can irreversibly adsorb onto the surface. To minimize the irreversible adsorption, modifications to the input waveform can allow for some of the byproducts to be pushed off by ending and holding the electrode at a positive potential. Furthermore, Nafion coating allows for a positively charged barrier to prevent irreversible adsorption.

CHAPTER 6

In-Vivo Testing

In the chapter, electrodes were tested on animal models. Electrophysiology and electrochemistry were tested at the University of California San Diego (UCSD) on a European starling. Stimulation tests were done at the University of Washington (UW) on a rat model. All tests were completed following Institutional Animal Care and Use Committee (IACUC) protocols.

6.1 Glassy Carbon and Electrophysiology

Electrophysiological signal recording was done using a surface glassy carbon electrode fabricated using the protocol described in 2.2.4. This electrode was placed on the HVc area of a European songbird (Starling) as shown in Figure 53. The HVc area of songbirds associated with song learning and song production (De Groof, 2016; Kubikova, 2010). Thus, after an initial recording was done during quiet time for baseline, the electrophysiological response to the audio stimulus was recorded. This stimulated signal is show in Figure 54 (a). Figure 54 (b) shows a data filtered to for alpha and beta frequencies (bellow 30 Hz) using a lowpass filter in Matlab. The filtered data show stereotypical beta burst that are often seen during a time when animal is being stimulated. From this data we can conclude that glassy carbon can reliably collect electrophysiological signals.

Figure 53: Surface Electrode on Songbird Cortex

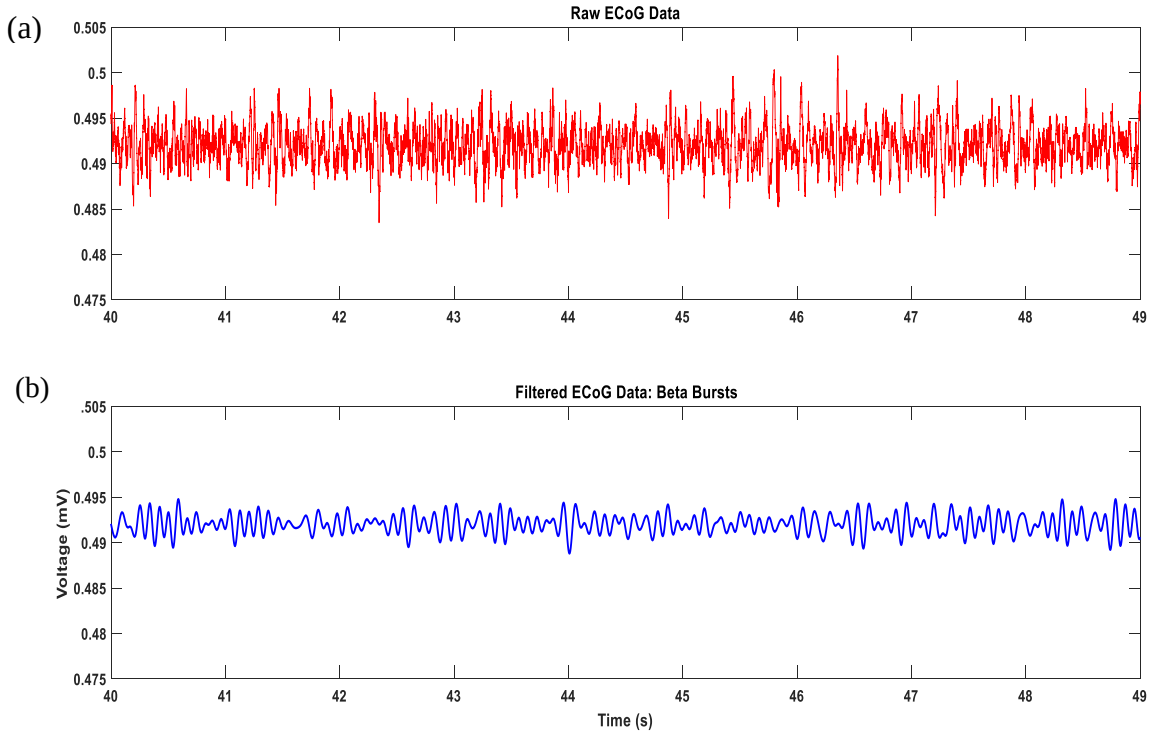

Figure 54: (a) Raw ECoG data (b) Beta Burst from ECoG signal

6.2 Glassy Carbon and Electrical Stimulation

In order to stimulate the spinal cord, the device needs to penetrate neural tissue. The 12 channel PeGESaS design, detailed in section 2.1.2, was designed for penetration into the rat spinal cord. In order to penetrate both sides of the of the device, the device needed to be bent and held in place. This was done by applying a small drop of polydimethylsiloxane (PDMS) to the center of the head, heating it for 20 seconds with a heat gun, then bending the device and fully curing the PDMS by heating for another 20 seconds with a heat gun. PDMS was prepared using the standard 10 to 1 ratio of polymer to curing agent. Penetration ability was tested using a 1% agar, a stiffness that is higher than the modulus of grey matter (Chen, 2011). As seen in Figure 55, this probe could penetrate to a depth of 1 mm after bending.

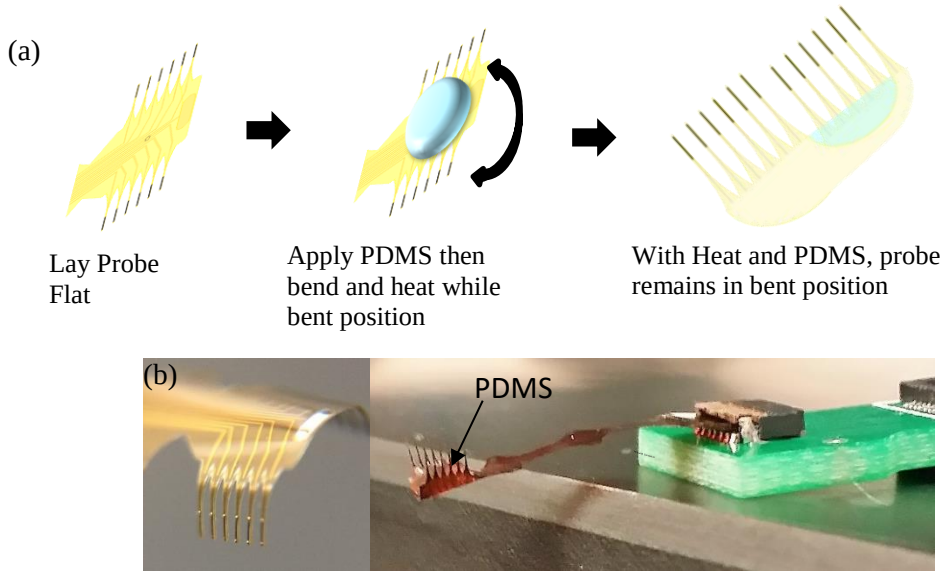

Figure 55: (a) Process for Bending the PeGeSaS Probe (b) Image of bent probe

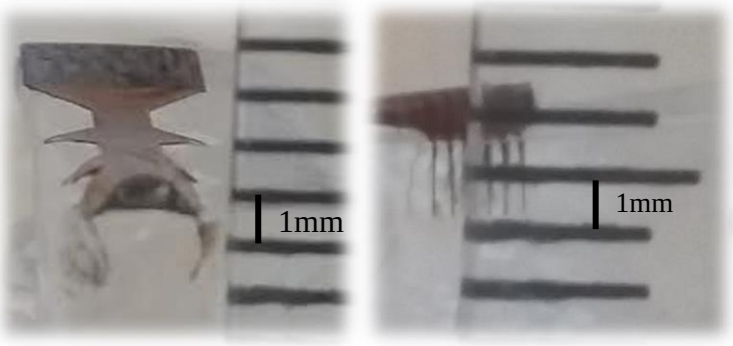

Figure 56: Penetration of PeGESaS probe into 1% agar

Electrical stimulation is often used in *in vivo* studies to stimulate a set of neurons; subsequently an electrophysiological, electrochemical signal, or physical changes are monitored determine the response of the stimulus. Glassy carbon 12-channel PeGESaS array was implanted in a rat cervical spinal cord, as shown in Figure 57, to determine the glassy carbon's effectiveness as a stimulating electrode. After implant, the amount of current required to induce a physical twitch was recorded. Table 8 shows that the maximum current required to induce a triceps twitch remained below 200 µA and at some channels required as little as 120 µA. This current is comparable to the 150-200 µA required when a 30 µm wide iridium wire was place in a similar location, or the 390-450 µA required by when using 200 µm stainless steel wires (Linderoth, 1995). Thus, initial *in vivo* testing suggests that not only can the glassy carbon probe penetrate the spinal cord, but it can also act as an electrical stimulator just as or more efficiently than stimulators currently used in research.

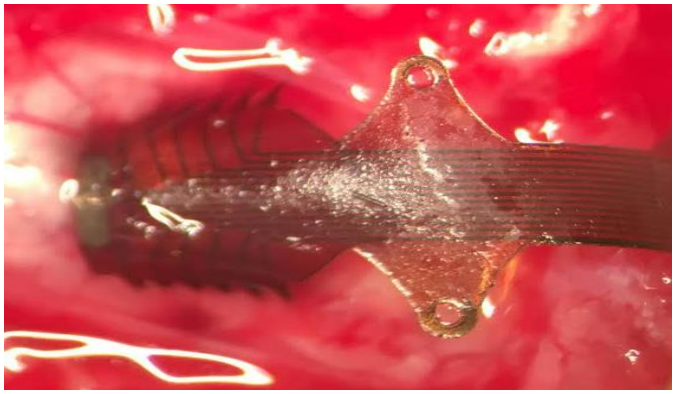

Figure 57: Penetration of PeGESaS probe into rat cervical spine

Table 8: Stimulation threshold measured for all 12 channels of implanted PeGESaS array

Ch	Threshold (µA)	Action	Cross Midline threshold
1	190	R Tricep	N/A
2	170	R Tricep	N/A
3	170	R Tricep	N/A
4	170	R Tricep	N/A
5	150	L Tricep	170
6	150	L Tricep	170
7	130	L Tricep	210
8	130	L Tricep	210
9	120	L Tricep	210
10	120	L Tricep	220
11	130	L Tricep	250
12	150	L Tricep	250

6.3 *In vivo* Electrochemistry

In vivo electrochemistry data was collected on a European starling using the penetrating PeGESaS Acute design described in section 2.1.3. The penetrating electrodes penetrated about 0.5 mm down in the hyperpallium near the HVc area of the brain as shown in Figure 56.

Data was collected using the WaveNeuro potentiostat using a triangle input waveform from -0.5 V to 1.3 V and a scan rate of 400 V/s. A platinum wire was used a counter/reference electrode.

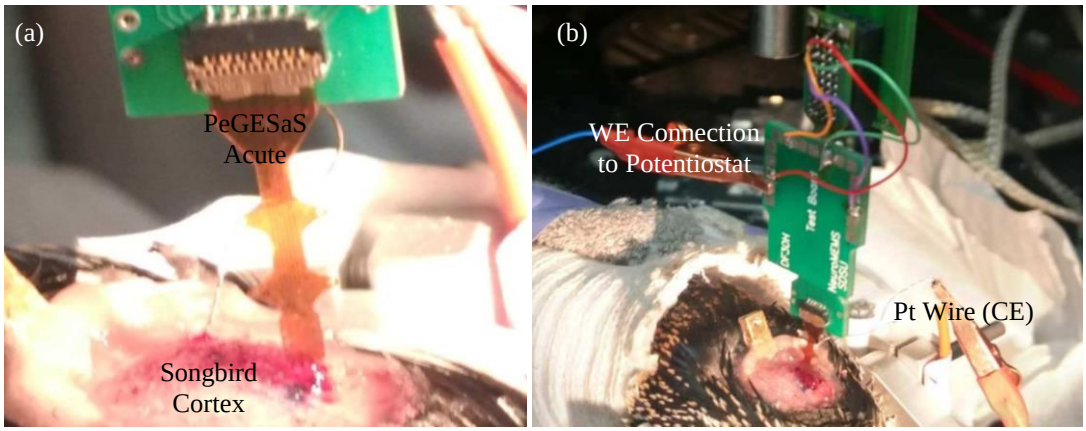

Figure 58: (a)PeGESaS Acute implanted in Songbrird (b) Working Electrode (WE) and Counter Electrode (CE) connections to potentiostat

Figures 59 thru 63 show oxidation voltages collected in the European songbird. Since the implant was near the HVc where dopaminergic and serotonergic neurons exist (Dutar, 1998; Kubikova, 2010). Thus, dopamine and 5-HT are among the electroactive compounds that could exist in this area. However, in addition to dopamine and 5-HT, are other signaling molecules like adenosine, histamine, norepinephrine, epinephrine, and metabolic byproducts like ascorbic acid and peroxide. Therefore, when attempting to determine the electroactive compound in Figures

59-63, other common signaling molecules and their oxidation voltages were considered as shown in table 9.

Figure 59 shows an oxidation voltage of about 0.45 volts. This oxidation produced the highest current during the experiment indicating a high concentration of some electroactive species. When compared to other literature, this peak best corresponds to the oxidation voltage of dopamine. Since the HVc has some dopaminergic neurons and its neural projections through the hyperpallium, a high concentration of dopamine is possible. However, Figure 60 shows a peak at about 0.55 V and the characteristic dopamine reduction peak at -0.2 V. This image suggests that the 0.45V oxidation peak is either another analyte, or the oxidation voltage of the dopamine is somehow decreased. Over time, a pH shift can cause drift in the oxidation voltage (Salimi, 2006). This is a likely scenario since the animal experiences localized pH changes in response to injury. However, a pH shift does not explain the missing reduction peak. Figure 61 shows what looks to be the oxidation of ascorbic acid at about 0.25 V. This peak is also very large in current and could shift down the dopamine peak if the concentration was large enough.

Table 9: Neurochemicals and their various oxidation voltages

Neurochemical	*Oxidation Voltage*	*Carbon electrode*	*Reference Electrode*	*Reference*
Serotonin	0.65	Carbon Fiber	Ag/AgCl	(Abdalla,2017)
	0.65	Carbon Fiber	Ag/AgCl	(Fang 2013)
	0.5-0.6V	Carbon Fiber	Ag/AgCl	(Griessenauer, 2010)
	0.8	Carbon Fiber	Ag/AgCl	(Van Gompel, 2010)
	0.45-0.65 (Variable Scan rate)	Carbon Fiber	Ag/AgCl	(Jackson,1995)
Dopamine	0.46	Carbon Fiber	Ag/AgCl	(Schmidt, 2013)
	0.34	Carbon Yarn	Ag/AgCl	(Schmidt, 2013)
	0.6	Carbon Fiber	Ag/AgCl	(Van Gompel, 2010)
	0.6	Carbon Fiber	Ag/AgCl	(Fang, 2013)
Adenosine	1V, 1.5V	Carbon Fiber	Ag/AgCl	(Swamy, 2007)
	1V, 1.5V	Carbon Fiber	Ag/AgCl	(Fang, 2013)
Histamine	1.2-1.3 V	Carbon Fiber	Ag/AgCl	(Chang, 2012)
Epinephrine	0.6 V	Carbon Fiber	Ag/AgCl	(Taleat, 2017)
Peroxide	1.1-1.3V (variation due to scan rate)	Carbon Fiber	Ag/AgCl	(Sanford, 2010)
Ascorbic Acid	0.24 V	Glassy Carbon	SCE	(Downard,1995)
	0.34 V	Carbon Fiber	Ag/AgCl	(Schmidt, 2013)
	0.3	Carbon Yarn	Ag/AgCl	(Schmidt, 2013)

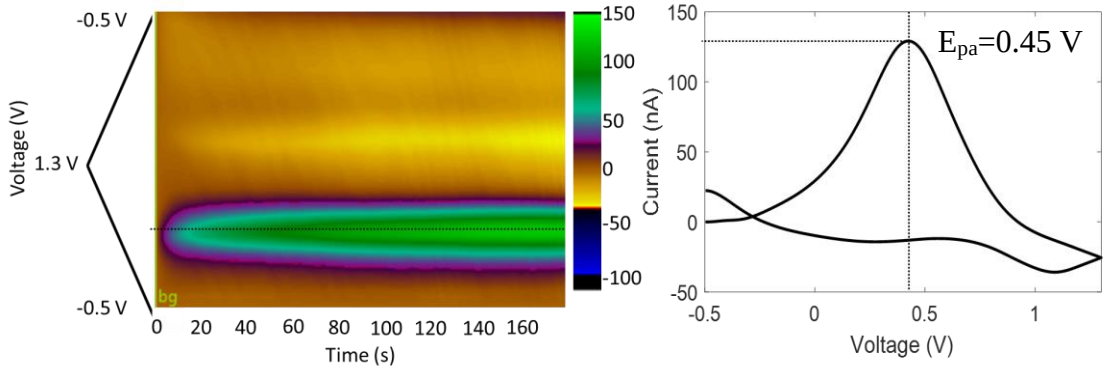

Figure 59: Possible detection of dopamine

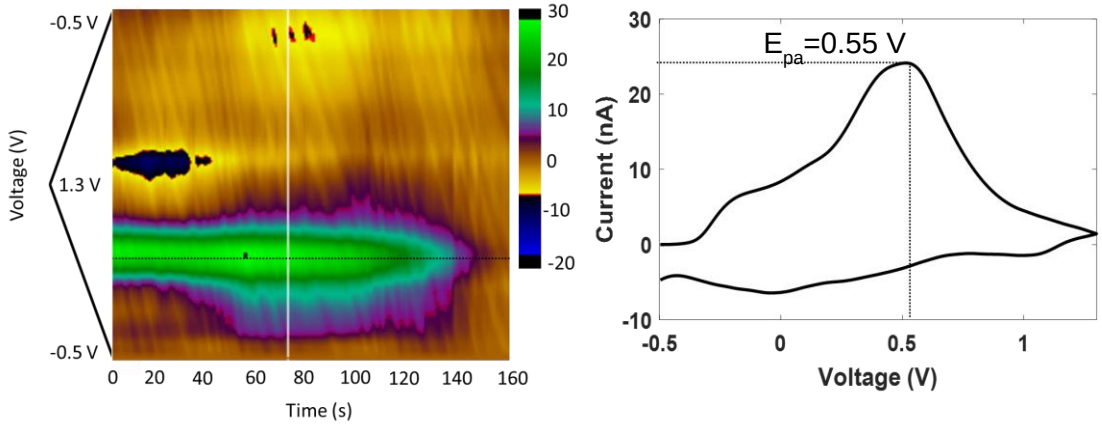

Figure 60: Detection of Dopamine

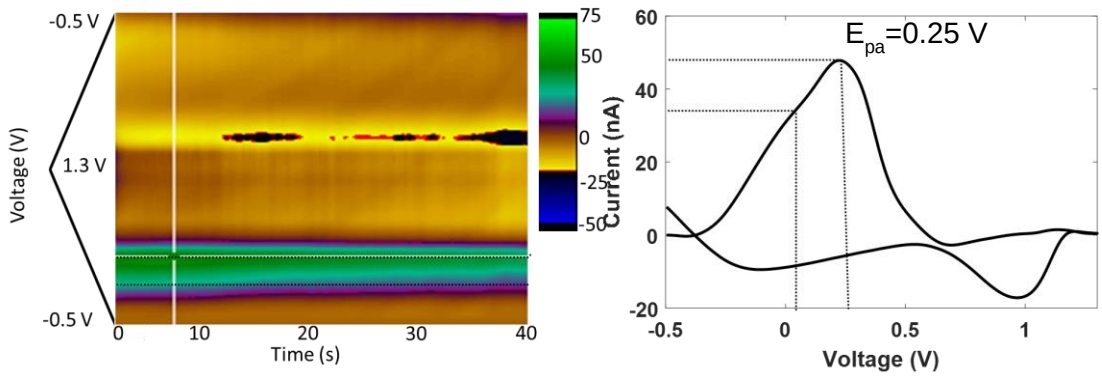

Figure 61: Oxidation of Ascorbic Acid

While serotonin (5-HT) is not widely studied in the HVc portion of the songbird brain, there has been some evidence of serotonergic neurons in the nucleus (Dutar, 1998). Thus, while the signal would be very small, it was still possible to pick up some signal from 5-HT. Two oxidations were found at about 0.7 V. Figure 62 shows the presence of 5-HT, however, the additional peaks at about 1.1 and 0.4 also indicate the presence of other neurochemicals which could obscure the reduction peak around 0 V to confirm that the oxidation was indeed 5-HT. However, Figure 63 shows a peak at 0.7 V and the reduction peak at 0 V indication a small concentration of 5-HT detected in the songbird brain.

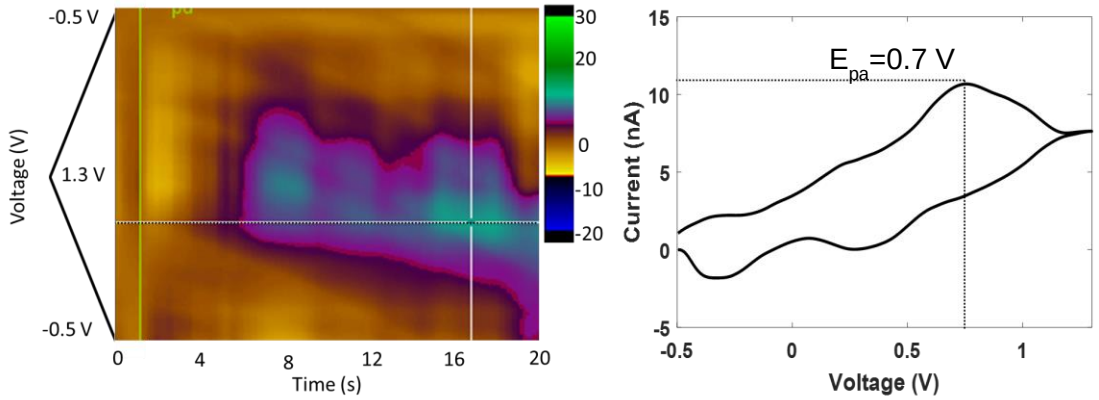

Figure 62: *In vivo* Detection of Serotonin

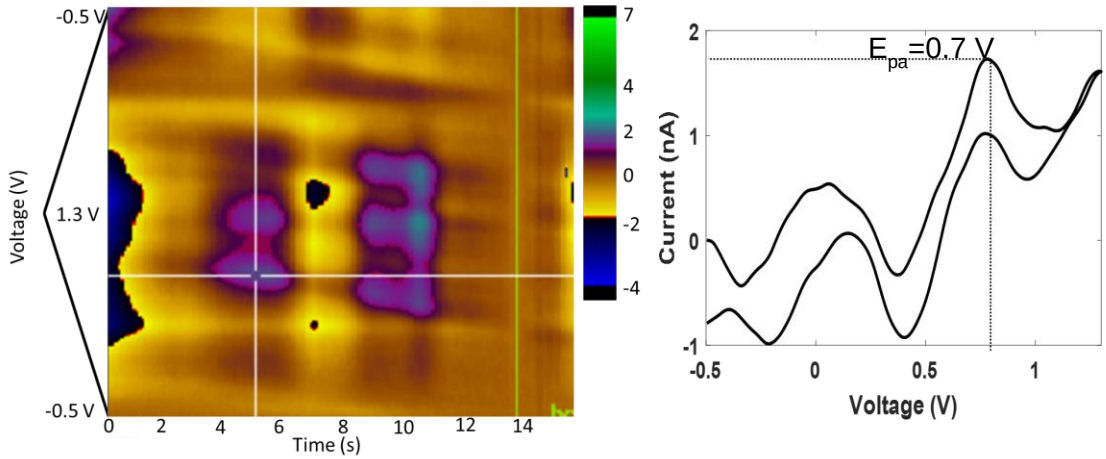

Figure 63: Second Detection of Serotonin

Figures 58 through 62 confirm the ability for glassy carbon to detect neurotransmitters *in vivo*. However, to use this measurement reliably, control tests using microdialysis would be necessary to ensure that the correlations between oxidation voltages and analyte species does not change dramatically when comparing *in vivo* to *in vitro* measurements.

CHAPTER 7

Summary and Conclusion

The research presented demonstrated the ability to generate glassy carbon microelectrodes arrays for the purposes of multi-modal neural signal detection and stimulation. First, protocols were developed to generate penetrating electrodes that could be implanted in a spinal cord or cortex. The body of the design was then modified for the specific application, PeGESaS for long term implants in the spinal cord, and PeGESaS Acute for either short term implant in the spinal cord or cortex, or long term in the cortex. The fabrication process was then optimized determining the bonding between the glassy carbon and the substrate material, polyimide. Through a study with FTIR, the interface bonds were found to include:

1. Hydrogen bonding through hydroxyls and carboxylic acid dimers
2. Cyclic anhydrides that could form without plasma etching
3. Anhydride or Ether linkages that would form as a result of plasma etching and heating.

Once a reliable probe could be fabricated, *in vitro* tests were performed. These studies showed that:

1. The probe could reliably detect 5-HT
2. Nafion coating and increasing scan rate greatly assisted in detecting 5-HT in the nanomolar range.
3. 5-HT and electrophysiological data could be collected simultaneously

Finally, the fundamental mechanisms behind neurotransmitter detection were investigate to determine the optimal set-up for *in vivo* experiment. These fundamental studies revealed that:

1. while dopamine and 5-HT should be theoretically detected in the same manner, subsequent oxidations of 5-HT cause deviations of this theory.
2. Changes to the input waveform, scan rate and starting and ending potentials could prevent oxidation of the 5-HT byproducts
3. Surface modifications to the glassy carbon, such as increasing porosity and coating the surface with Nafion to prevent irreversible adsorption, were determined to be methods for reliably increasing the probe's sensitivity to 5-HT oxidation and thus reliability of probe as an electrochemical sensor.

Finally, acute *in vivo* tests were performed to show that glassy carbon could indeed record electrophysiological signals, stimulate, and electrochemically detect neurotransmitters like dopamine and 5-HT.

Collectively, the results reported in this research demonstrate that glassy carbon offers a compelling microelectrode material for multi-modal detection and stimulation applications.

REFERENCES

Abdalla, Aya, Christopher W. Atcherley, Pavithra Pathirathna, Srimal Samaranayake, Beidi Qiang, Edsel Peña, Stephen L. Morgan, Michael L. Heien, and Parastoo Hashemi. "*In vivo* Ambient Serotonin Measurements at Carbon-Fiber Microelectrodes." *Analytical chemistry* 89, no. 18 (2017): 9703-9711.

Bath, Bradley D., Darren J. Michael, B. Jill Trafton, Joshua D. Joseph, Petrise L. Runnels, and R. Mark Wightman. "Subsecond adsorption and desorption of dopamine at carbon-fiber microelectrodes." *Analytical chemistry* 72, no. 24 (2000): 5994-6002.

Belle, Anna M., Catarina Owesson-White, Natalie R. Herr, Regina M. Carelli, and R. Mark Wightman. "Controlled iontophoresis coupled with fast-scan cyclic voltammetry/electrophysiology in awake, freely moving animals." *ACS chemical neuroscience* 4, no. 5 (2013): 761-771.

Branner, A., Stein, R. B., & Normann, R. A. (2001). Selective stimulation of cat sciatic nerve using an array of varying-length microelectrodes. *Journal of neurophysiology*, 85(4), 1585-1594.

Chang, Su-Youne, Inyong Kim, Michael P. Marsh, Dong Pyo Jang, Sun-Chul Hwang, Jamie J. Van Gompel, Stephan J. Goerss et al. "Wireless fast-scan cyclic voltammetry to monitor adenosine in patients with essential tremor during deep brain stimulation." In *Mayo Clinic Proceedings*, vol. 87, no. 8, pp. 760-765. Elsevier, 2012.

Chang, Su-Youne, Taylor Jay, Joel Muñoz, Inyong Kim, and Kendall H. Lee. "Wireless fast-scan cyclic voltammetry measurement of histamine using WINCS–a proof-of-principle study." *Analyst* 137, no. 9 (2012): 2158-2165.

Chen, C.H., Chuang, S.C., Su, H.C., Hsu, W.L., Yew, T.R., Chang, Y.C., Yeh, S.R. and Yao, D.J., 2011. A three-dimensional flexible microprobe array for neural recording assembled through electrostatic actuation. *Lab on a Chip*, 11(9), pp.1647-1655.

Chen, Changlun, Bo Liang, Akihisa Ogino, Xiangke Wang, Masaaki Nagatsu, Changlun Chen, et al. 2009. “Oxygen Functionalization of Multiwall Carbon Nanotubes by Microwave-Excited Surface-Wave Plasma Treatment Oxygen Functionalization of Multiwall Carbon Nanotubes by Microwave-Excited Surface-Wave Plasma Treatment.” doi:10.1021/jp9012015.

Chen, Qidao, Liming Dai, Mei Gao, Shaoming Huang, and Albert Mau. "Plasma activation of carbon nanotubes for chemical modification." The Journal of Physical Chemistry B 105, no. 3 (2001): 618-622.

Chen, Shen-Ming, and Kuo-Tzu Peng. "The electrochemical properties of dopamine, epinephrine, norepinephrine, and their electrocatalytic reactions on cobalt (II) hexacyanoferrate films." *Journal of Electroanalytical Chemistry* 547, no. 2 (2003): 179-189.

Chong Tai, and V. Reggie Edgerton. "Development of a multi-electrode array for spinal cord epidural stimulation to facilitate stepping and standing after a complete spinal cord injury in adult rats." *Journal of neuroengineering and rehabilitation* 10, no. 1 (2013): 2.

Cogan, Stuart F. "*Neural Stimulation and Recording Electrodes*." Annu. Rev. Biomed. Eng. 10 (2008): 275-309.

Colthup, N. B. "Spectra-structure correlations in the infra-red region." JOSA 40, no. 6 (1950): 397-400.

De Groof, Geert, Isabelle George, Sara Touj, Martin Stacho, Elisabeth Jonckers, Hugo Cousillas, Martine Hausberger, Onur Güntürkün, and Annemie Van der Linden. "A three-dimensional digital atlas of the starling brain." *Brain Structure and Function* 221, no. 4 (2016): 1899-1909.

De La Torre, J. C. "Spinal Cord Injury: Review of Basic and Applied Research." *Spine* 6, no. 4 (1981): 315-335.

Deepthi, R., Bhargavi, R., Jagadeesh, K. and Vijaya, M.S., 2010. Rheometric studies on agarose gel-a brain mimic material. *SASTECH Journal*, 9(2), pp.27-30.

DeWaele, Mark, Yoonbae Oh, Cheonho Park, Yu Min Kang, Hojin Shin, Charles D. Blaha, Kevin E. Bennet, In Young Kim, Kendall H. Lee, and Dong Pyo Jang. "A baseline drift detrending technique for fast scan cyclic voltammetry." *Analyst* 142, no. 22 (2017): 4317-4321.

Downard, Alison J., Alisa D. Roddick, and Alan M. Bond. "Covalent modification of carbon electrodes for voltammetric differentiation of dopamine and ascorbic acid." *Analytica Chimica Acta* 317, no. 1-3 (1995): 303-310.

Du, Jiao, Ruirui Yue, Fangfang Ren, Zhangquan Yao, Fengxing Jiang, Ping Yang, and Yukou Du. "Novel graphene flowers modified carbon fibers for simultaneous determination of ascorbic acid, dopamine and uric acid." *Biosensors and bioelectronics* 53 (2014): 220-224.

Dutar, Patrick, Huan M. Vu, and David J. Perkel. "Multiple cell types distinguished by physiological, pharmacological, and anatomic properties in nucleus HVc of the adult zebra finch." *Journal of Neurophysiology* 80, no. 4 (1998): 1828-1838.

Economou, A., S.d Bolis, C.e Efstathiou, and G.j Volikakis. "A “virtual” Electroanalytical Instrument for Square Wave Voltammetry." *Analytica Chimica Acta* 467, no. 1-2 (2002): 179-88. doi:10.1016/s0003-2670(02)00191-5.]

Fang, Huaifang, Megan L. Pajski, Ashley E. Ross, and B. Jill Venton. "Quantitation of dopamine, serotonin and adenosine content in a tissue punch from a brain slice using capillary electrophoresis with fast-scan cyclic voltammetry detection." *Analytical Methods* 5, no. 11 (2013): 2704-2711.

Fattahi, P., Yang, G., Kim, G. and Abidian, M.R., 2014. A review of organic and inorganic biomaterials for neural interfaces. *Advanced Materials*, 26(12), pp.1846-1885.

Ferrari, Andrea C., and Jf Robertson. "Interpretation of Raman spectra of disordered and amorphous carbon." *Physical review B* 61, no. 20 (2000): 14095.

Franklin, Rosalind E. "The structure of graphitic carbons." *Acta crystallographica* 4, no. 3 (1951): 253-261.

Gad, Parag, Jaehoon Choe, Mandheerej Singh Nandra, Hui Zhong, Roland R. Roy, Yu-Chong Tai, and V. Reggie Edgerton. "Development of a multi-electrode array for spinal cord epidural stimulation to facilitate stepping and standing after a complete spinal cord injury in adult rats." *Journal of neuroengineering and rehabilitation* 10, no. 1 (2013): 2.

Gillingham, Estelle L., David M. Lewis, and Bojana Voncina. "An FTIR study of anhydride formation on heating butane tetracarboxylic acid in the presence of various catalysts." *Textile Research Journal* 69, no. 12 (1999): 949-955.

Goldberg, Ethan M., and Douglas A. Coulter. "Mechanisms of epileptogenesis: a convergence on neural circuit dysfunction." *Nature Reviews Neuroscience* 14, no. 5 (2013): 337.

Griessenauer, Christoph J., Su-Youne Chang, Susannah J. Tye, Christopher J. Kimble, Kevin E. Bennet, Paul A. Garris, and Kendall H. Lee. "Wireless Instantaneous Neurotransmitter Concentration System: electrochemical monitoring of serotonin using fast-scan cyclic voltammetry-a proof-of-principle study: Laboratory investigation." *Journal of neurosurgery* 113, no. 3 (2010): 656-665.

Güell, Aleix G., Katherine E. Meadows, Petr V. Dudin, Neil Ebejer, Joshua C. Byers, Julie V. Macpherson, and Patrick R. Unwin. "Selection, characterisation and mapping of complex electrochemical processes at individual single-walled carbon nanotubes: the case of serotonin oxidation." *Faraday discussions* 172 (2014): 439-455.

Hashemi, Parastoo, Elyse C. Dankoski, Jelena Petrovic, Richard B. Keithley, and R. M. Wightman. "Voltammetric detection of 5-hydroxytryptamine release in the rat brain." A*nalytical chemistry* 81, no. 22 (2009): 9462-9471.

Hetke, Jamille F., Daryl R. Kipke, David S. Pellinen, and David J. Anderson. "Modular multichannel microelectrode array and methods of making same." U.S. Patent 7,941,202, issued May 10, 2011.

Hirabayashi, M., Huynh, NH., Witsell, S., Perez, A., Sandoval, L., Yamada, N., Kassegne, S., "In-Vitro Real-Time Coupled Electrophysiological and Electrochemical Signals Detection with Glassy Carbon Microelectrodes", *Journal of The Electrochemical Society* 164 (5), B3113-B3121.

Hirabayashi, Mieko, Beejal Mehta, Nasim W. Vahidi, Ajit Khosla, and Sam Kassegne. "Functionalization and characterization of pyrolyzed polymer based carbon microstructures for bionanoelectronics platforms." *Journal of Micromechanics and Microengineering* 23, no. 11 (2013): 115001.

Hirst, Judy, and Fraser A. Armstrong. "Fast-scan cyclic voltammetry of protein films on pyrolytic graphite edge electrodes: characteristics of electron exchange." *Analytical chemistry* 70, no. 23 (1998): 5062-5071.

Hu, Liang, Qin Wang, Zhen Qin, Kaiqi Su, Liquan Huang, Ning Hu, and Ping Wang. "Detection of 5-hydroxytryptamine (5-HT) *in vitro* using a hippocampal neuronal network-based biosensor with extracellular potential analysis of neurons." *Biosensors and Bioelectronics* 66 (2015): 572-578.

Hudspeth, A. James, Thomas M. Jessell, Eric R. Kandel, James Harris Schwartz, and Steven A. Siegelbaum, eds. *Principles of neural science*. McGraw-Hill, Health Professions Division, 2013.

Huynh, Nha Uyen. "Characterization of Surface Morphology of Thin-Film Platinum and Glassy Carbon Microelectrodes." *San Diego State University Master's Thesis* (2017).

Iijima, Sumio, and Toshinari Ichihashi. "Single-shell carbon nanotubes of 1-nm diameter." (1993): 603-605.

Jackson, Brad P., Susanne M. Dietz, and R. Mark Wightman. "Fast-scan cyclic voltammetry of 5-hydroxytryptamine." *Analytical chemistry* 67, no. 6 (1995): 1115-1120.

Jacobs, Christopher B., M. Jennifer Peairs, and B. Jill Venton. "Review: Carbon nanotube based electrochemical sensors for biomolecules." *Analytica Chimica Acta* 662, no. 2 (2010): 105-127.

Jenkins, G. M., and K. Kawamura. "Structure of glassy carbon." *Nature* 231 (1971): 175-176.

Jiang, Xiaowen, Yuezhen Bin, and Masaru Matsuo. "Electrical and mechanical properties of polyimide–carbon nanotubes composites fabricated by in situ polymerization." *Polymer* 46, no. 18 (2005): 7418-7424.

John, Carrie E., and Sara R. Jones. "Fast scan cyclic voltammetry of dopamine and serotonin in mouse brain slices." (2007).

Kassegne, Sam, Maria Vomero, Roberto Gavuglio, Mieko Hirabayashi, Emre Özyilmaz, Sebastien Nguyen, Jesus Rodriguez, Eda Özyilmaz, Pieter van Niekerk, and Ajit Khosla. "Electrical impedance, electrochemistry, mechanical stiffness, and hardness tunability in glassy carbon MEMS μECoG electrodes." *Microelectronic Engineering* 133 (2015): 36-44.

Kirkpatrick, D. C., C. J. McKinney, P. B. Manis, and R. M. Wightman. "Expanding neurochemical investigations with multi-modal recording: simultaneous fast-scan cyclic voltammetry, iontophoresis, and patch clamp measurements." *Analyst* 141, no. 16 (2016): 4902-4911.

Koehne, Jessica E., Michael Marsh, Adwoa Boakye, Brandon Douglas, In Yong Kim, Su-Youne Chang, Dong-Pyo Jang et al. "Carbon nanofiber electrode array for electrochemical detection of dopamine using fast scan cyclic voltammetry." *Analyst* 136, no. 9 (2011): 1802-1805.

Kong, K. C., Jamille Farraye Hetke, James A. Wiler, David S. Pellinen, and Mayurachat Gulari. "Implantable electrode lead system with a three dimensional arrangement and method of making the same." U.S. Patent Application 12/410,253, filed September 24, 2009.

Kubikova, Ľubica, and Ľubor Košťál. "Dopaminergic system in birdsong learning and maintenance." *Journal of chemical neuroanatomy* 39, no. 2 (2010): 112-123.

Kuncel, Alexis M., and Warren M. Grill. "Selection of stimulus parameters for deep brain stimulation." *Clinical neurophysiology* 115, no. 11 (2004): 2431-2441.

Lama, Rinchen D., Karl Charlson, Arun Anantharam, and Parastoo Hashemi. "Ultrafast detection and quantification of brain signaling molecules with carbon fiber microelectrodes." *Analytical chemistry* 84, no. 19 (2012): 8096-8101.

Li, W. S., Z. X. Shen, J. Z. Zheng, and S. H. Tang. "FT-IR study of the imidization process of photosensitive polyimide PMDA/ODA." *Applied spectroscopy* 52, no. 7 (1998): 985-989.

Li, Yu-Ting, Jeffery R. Wickens, Yi-Ling Huang, Wynn HT Pan, Fu-Yu Beverly Chen, and Jia-Jin Jason Chen. "Integrated wireless fast-scan cyclic voltammetry recording and electrical stimulation for reward-predictive learning in awake, freely moving rats." *Journal of neural engineering* 10, no. 4 (2013): 046007.

Linderoth, Bengt, Bertil Gazelius, Johan Franck, and Ernst Brodin. "Dorsal column stimulation induces release of serotonin and substance P in the cat dorsal horn." *Neurosurgery* 31, no. 2 (1992): 289-297.

Maynard, Edwin M., Craig T. Nordhausen, and Richard A. Normann. "The Utah intracortical electrode array: a recording structure for potential brain-computer interfaces." *Electroencephalography and clinical neurophysiology* 102, no. 3 (1997): 228-239.

Millar, Julian, Jonathan A. Stamford, Zygmunt L. Kruk, and R. Mark Wightman. "Electrochemical, pharmacological and electrophysiological evidence of rapid dopamine release and removal in the rat caudate nucleus following electrical stimulation of the median forebrain bundle." *European journal of pharmacology* 109, no. 3 (1985): 341-348.

Moran, Rosalyn J., Kenneth T. Kishida, Terry Lohrenz, Ignacio Saez, Adrian W. Laxton, Mark R. Witcher, Stephen B. Tatter et al. "The Protective Action Encoding of Serotonin Transients in the Human Brain." *Neuropsychopharmacology* (2018).

Mushahwar, Vivian K., David F. Collins, and Arthur Prochazka. "Spinal cord microstimulation generates functional limb movements in chronically implanted cats." *Experimental neurology* 163, no. 2 (2000): 422-429.

Nazari, Meisam Honarvar, and Roman Genov. "A Fully Differential CMOS Potentiostat." 2009 *IEEE International Symposium on Circuits and Systems*, 2009. doi:10.1109/iscas.2009.5118228.

Nghiem, Trang-Anh, Bartosz Telenczuk, Olivier Marre, Alain Destexhe, and Ulisse Ferrari. "Maximum entropy models reveal the correlation structure in cortical neural activity during wakefulness and sleep." *arXiv preprint* arXiv:1801.01853 (2018).

Njagi, John, Michael Ball, Marc Best, Kenneth N. Wallace, and Silvana Andreescu. "Electrochemical quantification of serotonin in the live embryonic zebrafish intestine." *Analytical chemistry* 82, no. 5 (2010): 1822-1830.

Novoselov, Kostya S., Andre K. Geim, Sergei V. Morozov, D. Jiang, Y. Zhang, Sergey V. Dubonos, Irina V. Grigorieva, and Alexandr A. Firsov. "Electric field effect in atomically thin carbon films." *science* 306, no. 5696 (2004): 666-669.

Ohuchi, F. S., and S. C. Freilich. "Metal polyimide interface: A titanium reaction mechanism." Journal of Vacuum Science & Technology A: Vacuum, Surfaces, and Films 4, no. 3 (1986): 1039-1045.

Patel, Anisha N., Patrick R. Unwin, and Julie V. Macpherson. "Investigation of film formation properties during electrochemical oxidation of serotonin (5-HT) at polycrystalline boron doped diamond." *Physical Chemistry Chemical Physics*15, no. 41 (2013): 18085-18092.

Patel, Bhavik Anil, Collin C. Luk, Pei Ling Leow, Arthur J. Lee, Wali Zaidi, and Naweed I. Syed. "A planar microelectrode array for simultaneous detection of electrically evoked dopamine release from distinct locations of a single isolated neuron." *Analyst* 138, no. 10 (2013): 2833-2839.

Pihel, Karin, Q. David Walker, and R. Mark Wightman. "Overoxidized polypyrrole-coated carbon fiber microelectrodes for dopamine measurements with fast-scan cyclic voltammetry." *Analytical chemistry* 68, no. 13 (1996): 2084-2089.

Porat, Ze'ev, Israel Rubinstein, and Baruch Zinger. "The effect of composition of Nafion deposition solutions on the diffusional properties of the films." *Journal of The Electrochemical Society* 140, no. 9 (1993): 2501-2507.

Rees, Hillary R., Sean E. Anderson, Eve Privman, Haim H. Bau, and B. Jill Venton. "Carbon nanopipette electrodes for dopamine detection in Drosophila." *Analytical chemistry* 87, no. 7 (2015): 3849-3855.

Rembado, Irene, Stavros Zanos, and Eberhard E. Fetz. "Cycle-triggered cortical stimulation during slow wave sleep facilitates learning a BMI task: a case report in a non-human primate." *Frontiers in behavioral neuroscience* 11 (2017): 59.

Roberts, James G., and Leslie A. Sombers. "Fast-Scan Cyclic Voltammetry: Chemical Sensing in the Brain and Beyond." *Analytical chemistry* 90, no. 1 (2017): 490-504.

Robinson, Donita L., B. Jill Venton, Michael LAV Heien, and R. Mark Wightman. "Detecting subsecond dopamine release with fast-scan cyclic voltammetry *in vivo." Clinical chemistry* 49, no. 10 (2003): 1763-1773.

Rothschild, R.M., 2010. Neuroengineering tools/applications for bidirectional interfaces, brain–computer interfaces, and neuroprosthetic implants–a review of recent progress. *Frontiers in neuroengineering*, *3*, p.112.

Rothstein, Jeffrey D., Lee J. Martin, and Ralph W. Kuncl. "Decreased glutamate transport by the brain and spinal cord in amyotrophic lateral sclerosis." *New England Journal of Medicine* 326, no. 22 (1992): 1464-1468.

Rousche, Patrick J., David S. Pellinen, David P. Pivin Jr, Justin C. Williams, and Rio J. Vetter. "Flexible polyimide-based intracortical electrode arrays with bioactive capability." *Biomedical Engineering, IEEE Transactions on* 48, no. 3 (2001): 361-371.

Salimi, Abdollah, Hussein MamKhezri, and Rahman Hallaj. "Simultaneous determination of ascorbic acid, uric acid and neurotransmitters with a carbon ceramic electrode prepared by sol–gel technique." *Talanta* 70, no. 4 (2006): 823-832.

Sanford, Audrey L., Stephen W. Morton, Kelsey L. Whitehouse, Hannah M. Oara, Leyda Z. Lugo-Morales, James G. Roberts, and Leslie A. Sombers. "Voltammetric detection of hydrogen peroxide at carbon fiber microelectrodes." *Analytical chemistry* 82, no. 12 (2010): 5205-5210.

Scaini, Denis, and Laura Ballerini. "Nanomaterials at the neural interface." *Current opinion in neurobiology* 50 (2018): 50-55.

Schmidt, Andreas C., Xin Wang, Yuntian Zhu, and Leslie A. Sombers. "Carbon nanotube yarn electrodes for enhanced detection of neurotransmitter dynamics in live brain tissue." *ACS nano* 7, no. 9 (2013): 7864-7873.

Schmidt-Rohr, Klaus, and Qiang Chen. "Parallel cylindrical water nanochannels in Nafion fuel-cell membranes." *Nature materials* 7, no. 1 (2008): 75.

Schwartz, Andrew B. "Cortical neural prosthetics." Annu. Rev. Neurosci. 27 (2004): 487-507.
Jaumard, N.V., Leung, J., Gokhale, A.J., Guarino, B.B., Welch, W.C. and Winkelstein, B.A., 2015. Relevant Anatomic and Morphological Measurements of the Rat Spine: Considerations for Rodent Models of Human Spine Trauma. *Spine*, 40(20), pp.E1084-E1092.

Schwerdt, Helen N., Hideki Shimazu, Ken-ichi Amemori, Satoko Amemori, Patrick L. Tierney, Daniel J. Gibson, Simon Hong et al. "Long-term dopamine neurochemical monitoring in primates." *Proceedings of the National Academy of Sciences* (2017): 201713756.

Seki, Kazuhiko, Steve I. Perlmutter, and Eberhard E. Fetz. "Sensory input to primate spinal cord is presynaptically inhibited during voluntary movement." *Nature neuroscience* 6, no. 12 (2003): 1309.

Sharma, Swati, and Marc Madou. "Micro and Nano Patterning of Carbon Electrodes for BioMEMS." *Bioinspired, Biomimetic and Nanobiomaterials* 1, no. 4 (2012): 252-265.

Si, Bo, and Edward Song. "Recent Advances in the Detection of Neurotransmitters." *Chemosensors* 6, no. 1 (2018): 1

Silverstein, Robert M., Francis X. Webster, David J. Kiemle, and David L. Bryce. Spectrometric Identification of Organic Compounds. John Wiley & Sons, 2007. Chapter 2.

Song, Yilin, Nansen Lin, Chunxiu Liu, Hong Jiang, Guogang Xing, and Xinxia Cai. "A novel dual mode microelectrode array for neuroelectrical and neurochemical recording *in vitro*." *Biosensors and Bioelectronics* 38, no. 1 (2012): 416-420.

Suzuki, Ikuro, Mao Fukuda, Keiichi Shirakawa, Hideyasu Jiko, and Masao Gotoh. "Carbon nanotube multi-electrode array chips for noninvasive real-time measurement of dopamine, action potentials, and postsynaptic potentials." *Biosensors and Bioelectronics* 49 (2013): 270-275.

Swamy, BE Kumara, and B. Jill Venton. "Carbon nanotube-modified microelectrodes for simultaneous detection of dopamine and serotonin *in vivo*." *Analyst* 132, no. 9 (2007): 876-884

Swamy, BE Kumara, and B. Jill Venton. "Subsecond detection of physiological adenosine concentrations using fast-scan cyclic voltammetry." *Analytical chemistry* 79, no. 2 (2007): 744-750.

Takmakov, Pavel, Collin J. McKinney, Regina M. Carelli, and R. Mark Wightman. "Instrumentation for fast-scan cyclic voltammetry combined with electrophysiology for behavioral experiments in freely moving animals." *Review of Scientific Instruments* 82, no. 7 (2011): 074302.

Takmakov, Pavel, Matthew K. Zachek, Richard B. Keithley, Paul L. Walsh, Carrie Donley, Gregory S. McCarty, *et al.* "Carbon Microelectrodes with a Renewable Surface." *Analytical chemistry* 82, no. 5 (2010): 2020-2028.

Taleat, Zahra, Judith Estévez-Herrera, Jose David Machado, Johan Dunevall, Andrew G. Ewing, and Ricardo Borges. "Electrochemical investigation of the interaction between catecholamines and ATP." *Analytical chemistry* (2017).

Tian, Bozhi, Jia Liu, Tal Dvir, Lihua Jin, Jonathan H. Tsui, Quan Qing, Zhigang Suo, Robert Langer, Daniel S. Kohane, and Charles M. Lieber. "Macroporous nanowire nanoelectronic scaffolds for synthetic tissues." *Nature materials* 11, no. 11 (2012): 986.

van den Brand, Rubia, Janine Heutschi, Quentin Barraud, Jack DiGiovanna, Kay Bartholdi, Michèle Huerlimann, Lucia Friedli et al. "Restoring voluntary control of locomotion after paralyzing spinal cord injury." *science* 336, no. 6085 (2012): 1182-1185.

Van Gompel, Jamie J., Su-Youne Chang, Stephan J. Goerss, In Yong Kim, Christopher Kimble, Kevin E. Bennet, and Kendall H. Lee. "Development of intraoperative electrochemical detection: wireless instantaneous neurochemical concentration sensor for deep brain stimulation feedback." *Neurosurgical focus29*, no. 2 (2010): E6.

Vomero, JM., Castagnola, E., Ciarpella, F., Maggiolini, E., Goshi, N., Zucchini, E., Carli, S., Fadiga, L., Kassegne, S., Ricci, D., "Highly Stable Glassy Carbon Interfaces for Long-Term Neural Stimulation and Low-Noise Recording of Brain Activity", *Science Reports*, Vol. 7, 4033, DOI: 10.1038/srep40332, 2017.

Vomero, M, Niekerk, P., Nguyen, V., Gong, N., Hirabayashi, M., Cinopri, A., et al. "A novel pattern transfer technique for mounting glassy carbon microelectrodes on polymeric flexible substrates." *Journal of Micromechanics and Microengineering* 26, no. 2 (2016): 025018.

Vomero, Maria, Ian Dryg, Tyler Maxfield, William Shain, Steve Perlmutter, and Sam Kassegne. "In-Vivo Characterization of Glassy Carbon μ-Electrodes and Histological Analysis of Brain Tissue after Chronic Implants." *ECS Transactions* 72, no. 1 (2016): 91-96.

Wang, Yan, Daniel C. Alsmeyer, and Richard L. McCreery. "Raman spectroscopy of carbon materials: structural basis of observed spectra." Chemistry of Materials 2, no. 5 (1990): 557-563.

Wrona, M.Z. and Dryhurst, G., 1990. Oxidation chemistry of 5-hydroxytryptamine: Part II. Mechanisms and products formed at millimolar concentrations in acidic aqueous solution. *Journal of electroanalytical chemistry and interfacial electrochemistry*, 278(1-2), pp.249-267.

Wrona, Monika Z., and Glenn Dryhurst. "Electrochemical oxidation of 5-hydroxytryptamine in aqueous solution at physiological pH." *Bioorganic Chemistry* 18, no

Wrona, Monika Z., and Glenn Dryhurst. "Oxidation chemistry of 5-hydroxytryptamine. 1. Mechanism and products formed at micromolar concentrations." *The Journal of Organic Chemistry* 52, no. 13 (1987): 2817-2825.

Yakushenko, Alexey, Volker Schöps, Dirk Mayer, Andreas Offenhäusser, and Bernhard Wolfrum. "On-chip fast scan cyclic voltammetry for selective detection of redox active neurotransmitters." *physica status solidi* (a) 211, no. 6 (2014): 1364-1371.

Yuan, Wei, Junluo Feng, Zaher Judeh, Jie Dai, and Mary B. Chan-Park. "Use of polyimide-graft-bisphenol a diglyceryl acrylate as a reactive noncovalent dispersant of single-walled carbon nanotubes for reinforcement of cyanate ester/epoxy composite." *Chemistry of Materials* 22, no. 24 (2010): 6542-6554.

Zachek, Matthew K., Andre Hermans, R. Mark Wightman, and Gregory S. McCarty. "Electrochemical dopamine detection: comparing gold and carbon fiber microelectrodes using background subtracted fast scan cyclic voltammetry." *Journal of Electroanalytical Chemistry* 614, no. 1-2 (2008): 113-120.

Zachek, Matthew K., Pavel Takmakov, Jinwoo Park, R. Mark Wightman, and Gregory S. McCarty. "Simultaneous Monitoring of Dopamine Concentration at Spatially Different Brain Locations In vivo." *Biosensors and Bioelectronics* 25, no. 5 (2010): 1179-1185.

Zhang, Limin, Fangling Liu, Xuemei Sun, Guang-feng Wei, Yang Tian, Zhi-pan Liu, Rong Huang, Yanyan Yu, and Huisheng Peng. "Engineering carbon nanotube fiber for real-time quantification of ascorbic acid levels in a live rat model of Alzheimer's disease." *Analytical chemistry* 89, no. 3 (2017): 1831-1837.

Zschoerper, Nicolas Peer, Verena Katzenmaier, Uwe Vohrer, Michael Haupt, Christian Oehr, and Thomas Hirth. "Analytical investigation of the composition of plasma-induced functional groups on carbon nanotube sheets." *Carbon* 47, no. 9 (2009): 2174-2185.

APPENDIX

Charge Transfer between Serotonin and Glassy Carbon

Electrostatic interaction, as discussed in the previous section, occurs before the electrochemical potential is applied. Once the potential is applied, in cyclic voltammetry, the voltage sweeps up. At this point the working electrode reads a positive voltage relative to the reference electrode. This can occur through reversible oxidation of the working electrode and a build-up of electrons at the counter electrode. At a sufficient voltage electrostatically interreacting 5-HT molecules give up electrons to the carbon electrode, causing the first oxidation. As the voltage increases further, a second electron can oxidize the 5-HT further. The electrons taken up from the 5-HT bring the carbon back to its original electronic state, leaving the 5-HT in an oxidized state.

(a)

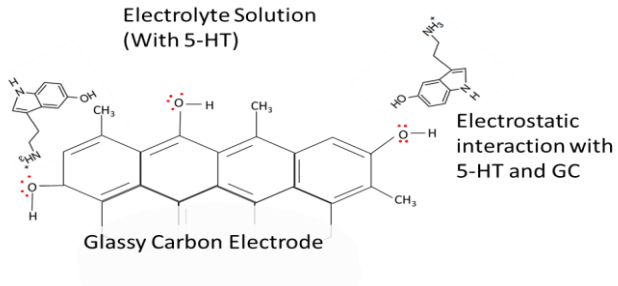

(b) Potential Applied causes oxidation of glassy carbon

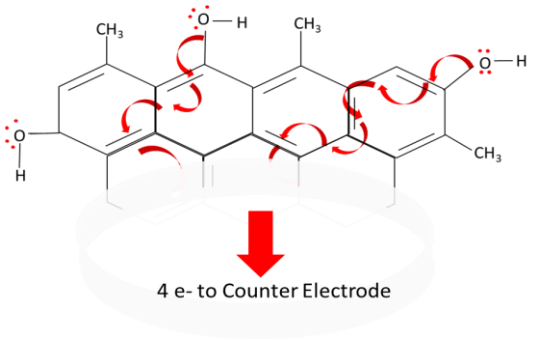

(c) Redistribution of electrons attracts 5-HT which leads to first and second oxidation as potential increases

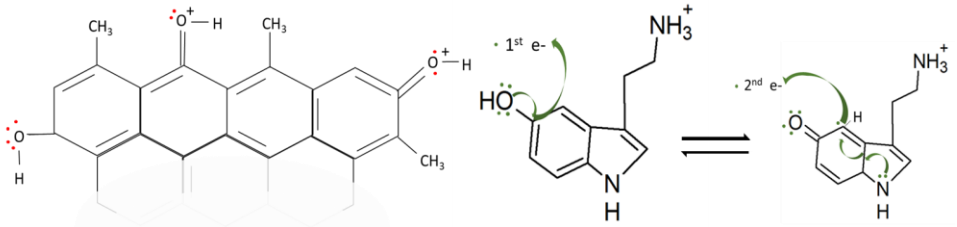

(d) Electrons from 5-HT reduce the surface of GC
Second oxidation produces quinone imine or another 5-HT by-product

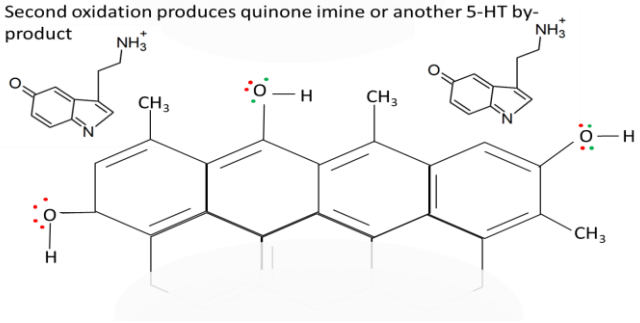

One possible scheme for charge transfer between glassy carbon and serotonin and resulting oxidization of 5-HT